ETHANOL CONVERSION TO HIGHER ALCOHOLS USING OCCLUDED $[Mg_4(OH)_4]^{4+}$ CLUSTERS IN MgO/KNaX AS CATALYSTS

NATTAPOL YOTKKHAM

A THESIS SUBMITTED IN PARTIAL FULFILLMENT OF THE REQUIREMENT FOR

THE DEGREE OF MASTER OF SCIENCE IN APPILED CHEMISTRY

DEPARTMENT OF CHEMISTRY SCHOOL OF SCIENCE

KING MONGKUT'S INSTITUTE OF TECHNOLOGY LADKRABANG

2022

KMITL-2022-SC-M-012-060

Title	ETHANOL CONVERSION TO HIGHER ALCOHOLS USING OCCLUDED $[Mg_4(OH)_4]^{4+}$ CLUSTERS IN MgO/KNaX AS CATALYSTS
Students Name	Mr. Nattapol Yotkkham
Students ID	62605050
Degree	Master of Science (Applied Chemistry)
Department	Chemistry
Academic year	2022
Advisor	Asst. Prof. Dr. Kittisak Choojun
Co-advisors	Prof. Dr. Tawan Sooknoi

Abstract

Conversion of ethanol to higher alcohols was studied over MgO/KNaX, prepared by ion exchange with Mg $(OAc)_2$, followed by KOH washing. The catalysts were characterized by XRF, XRD, SEM, BET, ^{27}Al MAS NMR, EXAFS, NH_3- and CO_2-TPD. All catalysts showing MgO nanopetals and aggregates on the external surface, contained occluded $[Mg_4(OH)_4]^{4+}$ clusters in the zeolite cavities, providing medium basic (M_b) and acid (M_a) sites. Ethanol conversion and higher alcohols selectivity (up to 78%) increased with M_b/M_a ratio due to the increase in both MgO (4–6 wt%) and K (14.7–17.3 wt.%) loadings. Decreasing occluded $[Mg_4(OH)_4]^{4+}$ clusters and/or increasing MgO aggregates led to the lower conversion and yields of higher alcohols. The essential role of the occluded $[Mg_4(OH)_4]^{4+}$ clusters in producing higher alcohols was verified by the reactions using various control catalysts. The MgO/KNaX showed high stability even after steaming at 380 °C, as well as being regenerated by calcination (450 °C in air)

Keywords: aldol condensation, ethanol, higher alcohols, Guerbet reaction, magnesium oxide (MgO), hydrogen transfer process and occluded $[Mg_4(OH)_4]^{4+}$ clusters

Acknowledgments

The author desires to appreciatively thank my advisor, Asst. Dr. Kittisak Choojun, and my co-advisor, Prof. Dr. Tawan Sooknoi, for any suggestions, inspiration, carefulness, reassurance, experimental instrument, and knowledge in catalysis throughout this research I would like to gratefully acknowledge chairperson and committee, Prof. Dr. Metta Chareonpanich and Asst. Prof. Dr. Karoon Sadorn for judgment and valuable comments.

Moreover, I would like to acknowledge the financial support from the Faculty of Science, King Mongkut's Institute of Technology Ladkrabang for the equipment, chemicals, and facilities.

Furthermore, I would like to grateful to my friends in Catalytic Chemistry Research Unit (CCR group) for their help, advice, support, and encouragement.

Last but not least, I deeply appreciate and thank my parents and family for their love and support.

Mr. Nattapol Yotkkham

Table of Contents

Table of Contents (Continue)

Table of Contents (Continue)

List of Tables

List of Figures

List of Figures (continue)

Chapter 1

Introduction

1.1 Research Motivation

Bioethanol has been commercially available and widely used in transportation fuel, however its business profit margin is not high. Conversion of bioethanol into value-added chemicals is the promising alternative to not only increase the profitability but also subsidize the petrochemical dependence. The conversion of bioethanol to higher alcohols derivatives, such as butanol, hexanol, and octanol, has been extensively investigated because they have a strong relevance to various industries [1-3]. For instance, butanol and hexanol are used as a plasticizer and solvents in polymer production, and octanol is commonly used in foods, perfumes, and lubes [4-5].

To convert ethanol directly to a higher alcohol, hydrogen transfer with a simultaneous aldol condensation, known as Guerbet reaction [6-10], is involved. This reaction is catalytically promoted by different active sites in each step. Lewis basic/acid sites promote the dehydrogenation of ethanol to acetaldehyde and hydrogen transfer from the alcohol to higher aldehyde. While the aldol condensation of the aldehydes needs proximity of acid-base sites [11]. The rate of these steps must be deliberately adjusted. A faster hydrogen transfer leads to low conversion with small alcohol/aldehyde products. Conversely, a higher condensation rate results in coke formation. Accordingly, the basic and acid sites must be placed in close proximity [12] since isolated sites could promote side reactions, such as dehydration to ethylene or dehydrogenation to acetaldehyde.

Alumina [13, 14], MgO [15-20], $LaMnO_3$ [21] and basic zeolite [22-26] have been employed for ethanol conversion due to the presence of proximate Lewis acid-base pairs,

which can reduce the energy barrier to generate acetaldehyde and promotes the aldol condensation of two acetaldehydes. Although alumina and $LaMnO_3$ were reported to be active for ethanol conversion, the reaction yields only a trace amount of butanol, presumably due to their low basic/acid ratio. Regarding basic zeolite catalysts, such as Rb-KX, KX, the dehydration to ethylene is still more favorable despites their higher basic/acid ratio. Comparatively, MgO possessing high basicity with very low acidity is prone to promote aldol condensation, which can improve butanol yield with lower ethylene selectivity. Nevertheless, the low surface area of MgO tends to give a relatively low activity. To increase the MgO surface area, the highly dispersed MgO supported on SiO_2 (MgO/SiO_2) was developed [27-28]. However, MgO/SiO_2 has poor selectivity to higher alcohols and mainly promotes dehydration, due to the additional weak acid site from the silanol.

Zeolites as the catalyst support offer a high surface area with cavities to accommodate highly dispersed MgO. Incorporation of MgO in KNaX can be simply achieved by Mg^{2+} ion exchange, followed by base washing. The method can produce various types of MgO species, such as occluded MgO clusters, MgO nanopetals and MgO aggregates [29]. In addition to the increased active MgO surface area, the method is also able to brings up the proximate acid/basic pair for Guerbet reaction. Zhang, et al. reported that the presence of MgO nanopetals in MgO/KNaX promoted aldol condensation of the acetaldehyde-ethanol mixture in a batch reactor, providing about 94.5% C4-aldehyde selectivity and 5.5% butanol selectivity. Interestingly, Ricchiardi et al. showed that the occluded $[Mg_4(OH)_4]^{4+}$ clusters inside the faujasite zeolite cavities provided the "super basic site" [30]. This might offer a closed proximity of acid-base sites within the framework, which would be beneficial to balance H-transfer/aldol condensation in Guerbet reaction. However, relevant insights into the supported occluded $[Mg_4(OH)_4]^{4+}$ clusters in the catalysis are still lacking. Though, the role of this occluded $[Mg_4(OH)_4]^{4+}$ clusters inside the zeolite X cavities in Guerbet reaction has not been demonstrated.

Herein, MgO species supported in the cavity of zeolite X (i.e., the MgO/KNaX catalysts) were prepared (via ion exchange) for conversion of ethanol to higher alcohols

via Guerbet reaction. The findings provided additional evidence to support the presence of occluded $[Mg_4(OH)_4]^{4+}$ clusters inside KNaX zeolite and its essential role in promoting higher alcohols production directly from ethanol. The effect of $Mg(OAc)_2$ concentration (used in the ion exchange method for loading Mg species), crystal structure and surface area on higher alcohol selectivity was evaluated by various characterization of XRF, XRD, ^{27}Al MAS NMR and N_2 physisorption. The incorporated Mg species, including occluded $[Mg_4(OH)_4]^{4+}$ clusters, MgO nanopetals, and MgO aggregates over MgO/KNaX, were investigated by SEM and EXAFS. The acid/base properties deriving from the occluded $[Mg_4(OH)_4]^{4+}$ clusters were determined by NH_3- and CO_2-TPD. Ethanol conversion over MgO/KNaX was studied in a gas-phase reactor at 380 °C under atmospheric N_2. The importance of medium basicity to medium acidity (M_b/M_a) of the MgO/KNaX catalysts was demonstrated. The role of the occluded $[Mg_4(OH)_4]^{4+}$ clusters inside the zeolite cavity was also revealed. The stability of the MgO/KNaX catalysts was studied, as well as their ability to be regenerated.

1.2 Objectives of the study

1.2.1 To obtain high active, selective, and stable catalysts for the production of higher alcohols from ethanol.

1.2.2 To study effect of the MgO loading over KNaX prepared by Mg^{2+} ion exchange.

1.2.3 To investigate the presence of the occluded $[Mg_4(OH)_4]^{4+}$ clusters, MgO nanopetals and MgO aggregated species

1.2.4 To understand the effect of MgO species and stability of catalyst on the conversion of ethanol to higher alcohols

1.3 Scopes of the study

1.3.1 Synthesis of 4-8MgO/KNaX and MgKNaX catalysts by ion-exchange and precipitation technique

1.3.2 Synthesis of 6MgO/KNaX(imp) by wet-impregnation method

1.3.3 Synthesis of 5MgO/KNaX(PB) and 5MgO/KNaX(St) by pre coking and water steaming technique

1.3.4 Characterization of catalysts by NH_3-temperature programmed desorption (NH_3-TPD), CO_2-temperature programmed desorption (CO_2-TPD), surface area analysis, X-ray fluorescence (XRF), X-ray diffraction (XRD), Scanning electron microscopy (SEM) and Solid ^{27}Al magic angle spinning nuclear magnetic resonance spectra (^{27}Al MAS-NMR) and Extended X-ray absorption fine structure spectroscopy (EXAFS)

1.3.5 Study the ethanol conversion activity of the MgO/KNaX catalysts in a continuous fixed-bed reactor

1.3.6 Analysis of liquid products by on-line gas chromatography with flame ionization detector (GC-FID)

1.4 Benefits of the study

It is expected that this study could provide an alternative catalyst with high activity, selectivity, and stability for the production of higher alcohols from ethanol. This strategy could increase the value-added ethanol which is widely produced from raw materials available in our country.

Chapter 2

Theory and Literature Reviews

2.1 Alcohol

An organic compound that is composed of the hydroxyl functional group (-OH) is classified as an alcohol. There are three types of alcohols which are primary, secondary (*sec-, s-*), and tertiary (*tert-, t-*), based upon the number of carbon atoms connected to the carbon atom that bears the hydroxyl functional group [31]. In general, the hydroxyl group makes the alcohol molecule polar. In addition, these groups can form intermolecular hydrogen bonding causing alcohols to have higher boiling points than comparable hydrocarbons and ethers.

Industrially, the most important alcohols are methanol, ethanol, 1-propanol, 1-butanol, 2-methyl-1-propanol (isobutyl alcohol), the plasticizer alcohols (C_6-C_{11}), and the fatty alcohols (C_{12}-C_{18}). They are prepared mainly from synthesis gas (methanol), from olefins via the oxo synthesis, or by the Ziegler process. Alcohols are used as solvents and diluents for paints (mainly C_4-C_6 alcohols) [32], as intermediates in the manufacture of esters and a whole range of organic compounds [33], as flotation agents [34] and in recent times increasingly as fuel or fuel additives, e.g., methanol, ethanol, and tert-butyl alcohol [35]. For industrial purposes, isomeric mixtures are preferred since the pure alcohols are too expensive. Moreover, mixtures of alcohols with differing carbon numbers can be advantageous for certain purposes. Therefore, the amounts of alcohol mixtures available on the market are similar the quantities of the pure, individual alcohols.

Reactions of alcohols can be proceeded via cleavage of the O-H bond or the C-O bond either homolytic cleavage or heterolytic cleavage. Under normal conditions, alcohols are stable [36]. Alcohols can undergo oxidation to give aldehydes, ketones, or

carboxylic acids, or they can be dehydrated to alkenes. They can react to form ester compounds and undergo nucleophilic substitution reactions if activated first. The lone pair electrons on the oxygen of the hydroxyl group also make alcohols nucleophiles [37]. Catalytic oxidation or dehydrogenation of primary and secondary alcohols over copper, silver, iron, molybdenum, etc., leads to the formation of aldehydes and ketones [38].

2.1.1 Ethanol

Ethanol or ethyl alcohol, also called drinking alcohol, is the principal type of alcohol found in alcoholic beverages, produced by the fermentation of sugars by yeasts. It is a neurotoxic psychoactive drug and one of the oldest recreational drugs used by humans [39]. It can cause alcohol intoxication when consumed in sufficient quantity. Its structural formula, CH_3CH_2OH is often abbreviated as C_2H_5OH, C_2H_6O or EtOH [40]. Ethanol is also referred to an alcohol spirit, spirit of wine, grain alcohol, absolute alcohol, and ethyl hydrate. Depending on its water content, preparation, and final use, several ethanol products exist on the market. 99% alcohol (often referred to as absolute alcohol) is used extensively for tinctures and pharmaceutical preparations, as a solvent and preservative, as an antiseptic, and in perfume. If the alcohol is used for purposes other than as a beverage, it is denatured by the addition of substances such as methanol, pyridine, formaldehyde, or sublimate. The denatured alcohol is then used by industry and commerce, principally as a solvent, as a raw material for manufacturing chemicals, or as a fuel.

The chemical properties of ethanol are dominated by the OH-functional group, which can undergo many industrially important chemical reactions, e.g., dehydration, halogenation, ester formation, and oxidation [41]. Ethanol can also be produced efficiently not only by chemical synthesis from petroleum and coal-based feedstock. It can thus play a commercial role as a raw material for various chemicals with increasing importance. Conversion of ethanol to "alkochemicals" is an entirely new approach to producing familiar

petrochemicals. Some of these routes are already being used industrially in large alcohol producing countries [42].

2.2 Higher alcohols

2.2.1 Butanol

Butanol (butyl alcohol) refers to a four-carbon alcohol with a formula of C_4H_9OH. There are four possible isomeric structures for butanol, from a straight chain primary alcohol to a branched-chain tertiary alcohol [43]. Butanol is considered as a potential biofuel (butanol fuel). Butanol at 85% strength can be used in cars designed for gasoline (petrol) without any change to the engine (unlike 85% ethanol), and it contains more energy for a given volume than ethanol and almost as much as gasoline, so a vehicle using butanol would return fuel consumption more comparable to gasoline than ethanol. Butanol can also be used as a blended additive to diesel fuel to reduce soot emissions. It is used as a solvent for a wide variety of chemicals and textile processes, in organic synthesis and as a chemical intermediate. It is also used as paint thinner and a solvent in other coating applications, where it is used as a relatively slow evaporating latent solvent in lacquers and ambient-cured enamels. It finds other uses such as a component of hydraulic and brake fluids [44].

2.2.2 Hexanol

1-Hexanol $CH_3(CH_2)_4CH_2OH$, is prepared according to the Ziegler process from ethylene or is made from natural products derived from coconut or palm oils. It is used as a solvent, as a basic material for the perfume industry, and to produce plasticizers (in this case usually as a mixture with higher n-alcohols). Nitrates of 1-hexanol are recommended as cetane number improvers. 2-Methyl1-pentanol $CH_3(CH_2)_2CH(CH_3)CH_2OH$,is prepared by aldol condensation of propionaldehyde and subsequent hydrogenation of the intermediate 2-methyl-2- pentanal, it is used as a solvent [45].

2.2.3 Octanol

2-Ethyl-1-hexanol [$CH_3(CH_2)_3CH(C_2H_5)CH_2OH$] is the most important C_8 alcohol. 1-Octanol [$CH_3(CH_2)_6CH_2OH$] capryl alcohol. Its esters are widespread in nature e.g., they occur in grapefruits, oranges, or green tea. 1-Octanol is manufactured by the Aldol process and from natural products. The alcohol is used in the perfume industry. 2-Octanol is obtained by the alkaline hydrolysis of castor oil. It is used as a solvent in the paint industry, as a wetting agent in the textile industry, and as a component of brake fluids [46].

2.3 Aldehyde

Aldehydes are represented by the general formula RCHO, where R can be hydrogen or an aliphatic, aromatic, or heterocyclic group. According to IUPAC nomenclature, aldehydes are identified by the ending "al." However, many of them still are called by their common names. The polarity of the carbonyl group of aldehydes not only facilitates the typical aldehyde reactions-addition of nucleophiles, reduction, and oxidation but it also makes the α-hydrogen atom acidic. For these reasons, aldehydes can undergo a wide variety of reactions [47].

2.3.1 Acetaldehyde

Acetaldehyde (CH_3CHO) was observed in 1774 by SCHEELE during reaction of black manganese dioxide and sulfuric acid with alcohol. Its constitution was explained in 1835 by LIEBIG who prepared pure acetaldehyde by oxidation of ethanol with chromic acid and designated this product “aldehyde”. A concentration of the term “alcohol dehydrogenatus”.

Acetaldehyde is mobile, low-boiling, highly flammable liquid with a pungent odor. Because of its high chemical reactivity, acetaldehyde is an important intermediate in the production of acetic acid, acetic anhydride, ethyl acetate, peracetic acid, butanol, 2-ethylhexnaol, pentaerythritol, chlorinated acetaldehyde (chloral), glyoxal, alkyl amines,

pyridines, and other chemicals. Acetaldehyde is an intermediate in the metabolism of plant and animal organisms, in which it can be detected in small amounts. Lager amounts of acetaldehyde interfere with biological processes. As an intermediate in alcoholic fermentation processes, it is present in small amounts in all alcoholic beverages, such as beer, wine, and spirits. Acetaldehyde also has been detected in plant juices and essential oils, roasted coffee, and tobacco smoke [48].

2.3.2 Butanal

Butanal is an organic compound with the formula $CH_3(CH_2)_2CHO$. This compound is the aldehyde derivative of butane. It is a colorless flammable liquid with an acrid smell. It is miscible with most organic solvents. It can be produced by the catalytic dehydrogenation of n-butanol. At once, it was produced industrially by the catalytic hydrogenation of crotonaldehyde, which is derived from acetaldehyde [49].

2.3.3 Hexanal

Hexanal is an alkyl aldehyde found in human biofluids. Human milk samples collected from women contains hexanal. Among mediators of oxidative stress, highly reactive secondary aldehydic lipid peroxidation products can initiate the processes of spontaneous mutagenesis, carcinogenesis, can also act as a growth-regulating factors and signaling molecules. In specimens obtained from adult patients with brain astrocytoma's, lower levels of n-hexanal are associated with poorer patient prognosis [50].

2.4 Guerbet reaction

An important reaction to produce higher alcohols from ethanol is "Guerbet reaction". The Guerbet reaction of alcohols is the oldest and best understood material in the class of compounds first synthesized by Marcel Guerbet [51].

In these reactions, ethanol is adsorbed on the catalyst surface and dehydrogenated to acetaldehyde, follows by aldol condensation of aldehydes to larger unsaturated aldehyde. Final step is hydrogen transfer, which promotes the formation of higher alcohol from unsaturated aldehyde. The reaction mechanism is on both acidic and basic active sites [52].

Dehydrogenation starts by alcohol chemisorption on acid- basic site pairs, which cleaves O-H bonds to form surface alkoxide intermediates bound to the acid center. The α-hydrogen in the alkoxide group is then abstracted by a neighboring basic site to form adsorbed aldehydes. Then, aldol condensation reactions on MgO samples involved also the formation of a carbanion intermediate on Lewis acid strong Brønsted base pair sites. After aldol condensation, the product of aldol condensation will be dehydrated to crotonaldehyde. Finally, crotonaldehyde will be hydrogenated to 1- butanol as shown in Figure 2.1

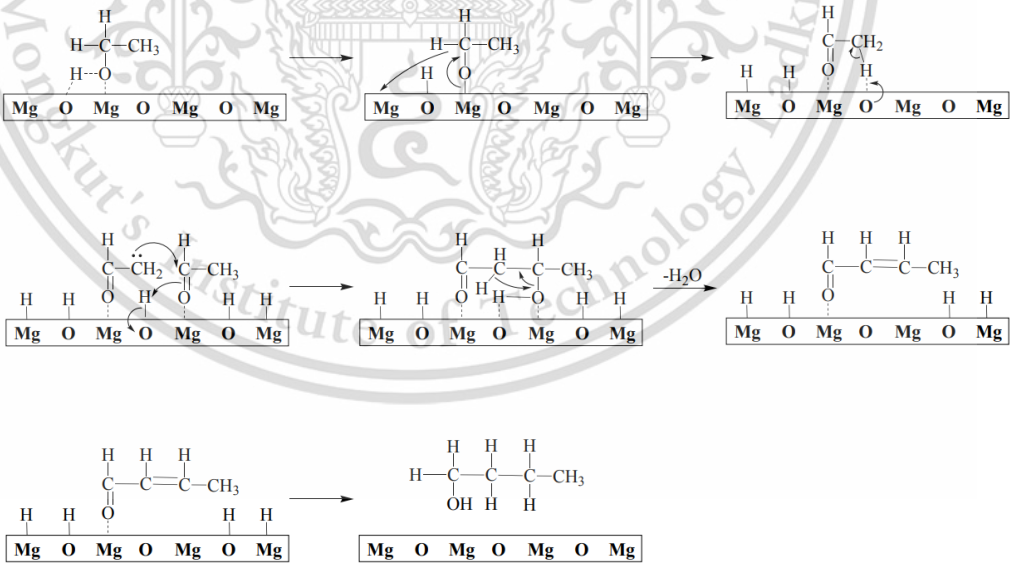

Figure 2.1 Mechanism of Guerbet reaction [52]

2.5 Catalyst

In 1931, ethanol coupling was first observed over mixtures of MgO, Al_2O_3, and CuO_x. Metal oxides are promising catalysts for ethanol conversion because they give high product selectivity and controllable synthetic processes; for instance, Mg - Al oxide catalysts with different structures show high selectivity for n-butanol in ethanol conversion. Mixed metal oxides catalysts have acid and basic sites, which active in aldol condensation reactions [53].

2.5.1 Magnesium oxide

Magnesium oxide (MgO), or magnesia, is a white hygroscopic solid mineral that occurs naturally as periclase and is a source of magnesium. It has an empirical formula of MgO and consists of a lattice of Mg^{2+} ions and O^{2-} ions held together by ionic bonding. MgO has Brønsted basic site that can promote aldol condensation in Guerbet reaction. The isolated O^{2-} ion on MgO surface would be unable to from ethoxide intermediates. Thus, the incorporation of small amounts of metal cations to MgO drastically increased the acetaldehyde formation rate because of the generation of new surface Lewis acid-strong base pair sites [54].

Basic mixed oxides are mostly based on MgO. It was found that the selectivity to 1-butanol increased with the number of strong basic sites. Catalysts with higher concentration and strength of the basic sites lead to high selectively to C_4 products whereas the presence of acid sites promotes ethanol dehydration [15]. However, it provides low surface area in comparable to other metal oxide. Therefore, the improvement of surface area can be achieved by supporting on high surface material such as zeolite X.

2.5.2 Faujasite zeolite (NaX)

Zeolites are porous crystalline aluminosilicates of SiO_4^{4-} and AlO_4^{5-} tetrahedra connected by oxygen bridges. Among various types of zeolites, NaX zeolite offers a large

pore diameter (0.74 nm). The framework is composed by linking sodalite cavity through double six-rings which create a large super-cage cavity accessible by a three-dimensional 12-ring pore system shown in Figure 2.4, and 2.5 [55]. Because of its well-defined structure, large pore volume, and appropriate ion exchange capability, NaX zeolite is widely used as ion-exchanger, absorbent and catalyst [56].

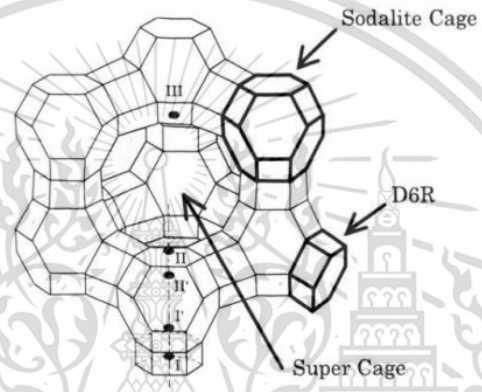

Figure 2.2 The crystal structure of NaX Zeolite [55].

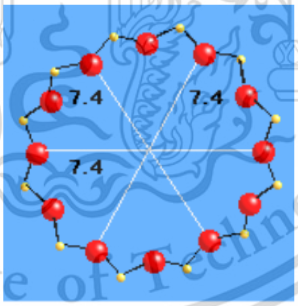

Figure 2.3 12-Ring of the NaX [55]

NaX are commonly used in base-catalyzed reactions since the strength of their basic sites (framework O ions) can be adjusted by varying the Si/Al ratio and the electronegativity of the exchangeable alkali metal cations used for compensating the

negative framework charges. At the same time, zeolites offer the possibility of controlling reaction selectivity by adjusting the extent of molecular confinement. In consecutive reactions like the acetaldehyde self-condensation of interest in this work, the formation of the higher alcohol products (>C_6) may be inhibited by confinement. This characteristic distinguishes zeolites from other types of basic catalysts and makes them a better candidate for obtaining high selectivity to C_4 products since further condensation to heavier C_6 and C_8 hydrocarbons may be inhibited. While the aldol condensation of acetaldehyde in the vapor phase has been previously investigated on NaX, no reports have been found on the aldol condensation of acetaldehyde in liquid phase over NaX, which is the focus of the present contribution. Moreover, in this work, we have investigated the aldol condensation in the presence of an alcohol, which can undergo hydrogen transfer via Meerwein-Pondorf-Verley (MPV) reaction and significantly affect the product distribution [57].

Apart from impregnation, to obtain highly dispersed MgO, the addition of MgO to NaX can be obtained by ion-exchange but it is unfavorable because Na^+ is a hard cation. The new strategy is firstly exchange Na^+ with K^+ at 80 °C and then re-exchange to Mg^{2+} washing by KOH solution. As a result, MgO forms white small extra-framework crystal that gain much of potential for Guerbet reaction.

2.6 Literature review

In 1890, the Guerbet reaction involving the coupling of two alcohol molecules was first named after Marcel Guerbet, who studied the self-coupling of 1-butanol to produce the branched saturated alcohol, 2-ethylhexananol ($C_8H_{18}O$) [51]. The Guerbet reaction involves a complex sequence of many other reactions such as dehydrogenation, aldolization, dehydration, and hydrogenation. Many recent publications on Guerbet reactions over heterogeneous catalysts are widely done using basic zeolite [22], and magnesia (MgO) [15]. C. Yang, *et al*., studied the synthesis of 1-butanol in single step over

zeolites in 20th century. They found that ethanol can mainly convert to 1-butanol over Li, K and Rb cation-exchanged 13X zeolites by bimolecular condensation. Even though, the selectivity was higher than 40%, the conversions were lower than 0.2% [22]. In addition, the distribution of acid sites and basic sites on the catalyst surface are related to the Ca/P ratio of HAP as an account of the yields of ethylene, 1-butanol, and 1,3- butadiene. In our CCR work group, T. Klinubon, and A. Hongmeuan, [58], prepared MgO by sol-gel method. They found that, because of the high dispersion, the conversion can be enhanced 30%. Moreover, the incorporation of Zn, Ni, and Cu over MgO by strong electrostatic adsorption (SEA) increases the Lewis acid characteristic. As such, the ethanol conversion was improved. In similar to Toni Riittonen's work, the most promising catalyst (20.7% Ni/Al_2O_3 and HTC-500) showed 25% ethanol conversion with 80% selectivity to 1-butanol could be reached [59]. The addition of Lewis acid additive can assist in the hydrogen transfer process.

In 2013, S. Ndou, *et al*., investigated dimerization of ethanol to 1-butanol over alkali earth metal oxides and modified MgO catalysts for the synthesis of fine chemicals from alcohols. Higher alcohols are produced through Guerbet reaction, which is an important industrial process that is used to increase the carbon number of alcohols. In this reaction, a primary or secondary alcohol react with itself or another alcohol to produce a higher alcohol. Magnesium oxide was suspended in warm water with stirring and then solidified by evaporation of water. It was dried at 120°C for 16 h and finally calcined in air at 400°C for 6 h. The metal oxide supported catalysts were prepared by an impregnation procedure using an appropriate amount of aqueous metal hydroxide/nitrate solutions (incipient wetness method). The catalysts were dried at 120°C for 16 h and calcined in air at 400°C. The catalytic experiments were carried out in a vertical fixed-bed glass reactor. Using of magnesium oxide and metal oxide supported catalysts provided 18.39% and 7.33% yield of butanol, respectively [15].

In 2016, L. Zhang *et. al.,* [29] studied the effects of different types of zeolite faujasite catalysts to selective aldol condensation of acetaldehyde in the liquid phase.

From CO_2 TPD, the addition of K reduced total basic sites, resulting in increased aldol condensation of NaX. However, NaX products have a lower C_4 / (C_6 + C_8) ratio than NaY because NaX has a higher total base site. As a result, increased activity for condensation reactions but decreased C_4 product yield. Therefore, it can be concluded that the addition of K into NaX results in higher carbon product yield and increase the aldol condensation of acetaldehyde. They also investigated the acetaldehyde-ethanol conversion activity of MgO-KNaX with different MgO amounts and compared with MgO and KNaX. The basicity and scope of molecular captivity in KNaX zeolites have been adjusted by controlled agglomeration of Mg as extra-framework species through ion-exchange and precipitation. The extent of condensation of C_2 aldehyde, depends on the amount of extra-framework MgO. An increasing amount of Mg outside the framework increased the (C_6+C_8)/C_4 and C_8/C_6 ratios. Especially, MgO-KNaX-0. 99, which only has Mg in the cation form, is the lowest active condensation catalyst. MgO-KNaX-1. 32 results in higher (C_6+ C_8)/ C_4 and C_8/C_6 ratios than those of MgO-KNaX-1.14, specifically at increase C_2 aldehyde conversion levels. Differences in the product distribution are attributed not only to the inflated basicity of MgO-KNaX-1.32, but also to the increased number of K^+ ions inside the super cages that increase the steric confinement and enhance conversion outside the zeolite cages.

Chapter 3

Research methodology

3.1 Reagents

Chemicals	Grade of purity	Manufacturers
1. Ethanol (C_2H_5OH)	99.99%	Carlo Erba
2. Nitrogen gas (N_2)	High purity (99.99%)	Praxair
3. Air	High purity (99.99%)	Praxair
4. Hydrogen gas (H_2)	High purity (99.99%)	Praxair
6. Potassium carbonate (K_2CO_3)	99.0%	Carlo Erba
7. Magnesium acetate ($Mg(CH_3COO)_2$)	-	Carlo Erba
8. Potassium hydroxide pellets (KOH)	85.0%	Merck
9. Deionized water	-	
10. Sodium hydroxide pellets (NaOH)	99.0%	Carlo Erba
11. Sodium aluminate ($NaAlO_2$)	56.0%	Sigma-aldrich
12. Sodium silicate solution ($Na_2Si_3O_7$)	26.5%	Sigma-aldrich
13. Furfuryl alcohol ($C_5H_6O_2$)	98.0%	Sigma Aldrich

3.2 Apparatus

1. Laboratory glassware
2. Reflux setup
3. Thermometer
4. Hotplate & stirrer
5. Magnetic bar
6. Vacuum pump
7. pH meter
8. Oven

9. Syringe (10mL)

10. Syringe pump (KD Scientific)

11. Furnace

12. USA standard sieve; 600 and 850 microns

13. Catalytic testing rig

14. Mass flow controller

15. Gas chromatograph with flame ionization detector (GC-FID)

16. Temperature programmed desorption (TPD) system

17. X-ray diffractometer (XRD)

18. X-ray fluorescence spectrometers (BRUKER S8 TIGER, Scientific and Technological

Research Equipment Centre, Chulalongkorn University)

19. Scanning electron microscope (LEO 1455 VP, Scientific Instrument Service Center,KMITL)

20. Surface area analyzer

3.3 Experimental procedure

3.3.1 Catalyst preparation

3.3.1.1 Preparation of Zeolite X

The zeolite X samples were prepared according to those reported by Yao et al. [60], with a slight modification. In synthesis, the freshly prepared sodium aluminate solution containing 3.0 g of $NaAlO_2$, 1.5 g of NaOH and 9.6 g of DI water was dropped wisely added into the sodium silicate solution containing 11.1 g of $Na_2Si_3O_7$, 0.6 g of NaOH and 33.6 g of DI water. The molar composition of the synthesis gel was 3:3.5:1:180 of SiO_2: Na_2O : Al_2O_3 : H_2O. Subsequently, the slurry was aged at 30 ˚C for 30 min. The mixture was put into a Teflon-lined stainless-steel autoclave, then placed in an oven at 110 ˚C for 5 h. After that, the autoclave was naturally cooled to room temperature. Next, the solids were filtered and washed with deionized water until the pH of the filtrate reached ~6–7. Finally, the obtained solids were dried overnight at 110 ˚C and calcined in a horizontal tube furnace air at 450 ˚C (1 ˚C/min) under air (30mL/min) for 3 h.

3.3.1.2 Preparation of KNaX catalyst

The KNaX zeolite was synthesized by the ion exchange method, as reported by Kim, et al [61]. Briefly, 6 g of NaX was added into 300 mL of 0.1 M potassium carbonate (K_2CO_3) solution. This solution was stirred (900 rpm) at 80˚C for 24 h. Then, the mixture was vacuum filtered and dried at 110˚C for 8 h.

3.3.1.3 Synthesis of MgO/KNaX catalyst

The xMgO/KNaX catalysts – x is the wt.% MgO loading - were prepared by the Mg^{2+} ion exchange and precipitation, respectively. Briefly, 2 g of KNaX was added into 100 mL of the desired magnesium acetate ($Mg(OAc)_2$) solution (0.1, 0.3, 0.5, 0.6 or 1.0 M for 4, 5, 6, 7, or 8). The mixture was stirred at room temperature for 24 h. Then, the solids were vacuum filtered and dried overnight at 110˚C. Afterward, the obtained

solid were added to 100 mL of KOH solution and stirred at room temperature for 20 min in order to precipitate the Mg^{2+} ions to $Mg(OH)_2$. It is noted that in this step, the concentration of the KOH solution use for the precipitation is the same as the concentration of $Mg(OAc)_2$. The solids were vacuum filtered, dried overnight at 110˚C, and followed by calcination in a horizonal tube furnace at 450˚C (1˚C/min) under air (30mL/min) for 3 h, to obtain the xMgO/KNaX catalysts.

3.3.1.4 Synthesis of exchangeable MgKNaX

The exchangeable MgKNaX catalyst was prepared by the ion exchange method similar to those of xMgO/KNaX sample but using only 0.01 M of $Mg(OAc)_2$ for the ion exchange. The obtained sample was denoted as MgKNaX.

3.3.1.5 Synthesis of 6MgO/KNaX(Imp)

The 6MgO/KNaX(Imp) was prepared by the wetness impregnation method. To prepare 2 g of the catalyst, magnesium acetate ($Mg(OAc)_2$) 0.64 g was dissolved in 20 mL deionized water. This magnesium solution was sprayed on the supports (1.88 g) till wetness, then the sample was dried at 80˚C. The process was repeated until the prepared $Mg(OAc)_2$ solution was used up. Then, the catalyst was dried overnight at 80 ˚C and calcined in a horizontal tube furnace at 450˚C (2˚C/min) for 3 h under air (30 mL/min).

3.3.1.6 Synthesis of pore blocking: 5MgO/KNaX(PB)

The selective pore blocking of 5MgO/KNaX would be prepared by following the procedure reported by Chen, et al [62]. Briefly, 0.3 g of 5MgO/KNaX was sieved and treated at 450 ˚C (2 ˚C/min) under atmospheric air (30 mL/min) in the fixed-bed reactor for 1 h. After that, furfuryl alcohol was fed by a syringe pump (1 mL/h) at 100 ˚C under atmospheric N_2 (160 mL/min) for 1 h. Then, the sample was thoroughly flushed under N_2 (160 mL/min) for 1 h to remove the external absorbed furfuryl alcohol. The sample was then heated to 420 ˚C (2 ˚C/min) for 1 h, to form a coke inside the zeolite cavity. The obtained sample was ascribed as 5MgO/KNaX(PB).

3.3.1.7 Synthesis of steaming treatment: 5MgO/KNaX(St)

The 5MgO/KNaX was treated under steam at 380 ˚C to test the stability. The procedure is listed as the following. Briefly, 0.3 g of 5MgO/KNaX was firstly calcined at 450 ˚C (2 ˚C/min) under air (30 mL/min) in the fixed-bed reactor for 1 h. After that, water was fed by a syringe pump (1 mL/min) at 380 ˚C under N_2 (160 mL/min) for 1 h. The obtained sample is denoted as 5MgO/KNaX(St).

3.4 Catalyst characterization

3.4.1 X-ray diffraction (XRD)

The structure and crystalline phase of the prepared catalyst can be determined by an X-ray diffractometer. The sample was prepared by packing material onto the sample holder. The analysis was done by employing Cu-K∝ radiation at 40 kV and 30 mA. The sample was scanned over the covering range of 2Θ = 5-75° with 1.20°/min, and a scanning rate of 1 s/step. X-ray diffraction pattern of the sample was compared with the X-ray diffraction pattern of standard catalyst for structure determination.

3.4.2 X-ray fluorescence (XRF)

X-ray fluorescence (XRF) is the issuing of characteristic "secondary" X-rays (or fluorescent) from a material that has been excited by bombarding with high-energy X-rays. The released energy is a characteristic radiation that tells the composition of the sample. This technique can be done according to the following procedure: approximately 0.5 g of the catalyst sample and 4.5 g of boric acid were weighed, then mixed together, and compressed into an alumina pan before bringing into the XRF sample holder in XRF instrument.

3.4.3 Scanning electron microscopy (SEM)

Scanning electron microscope (SEM) is a type of electron microscope that produces images of a sample by scanning the surface with a focused beam of electrons. The operating parameters for SEM used for imaging were 15 kV and magnification of about 40000x. In order to reveal the character of the surface, the sample was manually dispersed on a SEM stub and then coated with a gold thin film. After that, the sample was placed into a chamber. Then, the sample holder was adjusted, title and moved in the X, Y, and Z directions.

3.4.4 NH_3-temperature programmed desorption (NH_3-TPD)

The acid sites of the catalyst were identified using temperature-programmed desorption of ammonia (NH_3-TPD) measurement. Sample was preheated in the flow of air zero (30 mL/min) at 450˚C for 2 h and evacuated. After that, the sample was exposed in 20 kPa of 1%NH_3/He gas at 30˚C until saturation coverage was reached. Afterward, the sample was flushed with He at room temperature for 1 h, the temperature was then increased at a linear rate of 10˚C/min from 50 to 600˚C under vacuum.

3.4.5 CO_2-temperature programmed desorption (CO_2-TPD)

The basic sites of the catalyst were identified by CO_2-TPD measurement, using the same procedure as on the previous occasion described in NH_3-TPD.

3.4.6 Surface area analysis

The surface area of the catalysts can be determined by a nitrogen gas adsorption analyzer. The sample was prepared by weighing approximately 0.05 g of the sample and loaded into the sample cell, which was attached to the outgassing station equipped with a heating mantle. The temperature was raised to 300˚C during the outgassing process. After that, nitrogen gas was introduced to the sample cell where the adsorption isotherm can be measured in a pressure range of 10-6 to 1.0 P/P_0.

3.4.7 Solid^{27}Al magic angle spinning nuclear magnetic resonance spectra (^{27}Al MAS NMR)

Solid ^{27}Al magic angle spinning nuclear magnetic resonance spectra (^{27}Al MAS-NMR) were recorded using a JEOL Resonance JNM-ECZ400R spectrometer (400MHz). Roughly 100 mg of sample was loaded into the spinner. The spinning rate during the measurement was 10 KHz.

3.4.8 Extended X-ray absorption fine structure spectroscopy (EXAFS)

Extended X-ray absorption fine structure spectroscopy (EXAFS) was conducted at Beamline 8 of the Siam Photon Laboratory, Synchrotron Light Research Institute (SLRI), Thailand, with the electron beam energy of 1.2 GeV and beam current of 120-80 mA. ~10 mg of the sample was placed into the holder and placed in the experimental chamber. Spectra were recorded in transmission mode at room temperature for the Mg K-edges using Beryl (1010) crystals. Normalized spectra and data were processed with Athena software and analyzed by Artemis software.

3.4.9 Thermal gravimetric analysis (TGA)

. The carbon deposit was quantified by thermogravimetric analysis (TGA) on a Pyris 1 TGA (Perkin). Briefly, the sample (~10 mg) was heated from 50 to 900 ˚C with a heating rate of 10 ˚C/min under air (50 mL/min).

3.5 Catalytic activity testing

Ethanol conversion activity of the prepared catalysts was investigated in a continuous flow fixed-bed glass reactor (8.0 mm) at atmospheric pressure. The catalyst powders were pelletized and crushed to the desired size (850-600 μm). The catalyst was packed into a glass tube reactor and topped with glass wool and glass beads. The gas flow rate was controlled by a mass flow controller and checked by a bubble flow meter.

The schematic of the catalytic testing rig is shown in Figure 3.1. After that, the catalytic activity testing was carried out at 380°C under nitrogen flow (160 mL/min). Before the catalytic testing, the catalyst was activated at 450°C for 1 h (2°C/min heating rate) under 30 mL/min air zero flow. Ethanol was introduced into the reactor using a syringe pump at 1.0 mL/h. The catalytic testing was conducted for a total time on stream (TOS) of 8 h. The product steam was analyzed online through a gas chromatograph.

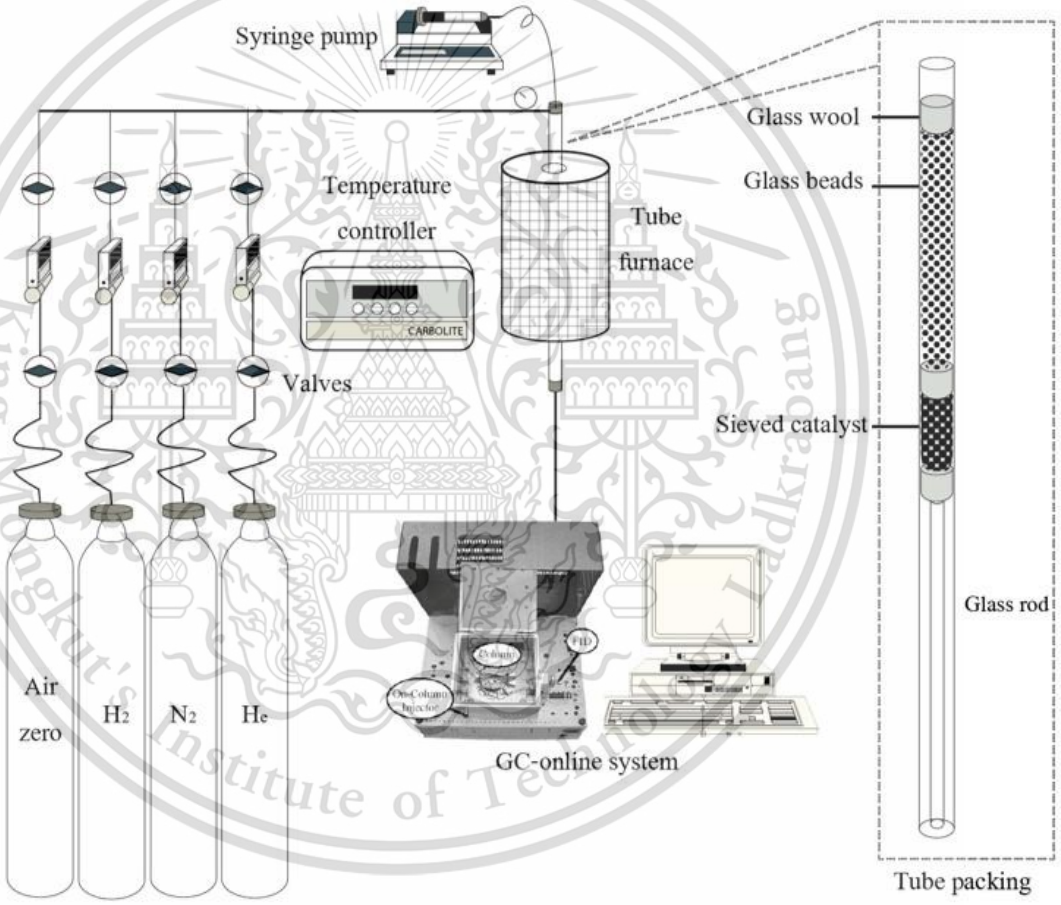

Figure 3.1 The schematic of the catalytic testing rig.

3.6 Products analysis

The product analysis was generally performed using an online gas chromatograph. The gas sample was collected in gas sampling loop, then periodically injected into GC column (Rt-Q-BOND columns) connected to flame ionized detectors (FID). The temperature of the injection port was set at 200°C, 35°C for column oven, and 250°C for FID detector. The GC temperature condition was started at 90°C, hold for 2 min, and then heated up to 250°C. Pressure of the carrier gas was fixed to 8.84 psi all time. Each component was separated as passed through the column with an inert N_2 carrier gas and their presence in the effluence were recorded as a chromatogram. Each peak area from the chromatogram was measured and calculated. Then each peak was determined by comparing with standard and the composition of each product was determined by calibration of standard.

Chapter 4

Results and Discussion

4.1 Catalyst characterization

The elemental composition of all samples is summarized in Table 4.1. After the ion exchange of NaX by 0.1 M K_2CO_3, a significant increase of K (12 wt.%) was observed for the KNaX sample, as compared to the parent NaX (Table 4.1, entry 1-2). While the amount of Na in the KNaX is decreased (from 12.3 to 4.6 wt.%). This indicates that the K^+ has replaced Na^+ in the NaX. Furthermore, the nominal positive/negative charge ratio ((Na^+ and K^+)/Al^{3+}) of KNaX is ~1, suggesting that the incorporation of K^+ is in the exchangeable sites of the zeolite X, similarly to those reported in the literature [63]. A slight decrease in the surface area (from 660 to 627 m^2/g, Table 4.1) was observed. This is presumably due to the incorporation of a larger cation, K^+ [63].

Table 4.1 Elemental composition and physical properties of the catalysts.

Entry	Catalyst	Concentration of [Mg^{2+}] for ion exchange (M)	S_{BET} (m^2/g) (Overall)	S_{BET} (m^2/g) (External Surface)	Pore volume (cc/g)	Elemental composition (wt.%)					(Na^+, K^+)/Al^{3+}	(Na^+, K^+, 2Mg^{2+})/Al^{3+}	MgO loading (wt.%)
						Si	Al	Na	K	Mg			
1	NaX	-	660	36	0.40	18.8	14.4	12.3	0.05	-	1.01	-	-
2	KNaX	-	627	57	0.40	17.5	12.8	4.6	12.0	-	1.07	-	-
3	4MgO/KNaX	0.10	617	87	0.45	16.3	12.0	2.2	14.7	2.65	1.06	1.56	4.4
4	5MgO/KNaX	0.30	539	83	0.39	15.9	11.2	1.1	16.0	3.01	1.10	1.71	5.0
5	6MgO/KNaX	0.50	518	64	0.29	15.6	11.2	0.6	17.3	3.60	1.13	1.86	6.0
6	7MgO/KNaX	0.60	402	48	0.28	16.0	11.9	0.8	16.0	3.92	1.01	1.75	6.5
7	8MgO/KNaX	1.00	306	116	0.24	15.2	11.1	0.4	19.7	4.97	1.27	2.28	8.3

Ion exchange of KNaX with 0.1 M $Mg(OAc)_2$ and subsequent washing with 0.1 M KOH yields a 4MgO/KNaX sample with 4.4 wt.% of MgO (Table 4.1, entry 3). The amount of Na^+ in this sample decreased further from 4.64 to 2.16 wt.%, whilst the K content

increased from 12 to 14.7 wt.%. The further incorporation of K^+ was due to the precipitation of Mg^{2+} in the exchangeable site with KOH rather than from the direct exchange of K^+ with Na^+. It is likely that, upon ion exchange of 0.1 M $Mg(OAc)_2$, Mg^{2+} could initially replace the remaining Na^+. However, such exchangeable Mg^{2+} was precipitated out as $Mg(OH)_2$ when washing with 0.1 M KOH (pH > 9) [64]. The similar concentration of KOH compared with [Mg^{2+}] is required to prevent reverse exchangeability of $Mg^{2+}$with K^+ or H_3O^+ during precipitation. Hence, the K^+ could be finally present as the countered ion of the negative framework charge, as deduced from a (Na^+, K^+)/Al^{3+} of ~1. Moreover, the nominal positive/negative charge ratio ((Na^+, K^+, $2Mg^{2+}$)/Al^{3+}) of the 4MgO/KNaX exceeds the theoretical value after calcination, emphasizing that the MgO could exist mainly as the extra-framework species.

As the $Mg(OAc)_2$ concentration used during the ion exchange increased from 0.1 to 1.0 M, the MgO loading increased from 4.4 to 8.3 wt.% (Table 4.1, entry 3-7). Consistently, the amount of Na^+ decreased from 2.2 to 0.4wt.% whilst the K^+ content increased from 14.7 to 19.7wt %. The nominal positive/negative charge ratio ((Na^+, K^+, $2Mg^{2+}$)/Al^{3+}) also increased from 1.56 to 2.28, indicating the presence of higher amount of extra-framework MgO species. Accordingly, the sample surface area decreased notably from 617 to 306 m^2/g for 4MgO/KNaX to 8MgO/KNaX. The two-fold decrease in surface area with only ~8 wt.% MgO loading also suggests that the extra-framework MgO species was occluded within the zeolite cavities. In line with this view, a significant drop in pore volume was evidenced for all MgO incorporated samples.

According to the XRD diffraction patterns, the faujasite zeolite characteristic diffraction peaks remained after catalyst preparation, with a slight decrease in crystallinity (~10%) after K^+ ion exchange (Figure 4.1, a-b). The crystalline sizes of NaX and KNaX are similar (~108 nm). The slight decrease in the intensity (10%) of KNaX could be attributed to the X-ray absorption by a heavier atomic weight, K^+. After MgO incorporation (in KNaX), the faujasite characteristics were still observed with a similar crystalline size (~105 nm) for all samples (Figure 4.1, c-g).

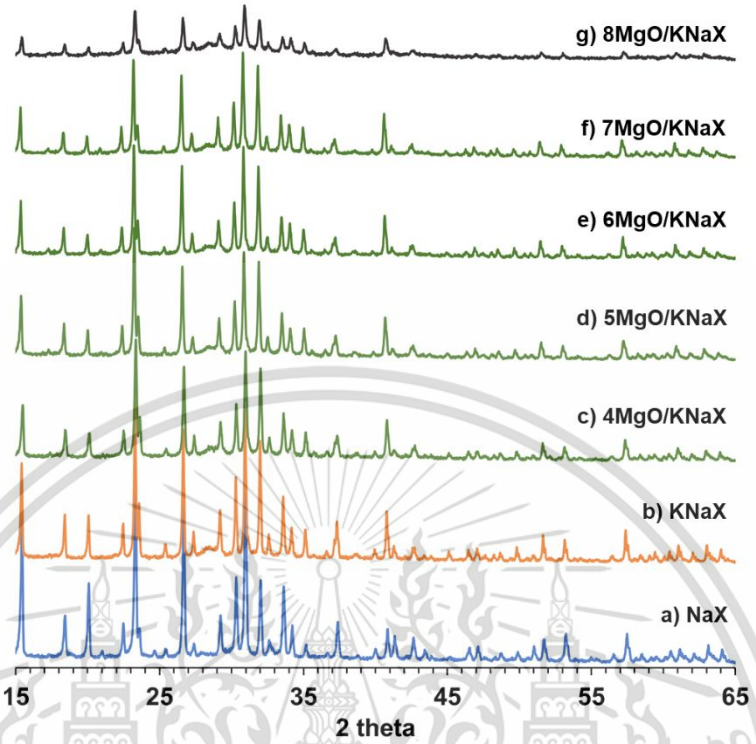

Figure 4.1 XRD pattern of all catalysts.

However, no MgO crystalline peak was detected. This could suggest that the incorporated MgO could be present as (i) occluded salt in zeolite cavities or (ii) highly dispersed MgO particles on the external surface. Although the XRD intensity of the MgO incorporated samples decreases, as compared to KNaX, these samples exhibit relatively the same intensity (~60%, for 4-7MgO/KNaX, Figure 4.2). Such decrease in the intensity could mainly derive from the perturbation of the occluded MgO species without the deconstruction of zeolite [65]. This is evidenced by ^{27}Al MAS-NMR showing only tetrahedral Al species (~66 ppm) for these samples (Figure 4.3). It is worth noting that a slight shift to a higher field of Al peak in the MgO/KNaX samples is detected compared with KNaX. This could be attributed to the shielding effect of the occluded salt [66], which again supports the co-existing of the extra-framework MgO and the framework Al. In support manner,

Ricchiardi, *et al.* have proposed that a highly solvated Mg cation cluster can exist as $[Mg(OH)_4]^{4+}$cluster within the sodalite and supercage cage of the faujasite framework [30].

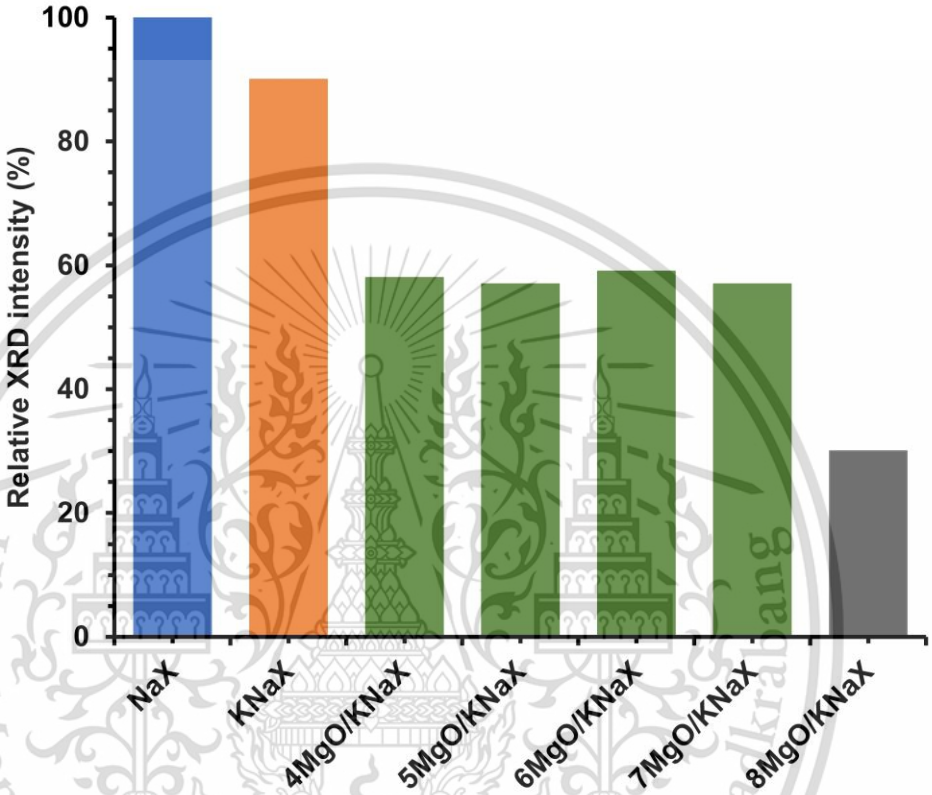

Figure 4.2 Relative XRD intensity of all catalysts using 2Θ at 6.10˚.

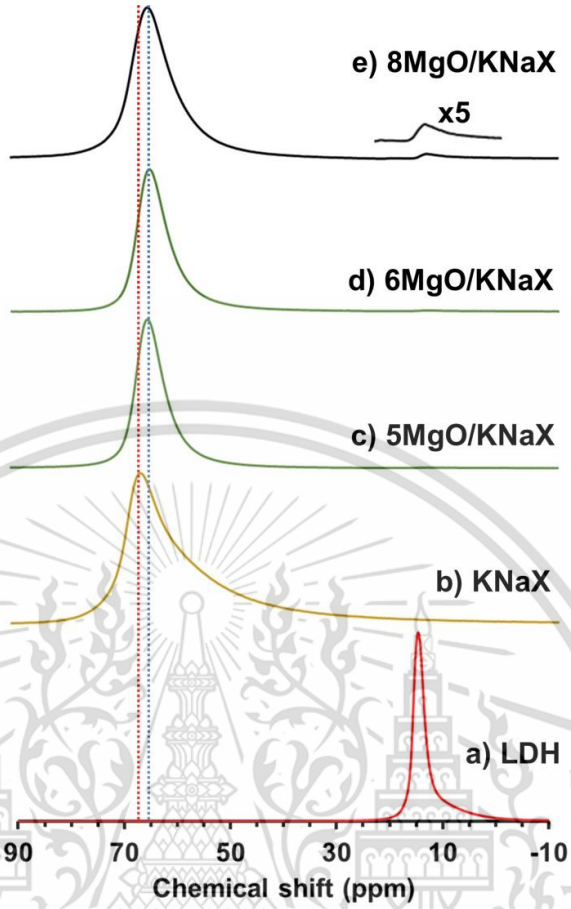

Figure 4.3 ^{27}Al MAS NMR spectra of samples.

In addition to the occluded $[Mg_4(OH)_4]^{4+}$clusters, highly dispersed MgO particles were evidenced on the external surface as well, particularly at high MgO loadings (Figure 4.4). As compared to the octahedral crystals with flat faces of NaX and KNaX, the rough external surfaces were observed without change in crystallite size (~6.5-7.0 μm, Figure 4.5). These petal-like nanostructures could be the anisotropic brucite structure of $Mg(OH)_2$ or MgO [67] as implied by the surface Mg composition of 5MgO/KNaX shown in Figure 4.6. As the concentration increased from 0.1 to 0.6 M $[Mg^{2+}]$, a higher amount of MgO nanopetals were decorated over the zeolite external surfaces. Excessive loading of these species could decrease the external surface, as evidenced by 4MgO/KNaX to 7MgO/KNaX, which could be presumably due to agglomeration of MgO nanopetals (into MgO aggregates).

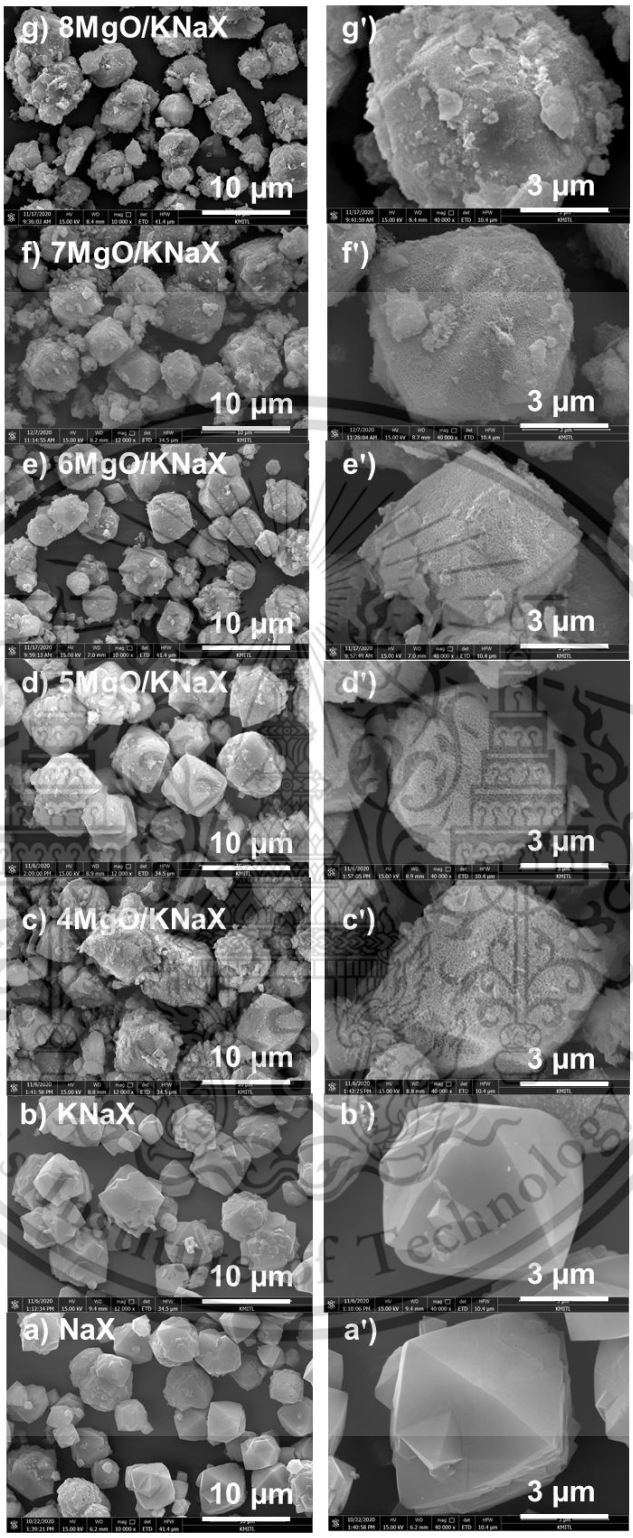

Figure 4.4 SEM images of (a, a') NaX, (b, b') KNaX, (c, c') 4MgO/KNaX, (d, d') 5MgO/KNaX, (e, e') 6MgO/KNaX, (f, f') 7MgO/KNaX and (g, g') 8MgO/KNaX.

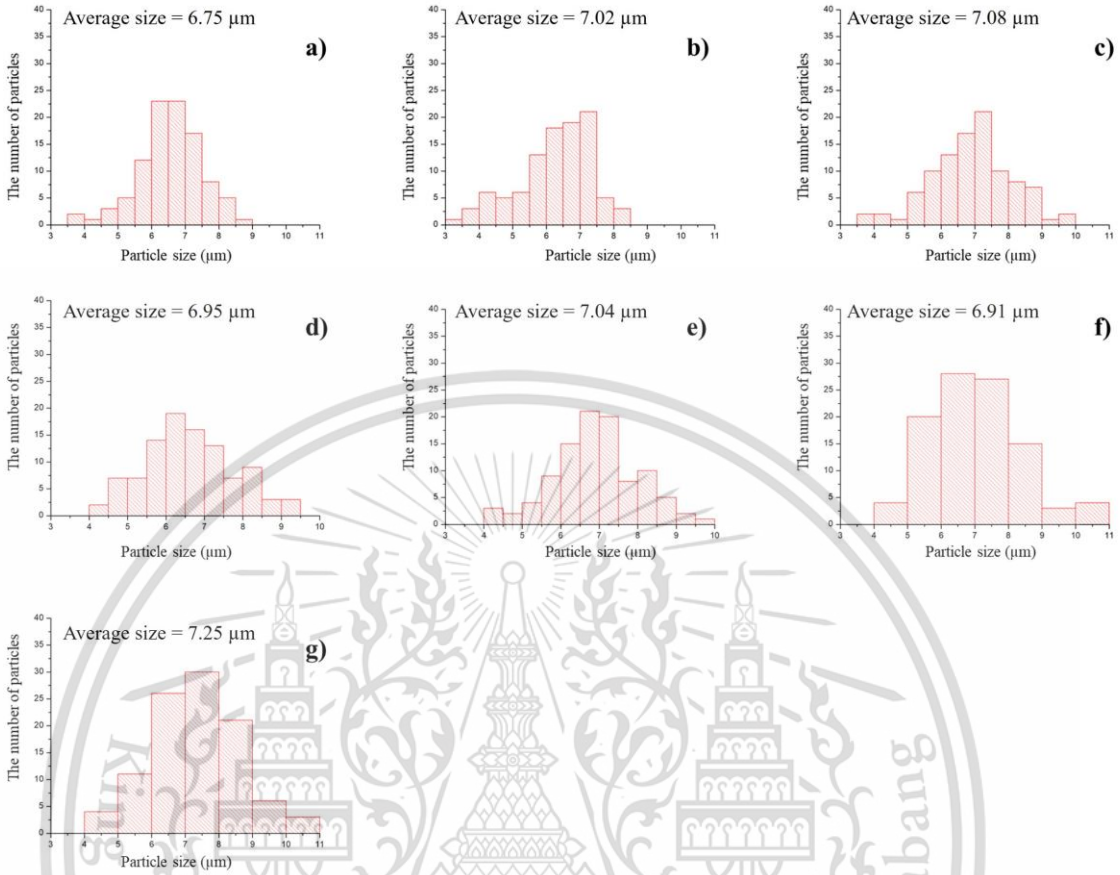

Figure 4.5 Particle size of a) NaX, b) KNaX, c) 4MgO/KNaX, d) 5MgO/KNaX, e) 6MgO/KNaX, f) 7MgO/KNaX and g) 8MgO/KNaX.

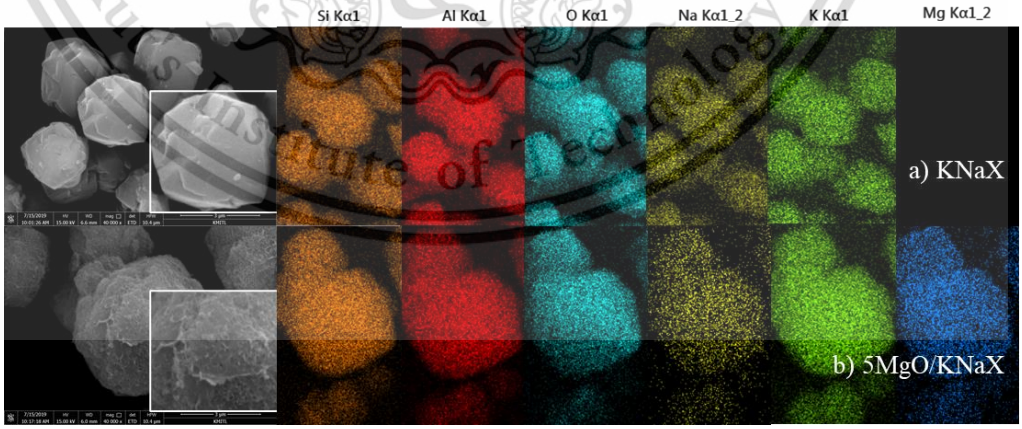

Figure 4.6 SEM images and elemental dispersion of a) KNaX and b) 5MgO/KNaX

Figure 4.4 also showed the agglomeration of MgO nanopetals on MgO/KNaX surface, for example on 8MgO/KNaX in Figure 3g. This could presumably be the MgO aggregate and/or the fragment of the destructed zeolite X at high MgO loadings. The finding is in line with the observed low XRD intensity (~29%) of 8MgO/KNaX, as compared to others (Figure 4.1-4.2). Additionally, destruction of zeolite structure was also evidenced by the additional signal at 15 ppm of the octahedral Al species in the ^{27}Al MAS-NMR spectrum (Figure 4.3e). The presence of the species suggests the leaching of framework Al from the zeolite, presumably due to the use of the exceedingly high concentration of $Mg(OAc)_2$ (1.0 M) during ion exchange, which resulted in the hydrolysis of the framework Al under the condition used. Destruction of zeolite was also supported by the significant decrease in the specific surface area of the samples, that is, 306 m^2/g for 8MgO/KNaX vs. 617 m^2/g for 4MgO/KNaX.

Incorporation of K^+ and Mg^{2+} modified the acid-base properties of the catalysts significantly, as shown by the NH_3- and CO_2-TPD profiles in Figure 4.7. The acidity (NH_3 μmol/g) and basicity (CO_2 μmol/g) calibrated with standard gas were tabulated in Table 4.2. The weak acid sites are referred to NH_3 adsorbed on the Lewis acid cations, *i.e.*, Na^+ or K^+, at external surface and those in the zeolite cavities (supercages and sodalite cages). The weak acid site at ~136˚C is more pronounced for NaX (Figure 4.7a) but disappeared when K was incorporated. More NH_3 desorbed from KNaX, as compared to NaX, particularly from sodalite cage (~220 ˚C) and double-6 ring (~260 ˚C) of the zeolite X. As Na^+ was exchanged by a larger K^+, the exchangeable site in those cages become more restricted. Therefore, the exchanged K^+ tends to occupy the supercage, leaving the small cages available for NH_3 adsorption.

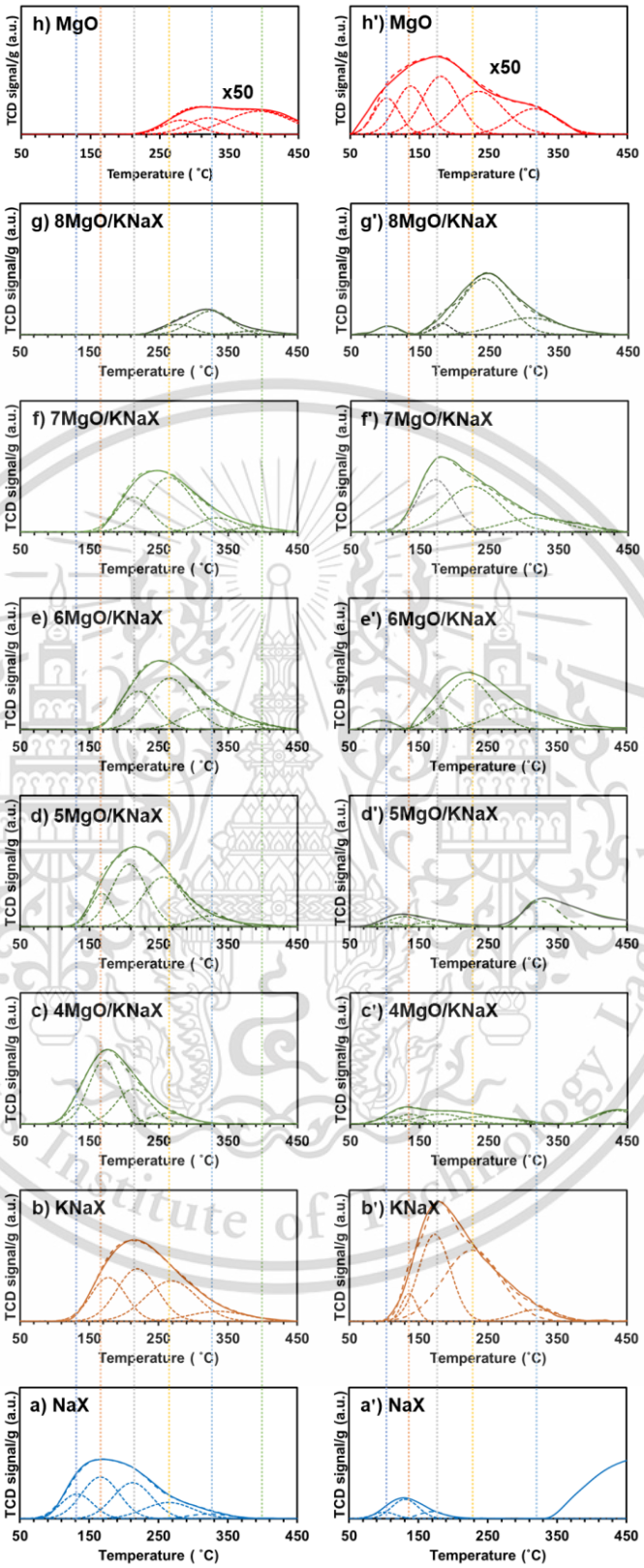

Figure 4.7 NH_3-TPD profiles (a-h) and CO_2-TPD profiles (a'-h') of all samples.

The weak basic sites are referred to physiosorbed CO_2 on the external surface (<150 ˚C) and those within the zeolite cavities (150-250˚C). The sharp increase in the basicity of KNaX (24.2 μmol/g), as compared to that of NaX (~2.7 μmol/g, Table 4.2) was observed, particularly with the new medium basic site at ~236 and 320 ˚C (Figure 4.7b). This is derived from the Lewis basic site at the negative framework charge, countered by a more polarizable K^+.

Table 4.2 Acidity and Basicity of all samples.

Entry	Catalysts	Acidity (μmol/g)							Basicity (μmol/g)					
		W_a1 (136 ˚C)	W_a2 (170 ˚C)	W_a3 (220 ˚C)	M_a1 (260 ˚C)	M_a2 (320 ˚C)	S_a1 (400 ˚C)	Total	W_b1 (100 ˚C)	W_b2 (130 ˚C)	W_b3 (176 ˚C)	W_b4 (236 ˚C)	M_b1 (320 ˚C)	Total
1	NaX	59	116	104	59	15	-	353	0.5	1.6	0.6	-	-	2.7
2	KNaX	-	114	160	156	43	-	473	-	1.3	8.6	12.7	1.6	24.2
3	4MgO/KNaX	33	148	92	30	-	-	303	0.6	0.8	1.5	1.3	0.1	4.3
4	5MgO/KNaX	-	50	140	135	27	-	352	0.3	1.1	0.6	0.2	2.8	5.0
5	6MgO/KNaX	-	-	104	167	77	13	361	0.7	-	0.2	7.7	4.0	12.6
6	7MgO/KNaX	-	-	87	186	39	13	325	-	-	6.6	8.8	3.0	18.4
7	8MgO/KNaX	-	-	-	23	70	11	93	0.5	-	0.6	7.8	2.9	11.8
8	MgO	-	-	-	0.4	0.6	1.2	2.2	0.06	0.09	0.13	0.13	0.07	0.48

W_a: Weak acid site, M_a: Medium acid site, S_a: Strong acid site, W_b: Weak basic site, M_b: Medium basic site

When 4.4wt.% MgO was incorporated, a significant decrease in the basicity (4.3 μmol/g) was observed for 4MgO/KNaX compared with its parent (24.2 μmol/g). It is possible that the extra-framework MgO species, formed by the precipitation of $Mg(OH)_2$ upon washing with 0.1 M KOH, could occupy inside the pore as occluded $[Mg(OH)_4]^{4+}$ clusters, as discussed earlier [30]. The presence of the $[Mg(OH)_4]^{4+}$ clusters also causes the decrease in NH_3 desorption of the 4MgO/KNaX (Table 4.2, Figure 4.7c). The observed weak

acid sites in 4MgO/KNaX could be attributed to some of the remaining exchangeable Mg^{2+} species, as typically observed in the literature [68]. Since a relatively low concentration of KOH was used in this sample, the Mg^{2+} in 4MgO/KNaX might not be entirely precipitated into $Mg(OH)_2$.

As MgO content increased from 4.4 wt.% to 6.5 wt.%, basicity of 7MgO/KNaX was enhanced to 18.2 μmol/g (Table 4.2, entry 3-6), particularly the medium basic site at 320 ˚C (Figure 4.7c'-f'). The rise of medium basic sites could be attributed to the presence of a higher amount of (i) the nanopetals as observed by SEM and (ii) the occluded $[Mg_4(OH)_4]^{4+}$ clusters. Ricchiardi, *et al*. also proved that the occluded $[Mg_4(OH)_4]^{4+}$ clusters are highly basic, interacting strongly with CO_2 [30, 69], supporting the findings in the current work. In addition, the observed increase in medium basic site with MgO content, may be derived from the increase in the softer exchangeable K^+ cation (Table 4.1). Such highly polarizable K^+ weakly interacts with the negative framework charge, leading to a higher electron density of the framework oxygen. This would generally result in higher basicity of the zeolite catalysts.

Furthermore, an increase in MgO loading also caused the increase in the medium acid sites (30 to 186 μmol/g, Table 4.2, entry 3-6) and a slight increase in the strong acid for the samples with >5 wt.% MgO loadings. The medium acid sites could be attributed to that the occluded $[Mg_4(OH)_4]^{4+}$ clusters that interact with NH_3 through hydrogen bonding [30]. While the acid sites could be attributed to the Mg^{2+} defect site of MgO aggregates [70]. In short summary, the occluded $[Mg_4(OH)_4]^{4+}$ clusters particularly provide both medium acid and medium basic sites.

It is worth noting that weak acid sites (~136 ˚C) due to the exchangeable cations cannot be found in the samples with MgO loading higher than 4.4wt.%. Further increase in MgO loadings to 8.3wt.% led to the decrease in both basic and acid sites, especially the medium acid site at 260 ˚C (Figure 4.7g, g'). This could result from the partial collapse of the framework, as discussed earlier, leading to the reduced number of occluded

$[Mg_4(OH)_4]^{4+}$ clusters. The observed basicity could be derived from the nanopetels and MgO aggregates on the external surface of the 8MgO/KNaX sample.

The existence of the occluded $[Mg(OH)_4]^{4+}$ clusters can be supported by Mg K-edge EXAFS spectra. It can be seen from Figure 4.8 that 6MgO/KNaX exhibits a relatively shorter Mg-O radial distance (1.63 Å), as compared to bulk MgO (1.66 Å). Similarly, their radial distance of the second coordination shell, presumably (Mg-Mg and/or Mg-Al), is shorter (2.64 vs. 2.67 Å, see Figure 4.8). This could be attributed to the presence of electropositive $[Mg(OH)_4]^{4+}$ clusters possessing a relatively lower electron density. Accordingly, the stronger interaction between Mg^{2+} and OH^- in this cation cluster would be expected, as compared to the bulk MgO. The shorter Mg-O radial distance was also observed for all samples with ≤6.5 wt.% MgO (see Figure 4.9). In a similar trend, the MgKNaX containing only the exchangeable Mg^{2+} (Table 4.3) shows an even shorter radial distance for both coordination shells (1.55, 2.60 Å, Figure 4.8). However, 8MgO/KNaX shows a similar Mg-O scattering (1.66 Å) as the bulk MgO. This emphasizes the increase in MgO nanopetals and/or MgO aggregates at the external surface at 8.3wt.% MgO loading, as discussed earlier.

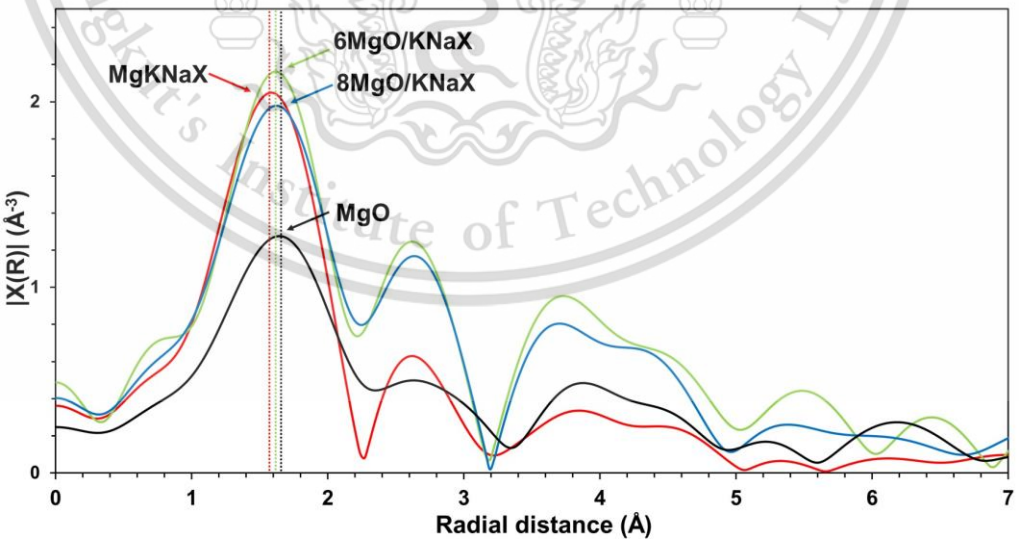

Figure 4.8 Magnitudes of k-weighted Fourier-transformed Mg K-edge EXAFS spectra of MgKNaX, 6MgO/KNaX, 8MgO/KNaX and MgO.

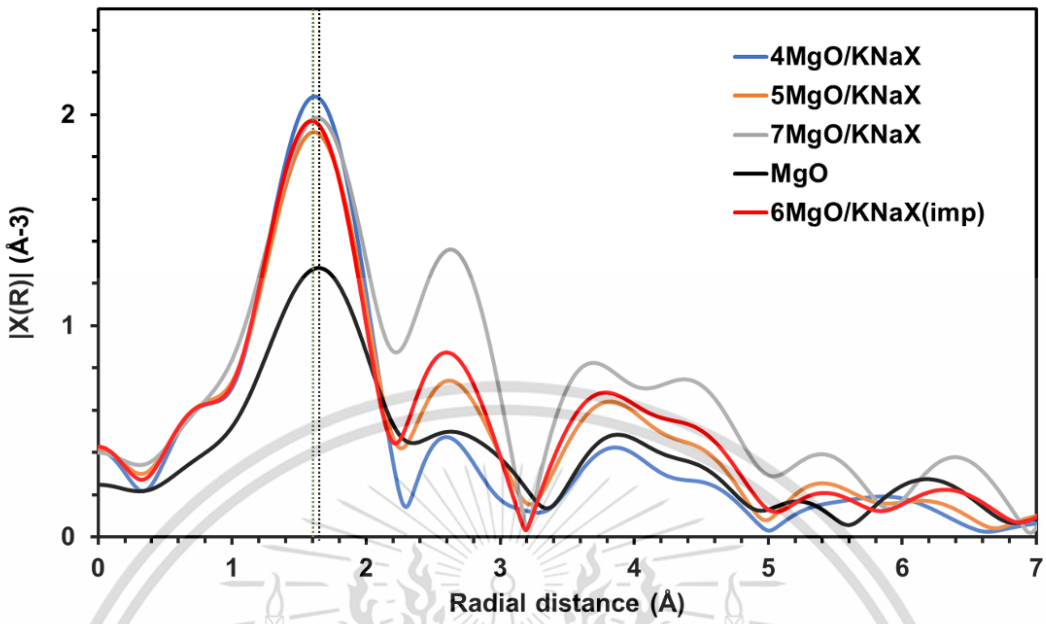

Figure 4.9 Magnitudes of k-weighted Fourier-transformed Mg K-edge EXAFS spectra of 4MgO/KNaX, 5MgO/KNaX, 7MgO/KNaX, MgO and 6MgO/KNaX(imp).

Table 4.3 Elemental composition and physical properties of the samples.

Entry	Catalyst	S_{BET} (m^2/g) (Overall)	S_{BET} (m^2/g) (External Surface)	Pore volume (cc/g)	Elemental composition (wt.%)					$(Na^+, K^+)/Al^{3+}$	$(Na^+, K^+, 2Mg^{2+})/Al^{3+}$	MgO loading (wt.%)
					Si	Al	Na	K	Mg			
1	MgKNaX	575	43	0.35	18.1	13.0	3.3	11.0	1.20	0.88	1.10	2.0
2	6MgO/KNaX(Imp)	390	37	0.25	17.2	12.6	4.85	11.2	3.70	1.07	1.73	6.1
3	5MgO/KNaX(PB)	26	26	0.01	-	-	-	-	-	-	-	-
4	5MgO/KNaX(St)	454	83	0.36	-	-	-	-	-	-	-	-

Imp – Impregnation, PB – Pore Blockage by treating with furfuryl alcohol at 420 ℃ and St – Steam treatment at 380 ℃

To get more details from the second coordination shell of the occluded $[Mg_4(OH)_4]^{4+}$ clusters, the wavelet transform function of k^2-weighted EXAFS was applied using HAMA software. The contour plot presenting the relation between wavenumber

space (k-space) and radial space (R-space) is shown in Figure 4.10. The 6MgO/KNaX and 8MgO/KNaX show two main features associated with the second coordination shell with wavelet coordinates {R-space, K-space} at {1.5-1.7Å, 4.0-5.0 $Å^{-1}$} and {1.5-1.7Å, 6.0-7.0 $Å^{-1}$}. These two features cannot be observed in the sample with exchangeable Mg^{2+} cation (MgKNaX, Figure 4.10a). Interestingly, the wavelet coordinate at {1.5-1.7Å, 4.0-5.0 $Å^{-1}$} was only observed in the samples with occluded $[Mg_4(OH)_4]^{4+}$ clusters (Figure 4.10b and c). While the wavelet coordinate at {1.5-1.7Å, 6.0-7.0 $Å^{-1}$} resembles that of bulk MgO (Figure 4.10d). Since the difference in k value for the observed backscattering amplitudes (values of *k*) would depend on the number of the nuclei in the second coordination shell of Mg, the wavelet coordinate at {1.5-1.7Å, 4.0-5.0 $Å^{-1}$} would represent the smaller MgO cluster, as compared to that at {1.5-1.7Å, 6.0-7.0 $Å^{-1}$}. Accordingly, it is reasonable to postulate that the first wavelet coordinate at {1.5-1.7Å, 4.0-5.0 $Å^{-1}$} could be attributed to the smaller cluster of occluded $[Mg_4(OH)_4]^{4+}$species. While the wavelet coordinate at {1.5-1.7Å, 4.0-5.0 $Å^{-1}$} could correspond to the larger clusters of MgO nanopetals and MgO aggregates on the external surface of all samples (Figure 4.8-4.10).

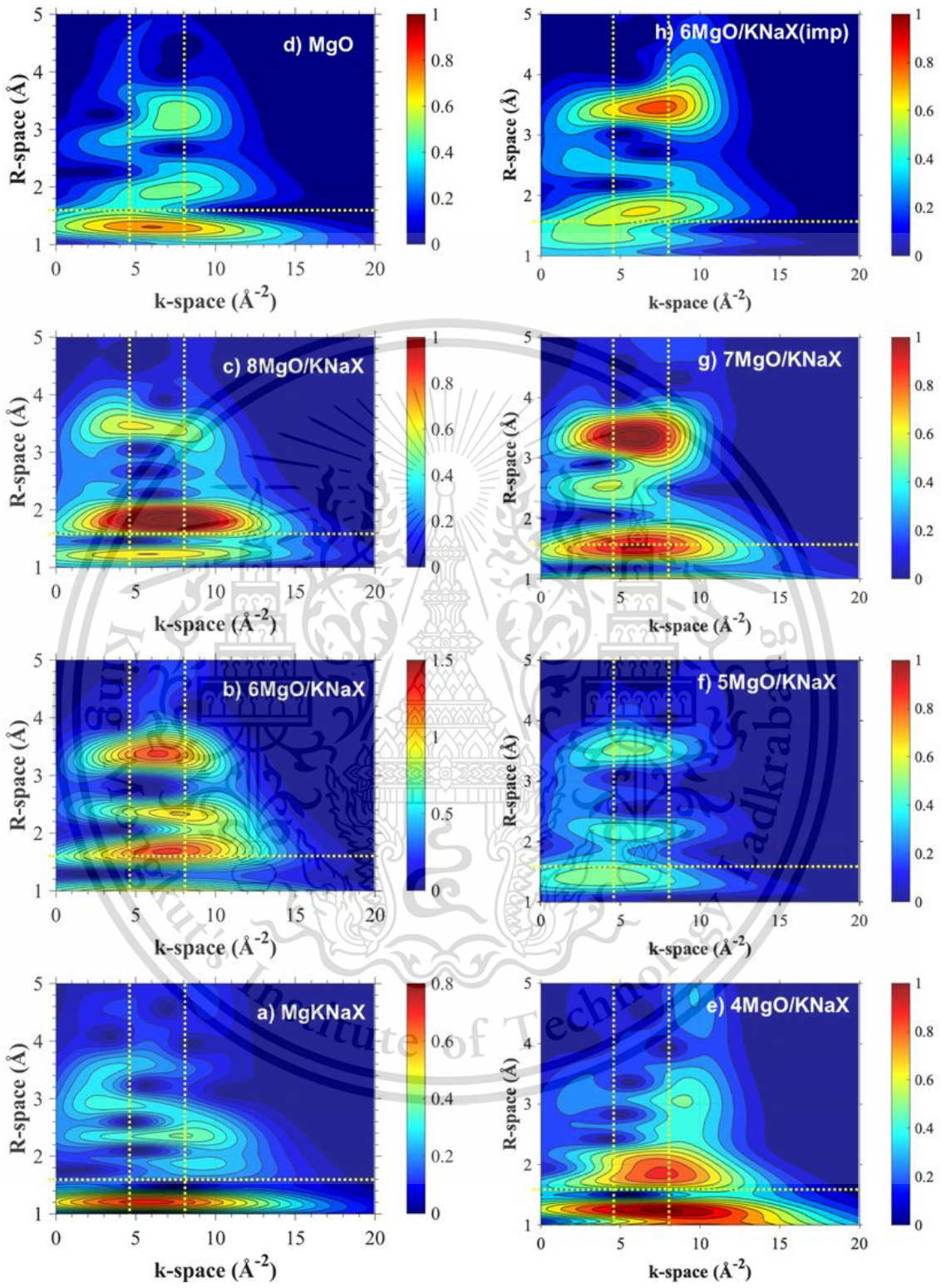

Figure 4.10 Wavelet transform of k^2-weighted Mg K-edge EXAFS spectra of catalysts.

4.2 Effect of the MgO loading over KNaX

Ethanol conversion over 6MgO/KNaX in a continuous flow gas-phase reactor at 380 ˚C produced C_4-C_8 products, with ~75% selectivity (~9.8% yield, as shown in Figure 4.11 and Table 4.4). Amongst these, higher alcohols, including C_4-/C_6-/C_8-alcohols, were identified as the major products (~55% selectivity), whilst acetaldehyde (~16%) and C_4-aldehyde (~7.7%) were detected as well. A much lower conversion of about 7% and yield of higher alcohols (~3.3 %in total) were obtained over the catalyst without occluded $[Mg_4(OH)_4]^{4+}$ clusters, KNaX (Table 4.4, entry 2). As the exchangeable K^+ was also increased in 6MgO/KNaX, the findings emphasize the key role of the occluded $[Mg_4(OH)_4]^{4+}$ clusters within the basic framework of KNaX, that promoted the Guerbet reaction of primary alcohol. It is worth noting that, under this reaction conditions, no ethanol conversion was observed thermally without catalyst.

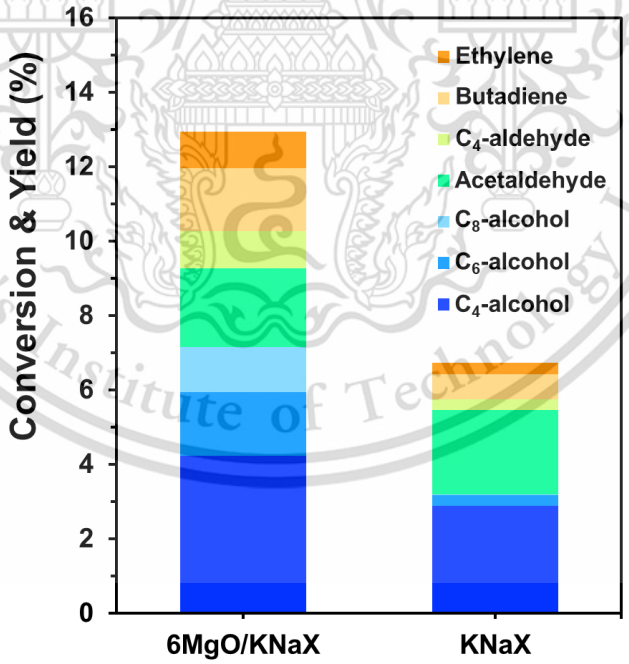

Figure 4.11 The ethanol conversion over 6MgO/KNaX and KNaX in a continuous flow gas-phase reactor (Reaction condition; temperature: 380 ˚C, EtOH feed rate: 1 mL/h, pressure: 1 atm, contact time: 16 g.h/mol, flow rate of N_2 carrier gas: 160 mL/min)

Table 4.4 Guerbet reaction over MgO/KNaX catalysts.

Entry	Catalysts	MgO (wt.%)	Conversion (%)	Yield (%)								
				Ethylene	Acetaldehyde	Butadiene	Diethyl ether	C_4-aldehyde	C_4-alcohol	C_6-alcohol	C_8-alcohol	Total higher alcohols
1	6MgO/KNaX	6.0	13.0	1.0	2.1	1.7	-	1.0	4.2	1.7	1.2	7.1
2	KNaX	-	7.0	0.3	2.3	0.7	-	0.3	2.9	0.3	0.1	3.3
3	NaX	-	36.0	32.0	-	-	4.0	-	-	-	-	-
4	MgKNaX	2.0	20.0	17.0	0.5	-	2.5	-	-	-	-	-
5	4MgO/KNaX	4.4	10.0	2.5	1.6	1.5	-	0.7	2.1	1.2	0.3	3.6
6	5MgO/KNaX	5.0	11.4	1.4	2.0	1.4	-	0.9	3.2	1.7	1.0	5.9
7	7MgO/KNaX	6.5	11.2	0.7	2.1	1.6	-	0.8	4.0	1.3	0.7	6.0
8	8MgO/KNaX	8.3	6.1	0.9	2.2	0.9	-	0.3	1.6	0.04	0.07	1.7
9	6MgO/KNaX(Imp)	6.1	9.4	0.6	2.8	0.9	-	0.5	3.4	0.2	0.9	4.5
10	5MgO/KNaX(PB)	5.0	2.7	0.8	1.3	0.1	-	-	0.6	-	-	0.6
11	5MgO/KNaX(St)	5.0	11.0	1.0	2.0	1.4	-	0.7	3.8	1.6	0.4	5.8

(Reaction condition; temperature: 380°C, EtOH feed rate: 1 mL/h, pressure: 1 atm, contact time: 16 g.h/mol, flow rate of N_2 carrier gas: 160 mL/min) Imp – Impregnation, PB – Pore Blockage by treating with furfuryl alcohol at 420 °C and St – Steam treatment at 380 °C

Dehydrogenation of ethanol can be activated by Lewis acid-base sites of the occluded $[Mg_4(OH)_4]^{4+}$ clusters to produce acetaldehyde as the intermediate (Scheme 1) [69, 71-75]. The basic site, derived from OH moiety of the clusters as discussed previously (Figure 4. 7), could also promote aldol condensation within the highly polarizable framework of the zeolites (KNaX) to produce higher aldehydes, i.e., crotonaldehyde [29, 7 6 -7 9]. In presence of Lewis acid sites, *i.e.*, Mg^{2+}, and the confinement within the highly polarizable micropores of the zeolite, H-transfer from the feed to the coupling products (higher aldehydes) can be facilitated to yield higher alcohols [8 0 -8 2]. However, dehydration of ethanol and crotyl alcohol can be competitively promoted over the acid sites, which produce unsaturated products, such as ethylene and butadiene (Scheme 1) [83-88].

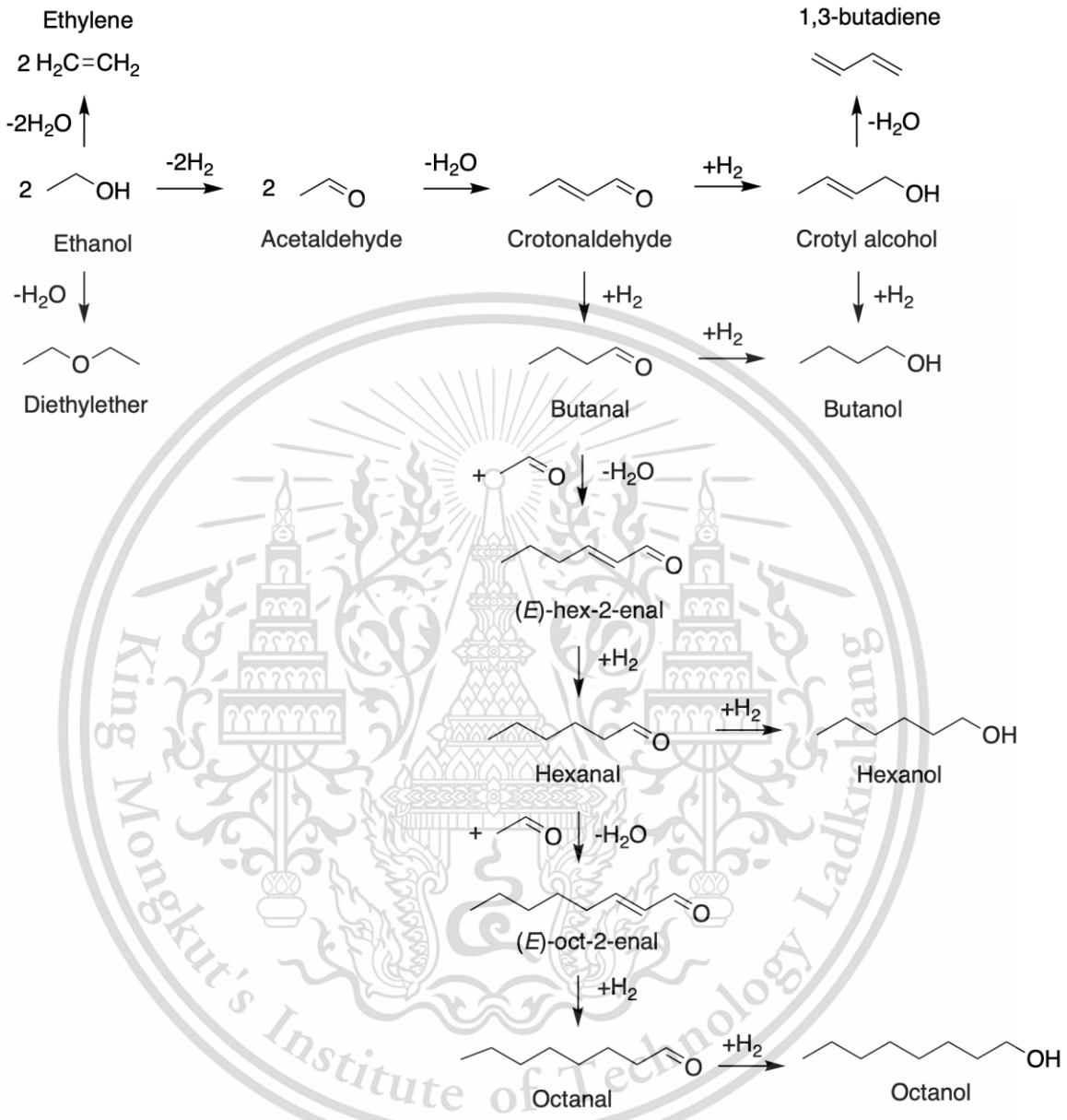

Scheme 4.1 Proposed reaction mechanism of ethanol conversion.

The ratio of the medium basic site (M_b) and medium acid site (M_a) of the catalysts seems crucial for the Guerbet reaction to produce higher alcohols. It can be seen from Figure 4.12 that without the medium basic site, higher alcohols could not be formed. Ethylene and diethyl ether were the only products for the catalysis over NaX and MgKNaX,

as shown in Table 4.4, entry 3-4. A linear relationship between the M_b/M_a and total higher alcohols was established, which prove the important effect of the basic site on dehydrogenation and condensation activity of the catalyst, particularly that from the occluded $[Mg_4(OH)_4]^{4+}$ species within the K^+ containing framework.

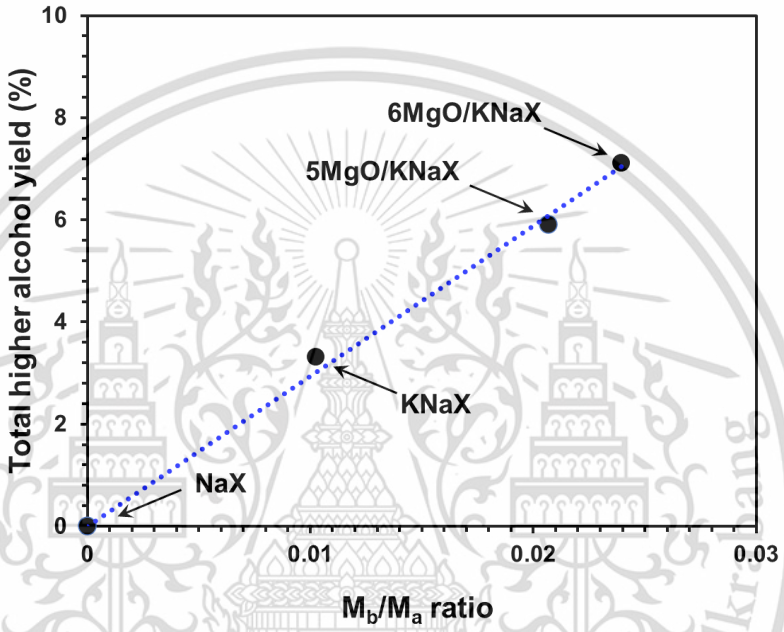

Figure 4.12 The relationship between M_b/M_a ratio and total higher alcohol yield. (M_b is medium base deriving from CO_2-TPD at 320 °C, and M_a is the medium acidity deriving NH_3-TPD at 260 °C)

As shown in Table 4.4 and Figure 4.13, the ethanol conversion and yield of higher alcohols follow the ratio of M_b/M_a with an increase of MgO loading. As the $[Mg_4(OH)_4]^{4+}$ clusters increase from 4MgO/KNaX to 6MgO/KNaX, the basicity derived from the -OH of this cationic cluster could be readily pronounced [20]. However, the rise in medium acidity from the hydrogen bonding of this -OH becomes less pronounced because the cluster is highly solvated and stabilized inside the zeolite cavities with polarizable K^+ cations [30].

Hence, some of the -OH moieties could already interact with the oxygen frameworks via H-bonding. Accordingly, the higher M_b/M_a ratio is enhanced upon the increase in the MgO and K content. The dehydrogenation and condensation are thus promoted, leading to the increased yield of higher alcohols, whilst the yield of ethylene from ethanol dehydration was decreased, as shown in Table 4.4.

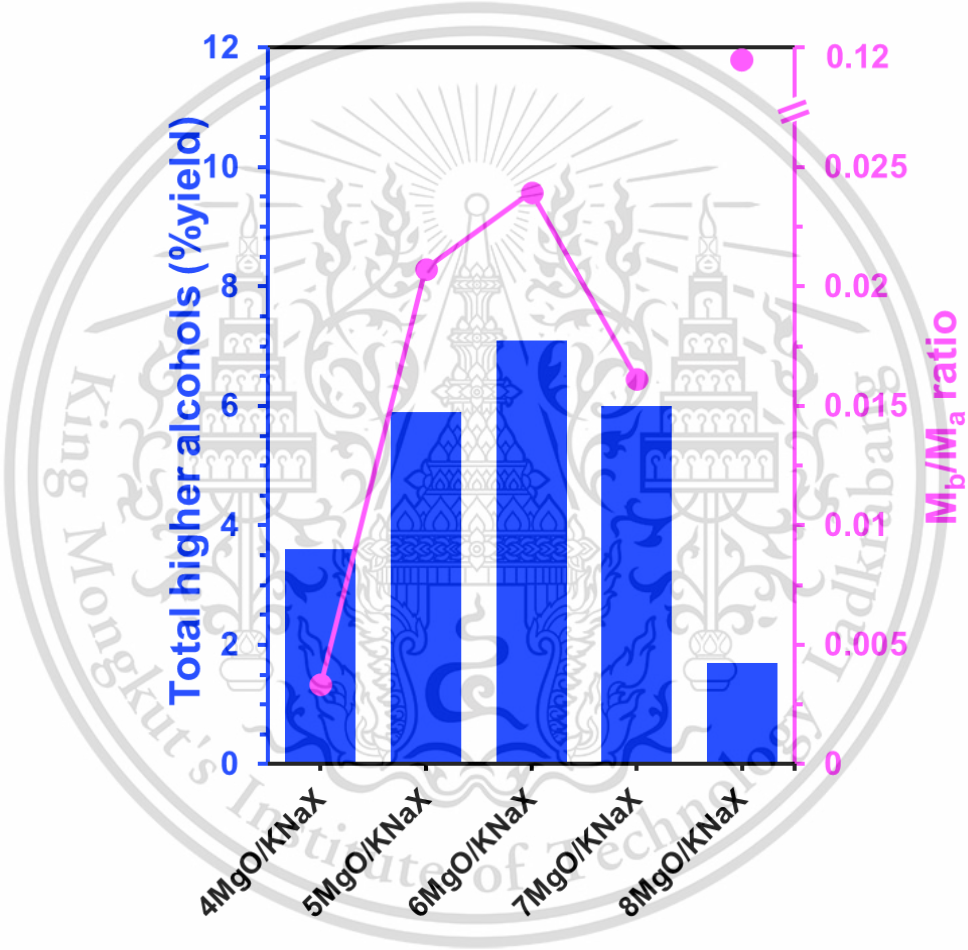

Figure 4.13 The corelation between the higher alcohol yields and the M_b/M_a ratio of the MgO/KNaX catalysts.

A further increase in MgO loading to 6.5wt.% (7MgO/KNaX) led to a decrease in the occluded $[Mg_4(OH)_4]^{4+}$ clusters and an increase in the MgO nanopetals, which hence

resulted in a decrease in the medium basic site and an increase in the medium acid site, respectively. Accordingly, a lower M_b/M_a ratio was obtained, causing a lower yield of higher alcohols. However, 8MgO/KNaX with a very high M_b/M_a ratio of 0.12 provided even lower yields of higher alcohols. Since the high basicity of 8MgO/KNaX is derived from the higher amount of MgO nanopetals and MgO aggregates on the external surface, as evidenced by SEM (Figure 4.4f-g) and EXAFS (Figure 4.8), the observed lower yields of higher alcohols suggest that incorporation of MgO at the external surface of the support is less active as compared with the occluded species.

Comparing at the similar 6 wt.% MgO loading, the impregnated catalyst (6MgO/KNaX(Imp)) showed a lower activity providing a lower yield of higher alcohols (Table 4.4, entries 1 and 9). This could be again derived from the high amount of the less active MgO aggregates and the low amount of the occluded $[Mg_4(OH)_4]^{4+}$ clusters in 6MgO/KNaX(Imp). The existence of MgO aggregates in the impregnated sample is evidenced by the EXAFS spectra, where the Mg-O radial distance of 6MgO/KNaX(Imp) is similar to that of the bulk MgO (Figure 4.9). During the impregnation, the incorporated $Mg(OAc)_2$ could be promptly precipitated on the basic surface of KNaX (as seen in the CO_2-TPD, Figure 4.7b´). In addition, the external surface area of 6MgO/KNaX(Imp) decreases by half (Table 4.3) compared with that of the ion exchange sample (6MgO/KNaX), whilst their crystallinity was maintained (Figure 4.14). Such external MgO nanopetals and MgO aggregates on 6MgO/KNaX(imp) also caused a significant decrease in NH_3 and CO_2 desorption signals, as shown in Figure 4.15 and Table 4.5.

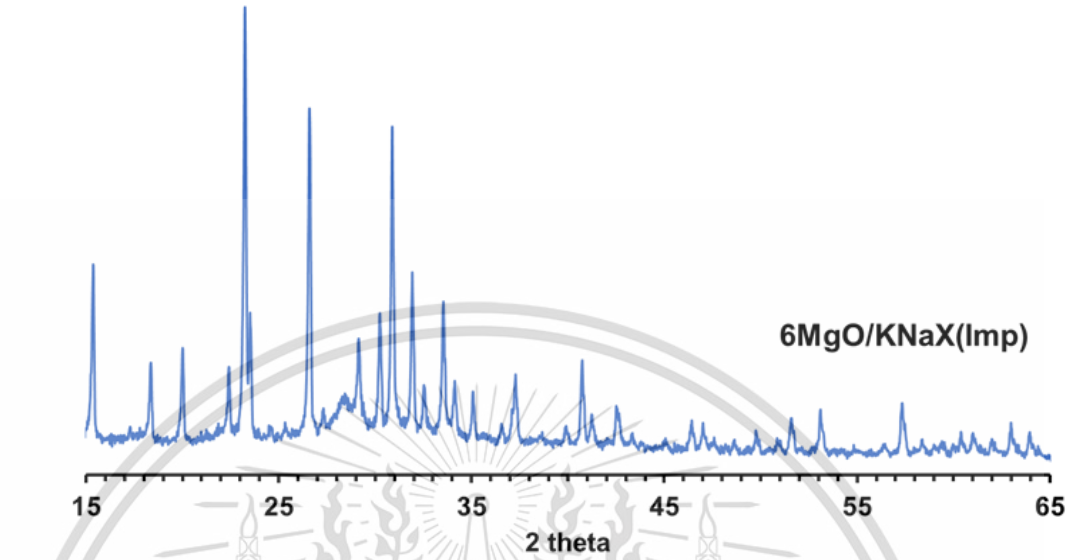

Figure 4.14 XRD pattern of 6MgO/KNaX(Imp).

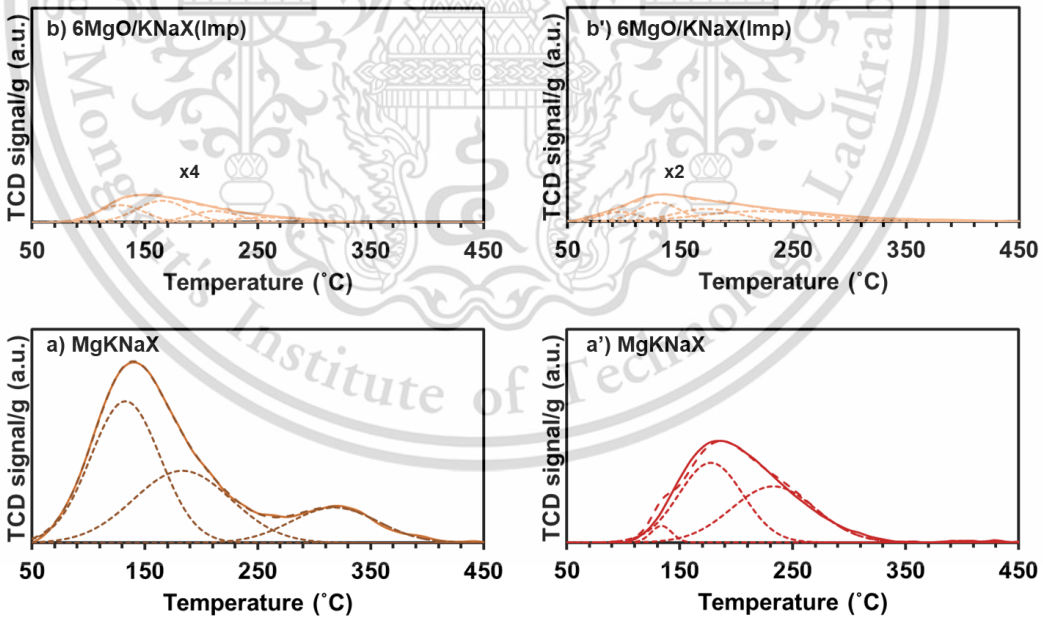

Figure 4.15 NH_3-TPD profiles (a-b) and CO_2-TPD profiles (a'-b') of MgKNaX and 6MgO/KNaX(Imp).

Table 4.5 Acidity and Basicity of catalysts.

Entry	Catalysts	Acidity (μmol/g)							Basicity (μmol/g)					
		W_a1 (136 °C)	W_a2 (170 °C)	W_a3 (220 °C)	M_a1 (260 °C)	M_a2 (320 °C)	S_a1 (400 °C)	Total	W_b1 (100 °C)	W_b2 (130 °C)	W_b3 (176 °C)	W_b4 (236 °C)	M_b1 (320 °C)	Total
1	MgKNaX	35	25	-	-	11	-	72	-	0.4	6	6	0.1	12.5
2	6MgO/KNaX (Imp)	10	13	7	4	0.4	-	34.4	0.6	1.3	1.3	1.9	0.5	5.6

W_a: Weak acid site, M_a: Medium acid site, S_a: Strong acid site, W_b: Weak basic site, M_b: Medium basic site

Based on the discussion above, it seems that the occluded $[Mg_4(OH)_4]^{4+}$ clusters inside the K^+ exchanged zeolite X provide the suitable medium acidity and medium basicity that would promote the Guerbet reaction selectively to produce higher alcohols. To gain further insights into the importance of the occluded $[Mg_4(OH)_4]^{4+}$ clusters in the cavity of zeolite X, the catalysis over the control of 5MgO/KNaX(PB), which was primarily treated with furfuryl alcohol at 420°C, was carried out. The surface area (26 m^2/g) and pore volume (0.01 cm^3/g) of 5MgO/KNaX(PB) are dramatically decreased (Table 4.3), as compared to that of its parent (539 m^2/g and 0.39 cm^3/g, respectively). This suggest that the cavity of this sample was blocked by the coke deposit (~5 wt.%, Figure 4.16). The activity of 5MgO/KNaX(PB) dropped significantly from 11.4% to 2.7% conversion, together with the consecutive decline of higher alcohol yield from 5.9 to 0.6% (Table 4.4, entry 11). Despite that the pore blockage cavity of 5MgO/KNaX(PB) was achieved, the external surface was still available as the sample was thoroughly flushed by N_2 (160 mL/min) for 1 h prior to heating to 420 °C. No structural collapse after the treatment was observed, as confirmed by the ^{27}Al MAS-NMR in Figure 4.17a. Accordingly, the decrease in the activity of 5MgO/KNaX(PB) could be due to the inaccessibility of the feed to the occluded $[Mg_4(OH)_4]^{4+}$ clusters inside the zeolite X. Whereas the MgO nanopetals on the external

surface mainly promoted ethanol dehydration to ethylene (Table 4.4, entry 10). This emphasizes the essential role of the occluded $[Mg_4(OH)_4]^{4+}$ clusters which promote the Guerbet reaction.

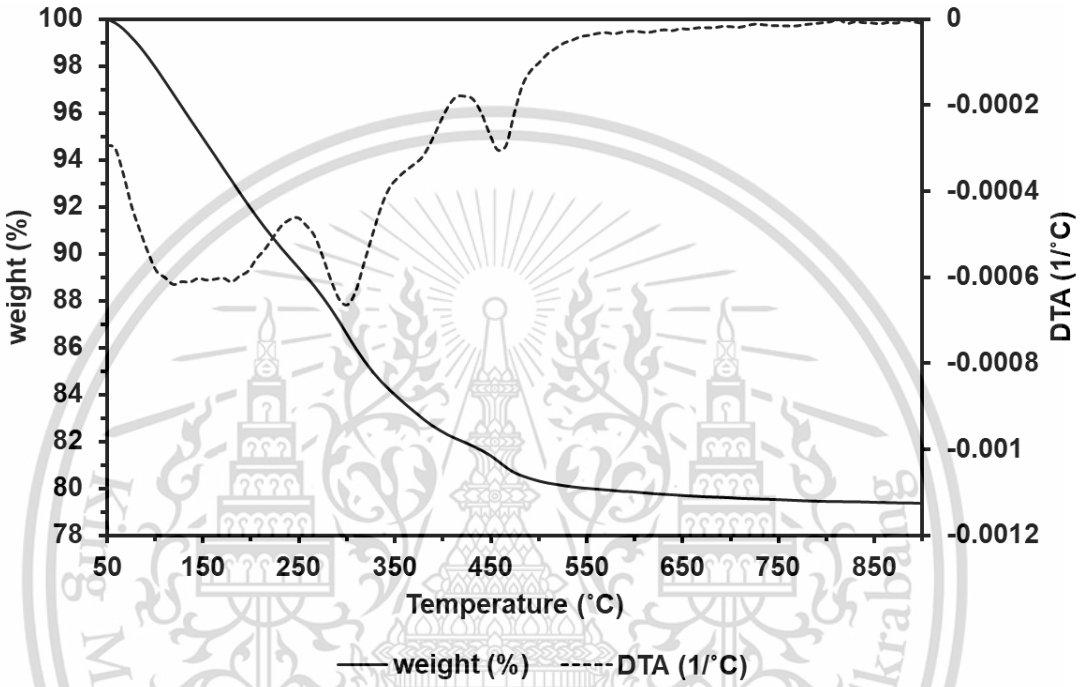

Figure 4.16 TGA of 5MgO/KNaX(PB).

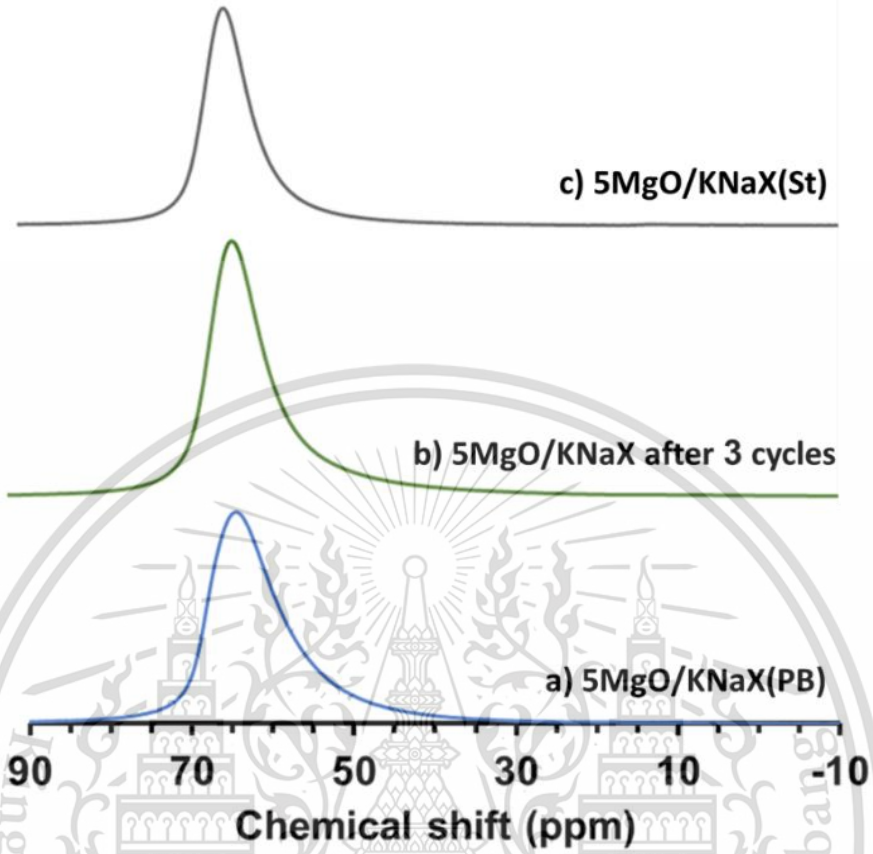

Figure 4.17 ^{27}Al MAS-NMR spectra of 5MgO/KNaX(PB), 5MgO/KNaX after 3 cycle and 5MgO/KNaX(St).

4.3 Catalytic stability

The ethanol conversion over the 5MgO/KNaX for 8 hours on stream is shown in Figure 4.18a. The activity of the catalyst is slightly decreased over time. The higher alcohols also decrease with a gradual increase in acetaldehyde. This suggests the deactivation of the catalyst, particularly the medium acid/base sites that are essential for the aldol condensation. The loss of these sites could presumably result from i) the structural collapse due to the presence of water produced during the reaction and/or ii) the coke formation blocking the active occluded $[MgOH]_4^{4+}$ clusters.

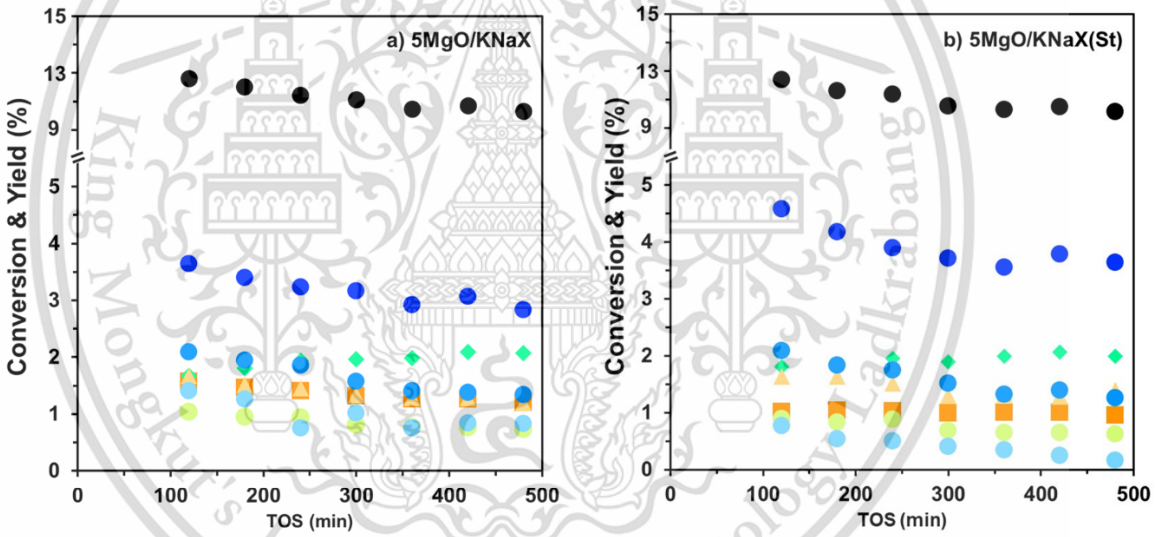

Figure 4.18 Time on steam of ethanol conversion over 5MgO/KNaX and 5MgO/KNaX(St) (●) Ethanol conversion, (■) Ethylene, (◆) Acetaldehyde, (▲) butadiene, (●) C4-aldehyde, (●) C4-alcohol, (●) C6-alcohol, and (●) C8-alcohol (Reaction condition: at 380 °C and 1 atm ; EtOH feed rate: 1 mL/h; contact time: 16 g.h/mol; flow rate of N_2 carrier gas: 160 mL/min).

To assess the first hypothesis, the ^{27}Al MAS-NMR spectra of the 5MgO/KNaX after 3 cycles on stream shows only tetrahedral Al^{3+} species (Figure 4.17b), indicating the well-defined framework structure. In a supportive manner, the reaction over 5MgO/KNaX(St) – primarily treated with steam at 380 ˚C for 1 h – showed a similar activity (Table 4.4) and time on stream profile (Figure 4.18 b). This clearly indicates that the presence of water produced during the reaction has no effect on the catalyst stability. In fact, only tetrahedral Al^{3+} species were detected in 5MgO/KNaX(St), as shown in Figure 4.17c.

In turn, the initial deactivation of the catalyst appears to result from the high molecular weight products deposit on the highly active acid/basic sites, as evidenced by the TGA of 5MgO/KNaX after 8 hours on stream (~10% of carbon deposit, Figure 4.19). The activity can be recovered simply by calcination under air at 450˚C for 1 hour to regenerate the catalyst up to three cycles, as shown in Figure 4.20. Higher alcohols were obtained as main products in all cycles, indicating the recovery of the active sites, particularly occluded $[MgOH]_4^{4+}$ clusters. Compared to other catalysts reported for the gas-phase ethanol conversion to higher alcohols (Table 4.6), this MgO/KNaX catalyst does provide not only high activity and selectivity for higher alcohols, but also offers high stability and regenerability.

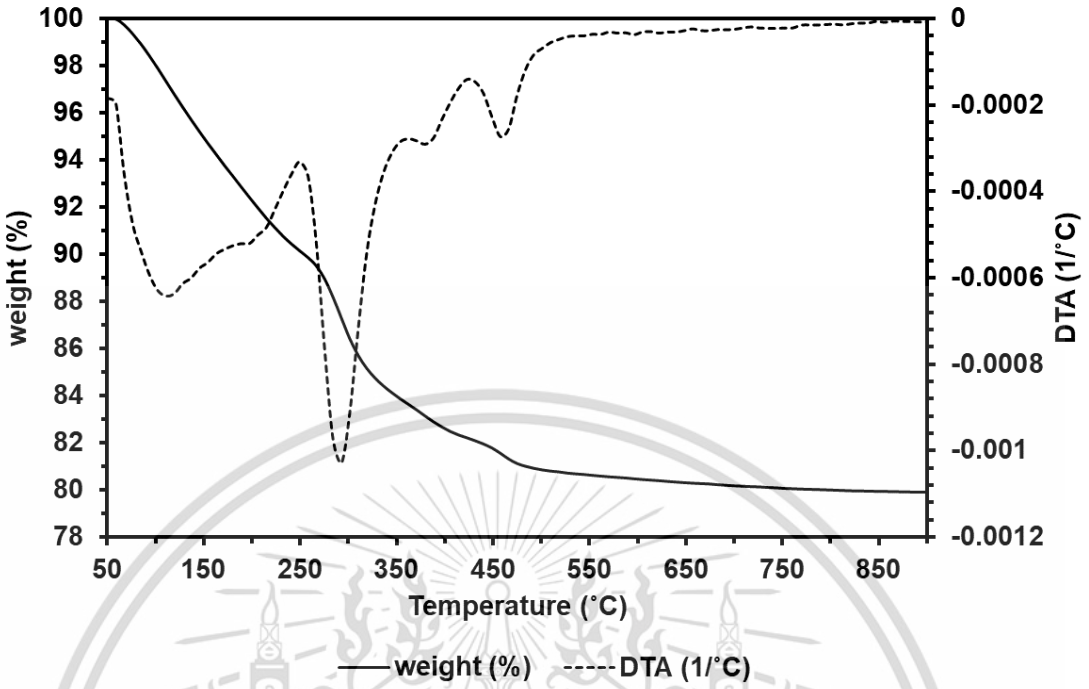

Figure 4.19 TGA of 5MgO/KNaX after 8 hours on stream.

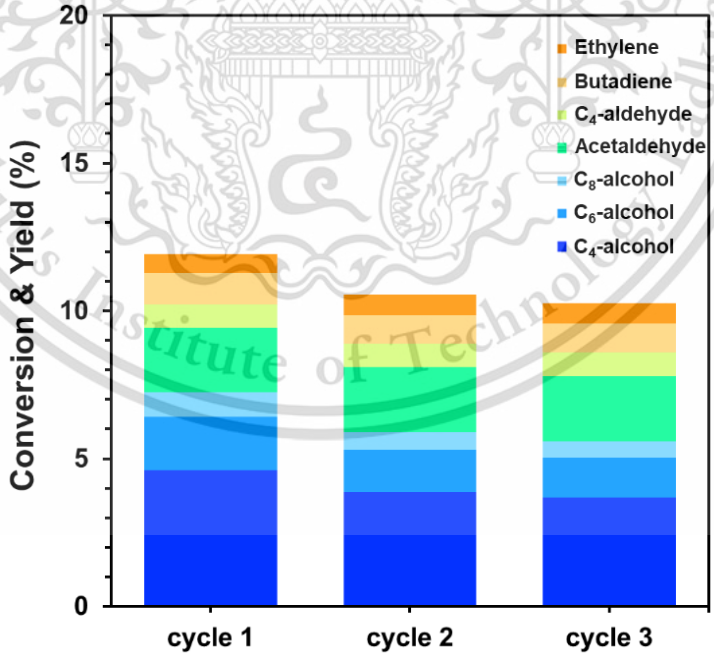

Figure 4.20 Regeneration of 5MgO/KNaX (Reaction condition: at 380 °C and 1 atm; EtOH feed rate: 1 mL/h; contact time: 16 g.h/mol; flow rate of N_2 carrier gas: 160 mL/min).

Table 4.6 Overview of the Catalysts for the Guerbet reaction.

Entry	Catalysts	W/F ($g.h.mol^{-1}$)	Temperature (°C)	Conversion (%)	Selectivity (%)		Ref.
					Total higher alcohol	Ethylene	
1	6MgO/KNaX	48.0	380	38.8[a]	78.5[a]	3.3[a]	This work
2	MgO	20.0	450	56.1	36.4	65.8	14
3	Mg_3AlO_x	23.3	350	34.0	37.0	Nd	83
4	$Mg_3Fe_nAl_{1-n}O_x$	24.7	350	80.0	14.0	Nd	84
5	HAP (Sr/P = 1.70)	130	300	24.0	75.3	Nd	85
6	Ni/MgO	200	400	18.0	8.0	Nd	86
7	YSZ 500	230	300	24.2	69.2	Nd	87
8	ZrO_2	230	300	9.9	19.9	Nd	88
9	ZrO_2-CeO_2	230	300	13.3	31.6	Nd	88

a: initial point, Nd: No data

CHAPTER 5

Conclusion and Suggestions

5.1 Conclusion

Higher alcohols, including C_4-C_8-alcohols, can be obtained as major products from the direct ethanol conversion over the MgO/KNaX catalysts. The occluded $[Mg_4(OH)_4]^{4+}$ clusters can be easily manipulated by the concentration of $Mg(OAc)_2$ (0.1-0.5 M) during ion exchange of the catalysts. A higher $Mg(OAc)_2$ concentration (≥0.6 M) leads to higher MgO nanopetals and MgO aggregates. The occluded $[Mg_4(OH)_4]^{4+}$ clusters inside the cavity of K^+ exchanged zeolite X are responsible for the observed activity for Guerbet reaction, as compared to the MgO nanopetals and MgO aggregates. Since the occluded $[Mg_4(OH)_4]^{4+}$ clusters offer both the medium basic (M_b) and medium acid (M_a) sites within the cavity, the dehydrogenation of ethanol, aldol condensation and H-transfer can be readily promoted. The total higher alcohol yields depend on the M_b/M_a ratio of the MgO/KNaX catalysts. 6MgO/KNaX with a M_b/M_a ratio of 0.024 offers relatively high alcohol selectivity (~80%), as compared to other catalysts reported in the literature. The MgO/KNaX showed high structural stability even after steaming at 380 ˚C. Despite a slight deactivation due to high MW molecule adsorption, the MgO/KNaX can be regenerated simply by calcination under air at 450 ˚C.

5.2 Suggestion

5.2.1 The activity and selectivity can be also enhanced by the use of highly crystallinity of zeolite X.

5.2.2 A high molecular weight molecule adsorption is a result of the over-potential active site, for overcome this, another metal oxide such as RuO would be a possibility.

References

[1] B. Rajesh Kumar and S. Saravanan, **"Use of higher alcohol biofuels in diesel engines: A review,"** *Renew. Sustain. Energy Rev.*, vol. 60, pp. 84–115, Jul. 2016, doi: 10.1016/j.rser.2016.01.085.

[2] C. Jin, M. Yao, H. Liu, C. F. Lee, and J. Ji, **"Progress in the production and application of n-butanol as a biofuel,"** *Renew. Sustain. Energy Rev.*, vol. 15, no. 8, pp. 4080–4106, Oct. 2011, doi: 10.1016/j.rser.2011.06.001.

[3] H. Yaman, B. Doğan, M. K. Yeşilyurt, and D. Erol, **"Application of Higher-Order Alcohols (1-Hexanol-C_6 and 1-Heptanol-C_7) in a Spark-Ignition Engine: Analysis and Assessment,"** *Arab. J. Sci. Eng.*, vol. 46, no. 12, pp. 11937–11961, Dec. 2021, doi: 10.1007/s13369-021-05765-7.

[4] I. V. Tetko and P. Bruneau, **"Application of ALOGPS to predict 1-octanol/water distribution coefficients, logP, and logD, of AstraZeneca in-house database,"** *J. Pharm. Sci.*, vol. 93, no. 12, pp. 3103–3110, Dec. 2004, doi: 10.1002/jps.20217.

[5] P. Li, J. Ge, Y. Gao, J. Wang, C. Zhang, and D. Xiao, **"A Seamless Gene Deletion Method and Its Application for Regulation of Higher Alcohols and Ester in Baijiu *Saccharomyces cerevisiae*,"** *BioMed Res. Int.*, vol. 2019, pp. 1–12, May 2019, doi: 10.1155/2019/6723849.

[6] F. Cheng, H. Guo, J. Cui, B. Hou, and D. Li, **"Guerbet reaction of methanol and ethanol catalyzed by CuMgAlO mixed oxides: Effect of M^{2+}/Al^{3+} ratio,"** *J. Fuel Chem. Technol.*, vol. 46, no. 12, pp. 1472–1481, Dec. 2018, doi: 10.1016/S1872-5813(18)30061-6.

[7] T. Matsu-ura, S. Sakaguchi, Y. Obora, and Y. Ishii, **"Guerbet Reaction of Primary Alcohols Leading to β-Alkylated Dimer Alcohols Catalyzed by Iridium Complexes,"** *J. Org. Chem.*, vol. 71, no. 21, pp. 8306–8308, Oct. 2006, doi: 10.1021/jo061400t.

[8] A. Ohligschläger, N. Staalduinen, C. Cormann, J. Mühlhans, J. Wurm, and M. A. Liauw, **"The Guerbet Reaction Network – a Ball-in-a-Maze-Game or: Why Ru-MACHO-**

BH is Poor in Coupling two Ethanol to n-Butanol," *Chemistry–Methods*, vol. 1, no. 4, pp. 181–191, Apr. 2021, doi: 10.1002/cmtd.202000056.

[9] H. Aitchison, R. L. Wingad, and D. F. Wass, **"Homogeneous Ethanol to Butanol Catalysis—Guerbet Renewed,"** *ACS Catal.*, vol. 6, no. 10, pp. 7125–7132, Oct. 2016, doi: 10.1021/acscatal.6b01883.

[10] J. Zhang *et al.*, **"Highly dispersed Pt nanoparticles supported on carbon nanotubes produced by atomic layer deposition for hydrogen generation from hydrolysis of ammonia borane,"** *Catal. Sci. Technol.*, vol. 7, no. 2, pp. 322–329, 2017, doi: 10.1039/C6CY01960A.

[11] J. C. Védrine, **"Acid–base characterization of heterogeneous catalysts: an up-to-date overview,"** *Res. Chem. Intermed.*, vol. 41, no. 12, pp. 9387–9423, Dec. 2015, doi: 10.1007/s11164-015-1982-9.

[12] A. Chieregato, J. Velasquez Ochoa, C. Bandinelli, G. Fornasari, F. Cavani, and M. Mella, **"On the Chemistry of Ethanol on Basic Oxides: Revising Mechanisms and Intermediates in the Lebedev and Guerbet reactions,"** *ChemSusChem*, vol. 8, no. 2, pp. 377–388, Jan. 2015, doi: 10.1002/cssc.201402632.

[13] A. Ndou, **"Dimerisation of ethanol to butanol over solid-base catalysts,"** *Appl. Catal. Gen.*, vol. 251, no. 2, pp. 337–345, Sep. 2003, doi: 10.1016/S0926-860X(03)00363-6.

[14] T. Tsuchida, T. Yoshioka, S. Sakuma, T. Takeguchi, and W. Ueda, **"Synthesis of Biogasoline from Ethanol over Hydroxyapatite Catalyst,"** *Ind. Eng. Chem. Res.*, vol. 47, no. 5, pp. 1443–1452, Mar. 2008, doi: 10.1021/ie0711731.

[15] S. Cimino, J. Apuzzo, and L. Lisi, **"MgO Dispersed on Activated Carbon as Water Tolerant Catalyst for the Conversion of Ethanol into Butanol,"** *Appl. Sci.*, vol. 9, no. 7, p. 1371, Apr. 2019, doi: 10.3390/app9071371.

[16] W. Janssens *et al.*, **"Ternary Ag/MgO-SiO_2 Catalysts for the Conversion of Ethanol into Butadiene,"** *ChemSusChem*, vol. 8, no. 6, pp. 994–1008, Mar. 2015, doi:10.1002/cssc.201402894.

[17] R. Velmurugan and A. Incharoensakdi, **"Metal Oxide Mediated Extracellular NADPH Regeneration Improves Ethanol Production by Engineered Synechocystis sp.**

PCC 6803," *Front. Bioeng. Biotechnol.*, vol. 7, p. 148, Jun. 2019, doi: 10.3389/fbioe.2019.00148.

[18] C. Angelici, M. E. Z. Velthoen, B. M. Weckhuysen, and P. C. A. Bruijnincx**, "Influence of acid–base properties on the Lebedev ethanol-to-butadiene process catalyzed by SiO_2 –MgO materials,"** *Catal. Sci. Technol.*, vol. 5, no. 5, pp. 2869–2879, 2015, doi: 10.1039/C5CY00200A.

[19] J. Wang, W. Yang, C. Wu, Y. Gong, J. Zhang, and C. Shen, **"Upgrading *n* -Butanol to Branched Alcohols over Ni/Ca $_x$Mg $_y$O,"** *ACS Sustain. Chem. Eng.*, vol. 8, no. 45, pp. 16960–16967, Nov. 2020, doi: 10.1021/acssuschemeng.0c07070.

[20] C. Wu, C. Shen, Y. Gong, and J. Wang, **"Domino Reactions for Biofuel Production from Zymotic Biomass Wastes over Bifunctional Mg-Containing Catalysts,"** *ACS Sustain. Chem. Eng.*, vol. 7, no. 23, pp. 18943–18954, Dec. 2019, doi: 10.1021/acssuschemeng.9b04311.

[21] T.-F. Yu, C.-W. Chang, P.-W. Chung, and Y.-C. Lin, **"Unsupported and silica-supported perovskite-type lanthanum manganite and lanthanum ferrite in the conversion of ethanol,"** *Fuel Process. Technol.*, vol. 194, p. 106117, Nov. 2019, doi: 10.1016/j.fuproc.2019.06.001.

[22] J. T. Kozlowski and R. J. Davis, **"Heterogeneous Catalysts for the Guerbet Coupling of Alcohols,"** *ACS Catal.*, vol. 3, no. 7, pp. 1588–1600, Jul. 2013, doi: 10.1021/cs400292f.

[23] T. Tsuchida, J. Kubo, T. Yoshioka, S. Sakuma, T. Takeguchi, and W. Ueda, **"Reaction of ethanol over hydroxyapatite affected by Ca/P ratio of catalyst,"** *J. Catal.*, vol. 259, no. 2, pp. 183–189, Oct. 2008, doi: 10.1016/j.jcat.2008.08.005.

[24] A. Lilić, S. Bennici, J. Devaux, J. Dubois, and A. Auroux, **"Influence of Catalyst Acid/Base Properties in Acrolein Production by Oxidative Coupling of Ethanol and Methanol,"** *ChemSusChem*, vol. 10, no. 9, pp. 1916–1930, May 2017, doi: 10.1002/cssc.201700230.

[25] A. Lilić, T. Wei, S. Bennici, J.-F. Devaux, J.-L. Dubois, and A. Auroux, **"A Comparative Study of Basic, Amphoteric, and Acidic Catalysts in the Oxidative Coupling of**

Methanol and Ethanol for Acrolein Production," *ChemSusChem*, vol. 10, no. 17, pp. 3459–3472, Sep. 2017, doi: 10.1002/cssc.201701040.

[26] L. Silvester *et al.*, **"Reactivity of ethanol over hydroxyapatite-based Ca-enriched catalysts with various carbonate contents,"** *Catal. Sci. Technol.*, vol. 5, no. 5, pp. 2994–3006, 2015, doi: 10.1039/C5CY00327J.

[27] S. Da Ros et al., **"Microkinetic analysis of ethanol to 1,3-butadiene reactions over MgO-SiO_2 catalysts based on characterization of experimental fluctuations,"** Chem. Eng. J., vol. 308, pp. 988–1000, Jan. 2017, doi: 10.1016/j.cej.2016.09.135.

[28] Y. Li, R. Zhang, L. Du, Q. Zhang, and W. Wang, **"Catalytic mechanism of C–F bond cleavage: insights from QM/MM analysis of fluoroacetate dehalogenase,"** Catal. Sci. Technol., vol. 6, no. 1, pp. 73–80, 2016, doi: 10.1039/C5CY00777A.

[29] L. Zhang et al., **"Synthesis of C4 and C8 Chemicals from Ethanol on MgO-Incorporated Faujasite Catalysts with Balanced Confinement Effects and Basicity,"** ChemSusChem, vol. 9, no. 7, pp. 736–748, Apr. 2016, doi: 10.1002/cssc.201501518.

[30] J. G. Vitillo, T. Fjermestad, M. D'Amore, M. Milanesio, L. Palin, G. Ricchiardi and S. Bordiga, "**On the structure of superbasic $(MgO)_n$ sites solvated in a faujasite zeolite,**"Phys. Chem. Chem. Phys., 2018, DOI: 10.1039/C8CP01788C

[31] **"Alcohol (Ethanol) Effects, Hazards & Warnings,"** *Drugs.com*. https://www.drugs.com/alcohol.html (accessed Dec. 15, 2020).

[32] J. Sha *et al.*, **"Solubility determination, model evaluation, Hansen solubility parameter and thermodynamic properties of benflumetol in pure alcohol and ester solvents,"** *J. Chem. Thermodyn.*, p. 106323, Oct. 2020, doi: 10.1016/j.jct.2020.106323.

[33] A. Neshat *et al.*, **"Catalytic alcohol oxidation using cationic Schiff base manganeseIII complexes with flexible diamino bridge,"** *Polyhedron*, vol. 193, p. 114873, Jan. 2021, doi: 10.1016/j.poly.2020.114873.

[34] P. E. Kee *et al.*, **"Primary capture of Bacillus subtilis xylanase from crude feedstock using alcohol/salt liquid biphasic flotation,"** *Biochem. Eng. J.*, vol. 165, p. 107835, Jan. 2021, doi: 10.1016/j.bej.2020.107835.

[35] S. P. Samudrala, S. Kandasamy, and S. Bhattacharya, **"One-pot synthesis of bio-fuel additives from glycerol and benzyl alcohol: Mesoporous MCM-41 supported iron (III) chloride as a highly efficient tandem catalyst,"** *Renew. Energy*, vol. 156, pp. 883–892, Aug. 2020, doi: 10.1016/j.renene.2020.04.111.

[36] D. Li, H. Zhen, L. Xingcai, Z. Wu-gao, and Y. Jian-guang, **"Physico-chemical properties of ethanol–diesel blend fuel and its effect on performance and emissions of diesel engines,"** *Renew. Energy*, vol. 30, no. 6, pp. 967–976, May 2005, doi: 10.1016/j.renene.2004.07.010.

[37] **"Alcohol Reactivity."** https://www2.chemistry.msu.edu/faculty/reusch/VirtTxtJml/alcohol1.htm (accessed Dec. 15, 2020).

[38] G. Litt and C. Almquist, **"An investigation of CuO/Fe_2O_3 catalysts for the gas-phase oxidation of ethanol,"** *Appl. Catal. B Environ.*, vol. 90, no. 1, pp. 10–17, Jul. 2009, doi: 10.1016/j.apcatb.2009.02.001.

[39] E. Lee and J.-E. Lee, **"Impact of drinking alcohol on gut microbiota: recent perspectives on ethanol and alcoholic beverage,"** *Curr. Opin. Food Sci.*, vol. 37, pp. 91–97, Feb. 2021, doi: 10.1016/j.cofs.2020.10.001.

[40] S. H. Haugland, **"Parental alcohol intoxication and adverse health outcomes among offspring. A 4-year follow up HUNT study among 2399 Norwegian adolescents,"** *Prev. Med. Rep.*, p. 6, 2020.

[41] J. M. Fraile, E. García-Bordejé, and L. Roldán, **"Deactivation of sulfonated hydrothermal carbons in the presence of alcohols: Evidence for sulfonic esters formation,"** *J. Catal.*, vol. 289, pp. 73–79, May 2012, doi: 10.1016/j.jcat.2012.01.017.

[42] **"Alcohol Consumption By Country,"** *WorldAtlas*. https://www.worldatlas.com/articles/who-drinks-the-most-alcohol-consumption-by-country.html (accessed Dec. 15, 2020).

[43] PubChem, **"1-Butanol."** https://pubchem.ncbi.nlm.nih.gov/compound/263 (accessed Dec. 15, 2020).

[44] **"Wamin Chemical,"** *Wamin Chemical*. http://www.waminchemical.com/Alcohols.html (accessed Dec. 15, 2020).

[45] PubChem, **"1-Hexanol."** https://pubchem.ncbi.nlm.nih.gov/compound/8103 (accessed Dec. 15, 2020).

[46] PubChem, **"1-Octanol."** https://pubchem.ncbi.nlm.nih.gov/compound/957 (accessed Dec. 15, 2020).

[47] N. Enomoto, S. Takase, M. Yasuhara, and A. Takada, **"Acetaldehyde Metabolism in Different Aldehyde Dehydrogenase-2 Genotypes,"** *Alcohol. Clin. Exp. Res.*, vol. 15, no. 1, pp. 141–144, 1991, doi: https://doi.org/10.1111/j.1530-0277.1991.tb00532.x.

[48] PubChem, **"Acetaldehyde."** https://pubchem.ncbi.nlm.nih.gov/compound/177 (accessed Dec. 15, 2020).

[49] PubChem, **"Butyraldehyde."** https://pubchem.ncbi.nlm.nih.gov/compound/261 (accessed Dec. 15, 2020).

[50] PubChem, **"Hexanal."** https://pubchem.ncbi.nlm.nih.gov/compound/6184 (accessed Dec. 15, 2020).

[51] **"Guerbet - Our History and Future,"** *Guerbet US*. /en-us/about-us/our-history-and-future/ (accessed Dec. 15, 2020).

[52] T. Tsuchida, J. Kubo, T. Yoshioka, S. Sakuma, T. Takeguchi, and W. Ueda, **"Reaction of ethanol over hydroxyapatite affected by Ca/P ratio of catalyst,"** *J. Catal.*, vol. 259, no. 2, pp. 183–189, Oct. 2008, doi: 10.1016/j.jcat.2008.08.005.

[53] J. T. Kozlowski and R. J. Davis, **"Heterogeneous Catalysts for the Guerbet Coupling of Alcohols,"** *ACS Catal*, p. 13, 2013.

[54] PubChem, **"Magnesium oxide."** https://pubchem.ncbi.nlm.nih.gov/compound/14792 (accessed Dec. 15, 2020).

[55] **"FAU: Framework Type."** https://asia.iza-structure.org/IZA-SC/framework.php?STC=FAU (accessed Dec. 15, 2020).

[56] H. E. Mgbemere, I. C. Ekpe, and G. I. Lawal, **"Zeolite Synthesis, Characterization and Application Areas: A Review,"** vol. 6, p. 15, 2017.

[57] W. Uhl and A. Kyriatsoulis, **"Meerwein-Ponndorf-Verley,"** in *Namen- und Schlagwortreaktionen in der Organischen Chemie*, W. Uhl and A. Kyriatsoulis, Eds. Wiesbaden: Vieweg+Teubner Verlag, 1984, pp. 111–112.

[58] **"Development of MgO based catalysts for conversion of ethanol to higher alcohols,"** KING MONGKUT'S INSTITUTE OF TECHNOLOGY LADKRABANG, 2019.

[59] T. Riittonen *et al.*, **"One-Pot Liquid-Phase Catalytic Conversion of Ethanol to 1-Butanol over Aluminium Oxide—The Effect of the Active Metal on the Selectivity,"** *Catalysts*, vol. 2, no. 1, Art. no. 1, Mar. 2012, doi: 10.3390/catal2010068.

[60] G. Yao, J. Lei, X. Zhang, Z. Sun, and S. Zheng, **"One-Step Hydrothermal Synthesis of Zeolite X Powder from Natural Low-Grade Diatomite,"** Materials, vol. 11, no. 6, p. 906, May 2018, doi: 10.3390/ma11060906.

[61] P. N. Joshi, U. D. Joshi, T. H. Kim, K. I. Kim, and V. P. Shiralkar, **"The Compatibility of Compositional and Structural Features of Aluminous Large Pore Zeolites with Sorption Characteristics,"** Adsorption, vol 7, p. 279-289, August 2001, doi: 10.1023/A:1013120916684.

[62] Z. Chen et al., **"Deactivation of a Y-zeolite based catalyst with coke evolution during the catalytic pyrolysis of polyethylene for fuel oil,"** Appl. Catal. Gen., vol. 609, p. 117873, Jan. 2021, doi: 10.1016/j.apcata.2020.117873.

[63] Yu. F. Shepelev, I. K. Butikova, and Yu. I. Smolin, **"Crystal structures of the partially K-, Rb-,and Cs-exchanged forms of NaX zeolite in both the hydrated and the dehydrated (400 °C) states,"** Zeolites, vol. 11, no. 3, pp. 287–292, Mar. 1991, doi: 10.1016/S0144-2449(05)80234-9.

[64] C. Yamagata and J. O. A. Paschoal, **"Systematic Precipitation of Magnesium Hydroxide Using NH_4OH to Preparing MgO-PSZ Precursor Powder,"** Mater. Sci. Forum, vol. 805, pp. 712–717, Sep. 2014, doi: 10.4028/www.scientific.net/MSF.805.712.

[65] F. T. Fanta, A. A. Dubale, D. F. Bebizuh, and M. Atlabachew, **"Copper doped zeolite composite for antimicrobial activity and heavy metal removal from waste water,"** *BMC Chem.*, vol. 13, no. 1, p. 44, Dec. 2019, doi: 10.1186/s13065-019-0563-1.

[66] Z. Adem, F. Guenneau, M.-A. Springuel-Huet, and A. Gédéon, **"PFG NMR investigation of hydrocarbon diffusion in large NaX zeolite crystals: Effect of internal field gradients on diffusion data,"** *Microporous Mesoporous Mater.*, vol. 114, no. 1–3, pp. 337–342, Sep. 2008, doi: 10.1016/j.micromeso.2008.01.019.

[67] X. Cao, H. Zhao, X. Liu, H.-H. Luo, and R. Liu, **"Preparation of petal-like magnesium hydroxide particles by adding sulfate ions,"** *J. Cryst. Growth*, vol. 550, p. 125841, Nov. 2020, doi: 10.1016/j.jcrysgro.2020.125841.

[68] A. Chatterjee and F. Mizukami, **"Location and role of exchangeable cations in zeolite catalysis: a first principle study,"** *Chem. Phys. Lett.*, vol. 385, no. 1–2, pp. 20–24, Feb. 2004, doi: 10.1016/j.cplett.2003.12.035.

[69] S. A. Halawy, M. A. Mohamed, and S. El-Nahas, **"A prolonged evaluation of air contamination level with CO_2 in a college student's laboratory using nanosized MgO,"** *Int. J. Environ. Sci. Technol.*, vol. 17, no. 3, pp. 1551–1566, Mar. 2020, doi: 10.1007/s13762-019-02584-0.

[70] T. L. Jordison, C. T. Lira, and D. J. Miller, **"Condensed-Phase Ethanol Conversion to Higher Alcohols,"** *Ind. Eng. Chem. Res.*, vol. 54, no. 44, pp. 10991–11000, Nov. 2015, doi: 10.1021/acs.iecr.5b02409.

[71] M. Szabó *et al.*, **"Outstanding Activity and Selectivity of Controlled Size Pt Nanoparticles Over WO_3 Nanowires in Ethanol Decomposition Reaction,"** *J. Nanosci. Nanotechnol.*, vol. 19, no. 1, pp. 478–483, Jan. 2019, doi: 10.1166/jnn.2019.15783.

[72] J.Ob-eye, P. Praserthdam, and B. Jongsomjit, **"Ethanol Dehydrogenation to Acetaldehyde over Activated Carbons-Derived from Coffee Residue,"** *Bull. Chem. React. Eng. Catal.*, vol. 14, no. 2, p. 268, Aug. 2019, doi: 10.9767/bcrec.14.2.3335.268-282.

[73] A. P. Farkas, Á. Szitás, D. Jurdi, K. Palotás, J. Kiss, and Z. Kónya, **"Selective transformation of ethanol to acetaldehyde catalyzed by Au/h-BN interface prepared on Rh(111) surface,"** *Appl. Catal. Gen.*, vol. 592, p. 117440, Feb. 2020, doi: 10.1016/j.apcata.2020.117440.

[74] A. Gazsi, A. Koós, T. Bánsági, and F. Solymosi, **"Adsorption and decomposition of ethanol on supported Au catalysts,"** *Catal. Today*, vol. 160, no. 1, pp. 70–78, Feb. 2011, doi: 10.1016/j.cattod.2010.05.007.

[75] L. N. Quintans, G. D. Castro, and J. A. Castro, **"Oxidation of ethanol to acetaldehyde and free radicals by rat testicular microsomes,"** *Arch. Toxicol.*, vol. 79, no. 1, pp. 25–30, Jan. 2005, doi: 10.1007/s00204-004-0609-5.

[76] C. Zhao *et al.*, **"Coupling of Acetaldehyde to Crotonaldehyde on CeO_{2-x}(111): Bifunctional Mechanism and Role of Oxygen Vacancies,"** *J. Phys. Chem. C*, vol. 123, no. 13, pp. 8273–8286, Apr. 2019, doi: 10.1021/acs.jpcc.8b08535.

[77] B. Szabó *et al.*, **"MgO–SiO_2 Catalysts for the Ethanol to Butadiene Reaction: The Effect of Lewis Acid Promoters,"** *ChemCatChem*, vol. 12, no. 22, pp. 5686–5696, Nov. 2020, doi: 10.1002/cctc.202001007.

[78] S. Chakraborty, P. E. Piszel, C. E. Hayes, R. T. Baker, and W. D. Jones, **"Highly Selective Formation of *n*-Butanol from Ethanol through the Guerbet Process: A Tandem Catalytic Approach,"** *J. Am. Chem. Soc.*, vol. 137, no. 45, pp. 14264–14267, Nov. 2015, doi: 10.1021/jacs.5b10257.

[79] J. E. Rekoske and M. A. Barteau, **"Kinetics, Selectivity, and Deactivation in the Aldol Condensation of Acetaldehyde on Anatase Titanium Dioxide,"** *Ind. Eng. Chem. Res.*, vol. 50, no. 1, pp. 41–51, Jan. 2011, doi: 10.1021/ie100394v.

[80] K. S. Rawat, S. C. Mandal, P. Bhauriyal, P. Garg, and B. Pathak, **"Catalytic upgrading of ethanol to *n*-butanol using an aliphatic Mn–PNP complex: theoretical insights into reaction mechanisms and product selectivity,"** *Catal. Sci. Technol.*, vol. 9, no. 11, pp. 2794–2805, 2019, doi: 10.1039/C9CY00501C.

[81] M. J. L. Gines and E. Iglesia, **"Bifunctional Condensation Reactions of Alcohols on Basic Oxides Modified by Copper and Potassium,"** *J. Catal.*, vol. 176, no. 1, pp. 155–172, May 1998, doi: 10.1006/jcat.1998.2009.

[82] K.-N. T. Tseng, S. Lin, J. W. Kampf, and N. K. Szymczak, **"Upgrading ethanol to 1-butanol with a homogeneous air-stable ruthenium catalyst,"** *Chem. Commun.*, vol. 52, no. 14, pp. 2901–2904, 2016, doi: 10.1039/C5CC09913G.

[83] D. L. Carvalho, R. R. de Avillez, M. T. Rodrigues, L. E. P. Borges, and L. G. Appel, **"Mg and Al mixed oxides and the synthesis of n-butanol from ethanol,"** *Appl. Catal. Gen.*, vol. 415–416, pp. 96–100, Feb. 2012, doi: 10.1016/j.apcata.2011.12.009.

[84] M. León, E. Díaz, A. Vega, S. Ordóñez, and A. Auroux, **"Consequences of the iron–aluminium exchange on the performance of hydrotalcite-derived mixed oxides for ethanol condensation,"** *Appl. Catal. B Environ.*, vol. 102, no. 3–4, pp. 590–599, Feb. 2011, doi: 10.1016/j.apcatb.2010.12.044.

[85] S. Ogo, A. Onda, and K. Yanagisawa, **"Selective synthesis of 1-butanol from ethanol over strontium phosphate hydroxyapatite catalysts,"** *Appl. Catal. Gen.*, vol. 402, no. 1–2, pp. 188–195, Jul. 2011, doi: 10.1016/j.apcata.2011.06.006.

[86] S. Cimino, L. Lisi, and S. Romanucci, **"Catalysts for conversion of ethanol to butanol: Effect of acid-base and redox properties,"** *Catal. Today*, vol. 304, pp. 58–63, Apr. 2018, doi: 10.1016/j.cattod.2017.08.035.

[87] N. V. Vlasenko, P. I. Kyriienko, K. V. Valihura, G. R. Kosmambetova, S. O. Soloviev, and P. E. Strizhak, **"Yttria-Stabilized Zirconia as a High-Performance Catalyst for Ethanol to *n* -Butanol Guerbet Coupling,"** *ACS Omega*, vol. 4, no. 25, pp. 21469–21476, Dec. 2019, doi: 10.1021/acsomega.9b03170.

[88] N. V. Vlasenko, P. I. Kyriienko, O. I. Yanushevska, K. V. Valihura, S. O. Soloviev, and P. E. Strizhak, **"The Effect of Ceria Content on the Acid–Base and Catalytic Characteristics of ZrO_2–CeO_2 Oxide Compositions in the Process of Ethanol to *n*-Butanol Condensation,"** *Catal. Lett.*, vol. 150, no. 1, pp. 234–242, Jan. 2020, doi: 10.1007/s10562-019-02937-x

Appendices

Appendix A

CALCULATION

Calculation of catalytic parameters

Contact time, W/F

To calculation, contact time (W/F) in reaction can used the equation below.

$$W/F = \frac{\text{Weight of catalyst (g)}}{\text{Molar feed rate } (\frac{\text{mol}}{\text{h}})}$$

In the reaction using ethanol feed 1 ml/h (density 0.789 g/ml) and using 0.275 g of catalyst, the W/F is calculated as follow

$$W/F = \frac{(0.275 \text{ g cat.})(46 \frac{\text{gEtOH}}{\text{mol}})}{(1\frac{\text{mL}}{\text{h}})(0.789\frac{\text{gEtOH}}{\text{mL}})}$$

$$= 16.0 \text{ g.h/mol}$$

In similar manner, W/F of catalysts with different catalyst weight and different feed rate are calculated as well as this method.

Calculation of %yield of products from gas chromatography

Table A1 The summation of the peak area of products.

Products	Peak area
Ethylene	146
Acetaldehyde	146
Butadiene	342
Ethanol (Feed)	8871
C_4- aldehyde	141
C_4-alcohol	617
C_6-alcohol	321
C_8-alcohol	554
Total	11157

(Information of ethanol conversion over 6MgO/KNaX, contact time = 16.0 g•h/mol, pressure = atmospheric, time on stream = 60 min, and flow rate of N_2 carrier gas = 160 ml/min)

The area of all peaks was computed accounting for variations in the detector response to different chemical types in the normalizing procedure. The ratio of area to total area was used to estimate the molarity of the examined. However, from table A1 these peak aera was modified by the response factor of each compound.

To calculate the percent yield of each component in sample as follow:

$$\%\text{Yield of each product} = \frac{\text{Peak area of product} \times 100}{\text{Total area}}$$

For example, % yield of C_4-alcohols can be calculated, as shown below

$$\%\ \text{Yield of } C_4\text{-alcohols} = \frac{617 \times 100}{11157}$$

$$= 5.5\ \%$$

The percent yield of each product obtained from above calculation is shown below.

Table A2 Yield of product derived from normalization method

Products	**%Yield**
Ethylene	1.1
Acetaldehyde	1.7
Butadiene	2.5
Ethanol (Feed)	79.5
C_4- aldehyde	1.7
C_4-alcohol	5.5
C_6-alcohol	2.9
C_8-alcohol	5.0
Total	100

Average % yield

The % yield for each product of all catalysts was averaged based on time on steam of each catalytic testing, which can be calculated from equation below, then these data were shown in table 4.4.

$$\text{Average \% yield of product} = \frac{\sum \text{\% yield of the product}}{\text{The number of injection point in time on steam}}$$

Conversion

%Conversion can be calculated using the total area and feed area (ethanol), as following equation below:

$$\%\text{conversion} = \frac{(\text{Total Area} - \text{Feed area}) \times 100}{\text{Total area}}$$

For example, from data in table A1

$$\% \text{ Conversion} = \frac{(11157\text{-}8871)\times 100}{11157}$$

$$= 20.5$$

Or another calculation, %conversion can be analyzed by yield of ethanol, which it equal to previously method.

$$\% \text{ Conversion} = 100 - 79.5$$

$$= 20.5\ \%$$

Average % conversion

The ethanol conversion of all catalysts was averaged based on time on steam of each catalytic testing, then these data was shown in table 4.4.

$$\text{Average \% conversion of product} = \frac{\sum \text{\% conversion of the product}}{\text{The number of injection point in time on steam}}$$

Selectivity

%Selectivity can be obtained from following equation:

$$\%\text{Selectivity of each product} = \frac{\%\text{Yield of each product}\times 100}{\%\text{Conversion}}$$

For example.

$$\%\text{Selectivity of } C_4\text{-alcohols} = \frac{5.5\times 100}{20.5}$$

$$= 27.0\ \%$$

Or other method, %selectivity can be direct calculated from peak area. Whilst follow by equation below.

$$\%\text{Selectivity of each product} = \frac{\text{peak area product} \times 100}{\text{total area of product}}$$

For example.

$$\%\text{Selectivity of } C_4\text{-alcohols} = \frac{617 \times 100}{2{,}286}$$

$$= 27.0\ \%$$

Average % selectivity

The products selectivity of all catalysts was averaged based on time on steam of each catalytic testing, then these data was shown in table 4.4.

$$\text{Average \% selectivity of product} = \frac{\sum \text{\% selectivity of the product}}{\text{The number of injection point in time on steam}}$$

Mass balance

The mass balance for this reaction is higher than 99%. The analysis was performed online with total gas counted. A very small coke deposit (27 mg on 275 mg catalyst) was obtained over 8 hours on stream (0.78 g/h ethanol feeding).

%Mass balance can be calculated following equation below.

$$\%\text{Mass balance} = \frac{\text{mol feed remain} \times 100}{\text{mol feed total}}$$

In this case, the feed remain was calculated from total feed (mol) minus the loss of converted feed (mol), whilst is high molecular weight adsorption product and infer to only butanol.

For example, the mass balance can be following from time on steam over 5MgO/KNaX, as shown below.

$$\text{Mol feed total} = \frac{1 \text{ mol ethanol}}{46 \text{ g ethanol}} \boldsymbol{x} \frac{0.789 \text{ g ethanol}}{1 \text{ ml ethanol}} \boldsymbol{x} \frac{1 \text{ ml ethanol}}{1 \text{ hour}} \boldsymbol{x}\ 8 \text{ hours}$$

= 0.13721 mol ethanol

From TGA in Figure 4.19, the catalyst shown 10 wt. % deposit of products adsorption. This result led to the finding in mol feed remain, as calculated below.

$$\text{Mol feed converted} = \frac{2 \text{ mol ethanol}}{1 \text{ mol butanol}} \boldsymbol{x} \frac{1 \text{ mol butanol}}{74 \text{ g butanol}} \boldsymbol{x} \frac{10 \text{ g butanol}}{100 \text{ g cat.}} \boldsymbol{x} \ 0.275 \text{ g cat.}$$

= 0.00074 mol ethanol

Indicating that, the mol remain ethanol in this reaction is

0.13721 − 0.00074 = 0.13647 mol ethanol remain

Therefore,

$$\%\text{Mass balance} = \frac{0.13647 \times 100}{0.13721}$$

= 99.47 %

The nominal negative framework charge ratio

This ratio can be calculated using the data from elemental compositions of each sample The nominal negative framework charge ratio of $(Na^+,K^+)/Al^{3+}$ as shown follow equation.

$$(Na^+,K^+)/Al^{3+} = \frac{(\text{mol } Na^+ + \text{mol } K^+)}{\text{mol } Al^{3+}}$$

For example, of NaX, the content of Na, K and Al were finding from the XRF in table 4.1

$$(Na^+,K^+)/Al^{3+} = \frac{\left(\frac{12.3 \text{ g Na}}{23 \text{ g Na}}\right)+\left(\frac{0.05 \text{ g K}}{39 \text{ g K}}\right)}{\left(\frac{14.4 \text{ g Al}}{27 \text{ g Al}}\right)}$$

= 1.01

Acidity and basicity

From raw signal of each sample was analyzed from TPD, these signals needed to calibration the baseline, in this work using origin program, then deconverloop and integration the other peak samples with magic plot student program.

To compare with other sample, the volume of standard gas and pulse standard gas of the instrument were needed to know. Therefrom, to calculation amount of acidity as follow equation below.

$$\text{Amount of acid site} = \frac{\text{raw signal peak x volume of standard ammonia gas (mol)}}{\text{signal peak of pluse standard ammonia gas x weight of sample}}$$

Similarly, for amount of basic site can be calculation with previous equation. Differently, the volume of standard gas and pulse standard gas were using carbon dioxide.

APPENDIX B

GAS CHROMATOGRAM

Analysis of gas product from gas chromatography

Prior to analysis, the structure of each product in the sample is identified by GCMS (Gas chromatography with mass spectrometer detector). Then, quantitative analysis of each product was carried out by GC-FID (Gas chromatography with flame ionization detector) with the condition expressed in **Table B1.**

Table B1 The GC condition for quantitative analysis

Column	RT®-Q-BOND, 30 m x 0.53 mm x 20 µm
Temperature program	90˚C (2 min hold) to 250˚C at 25˚C/min
Carrier gas	Nitrogen at 160 mL/min
Injection	250˚C
Detector	FID

In Gas chromatography analysis step, when initial feed was pump (1 ml/h) until 60 min, the first analysis point was become to injected until the gas in the loop runs out (30 second for sample loop size 15 µL). Then, over the next 8 hours, analyze each point every 1 hour. In addition, the sample out was connected to trap-waste 2 sections as i) potassium permanganate ($KMnO_4$) solution trap and ii) paraffin oil trap for polar and non-polar products trapped, respectively.

Table B2 The retention time and response factor of products

Products	Retention time	Response factor
Ethylene	2.03	1.20
Acetaldehyde	5.10	0.76
Butadiene	5.80	1.20
Ethanol	6.46	1.00
Diethyl ether	7.80	1.00
C_4-aldehyde	9.33	0.76
C_4-alcohols	9.96	1.00
C_6-alcohols	14.67	1.00
C_8-alcohols	26.33	1.00
C_{10}-alcohols	39.80	1.00

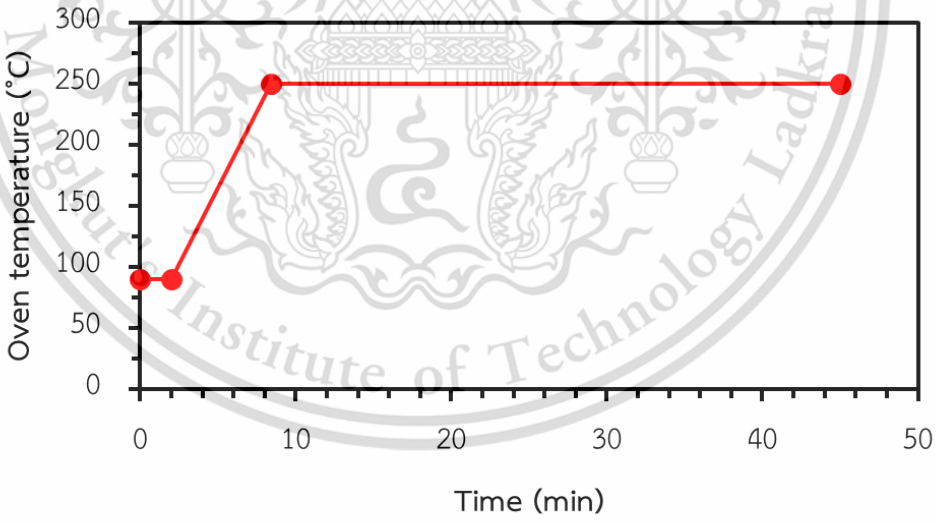

Figure B1 Analysis parameter for ethanol conversion

(Injection 200 °C and FID 250 °C)

APPENDIX C

CATALYTIC ACTIVITY DATA

The catalytic performances of all catalysts were investigated under N_2 atmospheric pressure with a rate 160 mL/min at temperature 380 ˚C condition, which using contact time as 16.0 g.h/mol. Except, table C14 was shown only catalytic testing of contact time as 48.0 g.h/mol, those data can be seen below respectively. This data was averaged depend on the time on steam of each catalyst, then these data were shown in table 4.4.

Table C1 Activity in Guerbet reaction over NaX

Time on stream (min)	30	60	90	120	150	180
Conversion (%)	36.6	35.0	37.0	35.4	35.5	35.9
Yield of product (%)						
Ethylene	32.8	31.1	33.2	31.3	31.5	31.8
Diethyl ether	3.9	4.0	4.1	4.1	4.0	4.1

The catalytic performances of catalyst were investigated under N_2 atmospheric pressure with a rate 160 mL/min at temperature 380 ˚C condition, which using contact time as 16.0 g.h/mol and run reaction for 3 h.

Table C2 Activity in Guerbet reaction over KNaX

Time on stream (min)	60	120	180	240	300	360	420	480
Conversion (%)	8.3	7.1	7.1	6.7	6.9	5.6	8.3	7.1
Yield of product (%)								
Ethylene	0.3	0.3	0.3	0.3	0.3	0.3	0.3	0.3
Acetaldehyde	2.3	2.2	2.3	2.3	2.4	2.0	2.3	2.2
Butadiene	0.9	0.7	0.7	0.7	0.6	0.5	0.9	0.7
C_4-aldehyde	0.4	0.3	0.3	0.3	0.3	0.2	0.4	0.3
C_4-alcohols[(a)]	3.7	3.0	3.1	2.8	2.9	2.3	3.7	3.0
C_6-alcohols[(b)]	0.5	0.3	0.3	0.2	0.2	0.2	0.5	0.3
C_8-alcohols[(c)]	0.2	0.2	0.0	0.0	0.0	0.0	0.2	0.2

[(a)] *n*-butanol and *i*-butanol, [(b)] *n*-hexanol and *i*-hexanol, [(c)] *n*-octanol and *i*-octanol

The catalytic performances of catalyst were investigated under N_2 atmospheric pressure with a rate 160 mL/min at temperature 380 ˚C condition, which using contact time as 16.0 g.h/mol and run reaction for 8 h.

Table C3 Activity in Guerbet reaction over 4MgO/KNaX

Time on stream (min)	60	120	180	240	300	360	420	480
Conversion (%)	14.0	11.2	10.7	10.7	10.1	9.8	9.4	9.5
Yield of product (%)								
Ethylene	2.8	2.8	2.7	2.8	2.4	2.2	2.1	2.1
Acetaldehyde	1.3	1.4	1.5	1.6	1.7	1.8	1.7	2.0
Butadiene	2.2	1.8	1.6	1.6	1.5	1.4	1.3	1.4
C_4-aldehyde	1.0	0.8	0.7	0.7	0.7	0.6	0.6	0.6
C_4-alcohols[(a)]	2.7	2.2	2.1	2.1	2.0	2.1	2.2	2.0
C_6-alcohols[(b)]	1.9	1.3	1.2	1.2	1.2	1.1	1.1	0.9
C_8-alcohols[(c)]	1.7	0.5	0.4	0.3	0.3	0.3	0.2	0.3

[(a)] *n*-butanol and *i*-butanol, [(b)] *n*-hexanol and *i*-hexanol, [(c)] *n*-octanol and *i*-octanol

The catalytic performances of catalyst were investigated under N_2 atmospheric pressure with a rate 160 mL/min at temperature 380 °C condition, which using contact time as 16.0 g.h/mol and run reaction for 8 h.

Table C4 Activity in Guerbet reaction over 5MgO/KNaX

Time on stream (min)	60	120	180	240	300	360	420	480
Conversion (%)	16.9	13.1	12.3	11.6	11.2	10.4	10.7	10.2
Yield of product (%)								
Ethylene	1.6	1.6	1.5	1.4	1.3	1.3	1.3	1.2
Acetaldehyde	1.5	1.7	1.8	1.9	2.0	2.0	2.1	2.1
Butadiene	2.0	1.7	1.5	1.5	1.3	1.3	1.3	1.2
C_4-aldehyde	1.3	1.0	0.9	0.9	0.8	0.8	0.8	0.7
C_4-alcohols[(a)]	4.3	3.6	3.4	3.2	3.2	2.9	3.1	2.8
C_6-alcohols[(b)]	3.2	2.1	1.9	1.9	1.6	1.4	1.4	1.3
C_8-alcohols[(c)]	2.9	1.4	1.3	0.8	1.0	0.8	0.8	0.8

[(a)] *n*-butanol and *i*-butanol, [(b)] *n*-hexanol and *i*-hexanol, [(c)] *n*-octanol and *i*-octanol

The catalytic performances of catalyst were investigated under N_2 atmospheric pressure with a rate 160 mL/min at temperature 380 °C condition, which using contact time as 16.0 g.h/mol and run reaction for 8 h.

Table C5 Activity in Guerbet reaction over 6MgO/KNaX

Time on stream (min)	60	120	180	240	300	360	420	480
Conversion (%)	20.5	17.1	14.0	13.3	12.3	12.2	11.8	10.9
Yield of product (%)								
Ethylene	1.1	1.1	1.0	1.0	1.0	1.0	0.9	0.9
Acetaldehyde	1.7	2..0	2.0	2.1	2.2	2.3	2.3	2.2
Butadiene	2.5	2.1	1.8	1.7	1.6	1.5	1.5	1.4
C_4-aldehyde	1.7	1.3	1.1	1.0	0.9	0.9	0.8	0.7
C_4-alcohols[(a)]	5.5	5.0	4.4	4.3	3.9	4.1	4.0	3.7
C_6-alcohols[(b)]	2.9	2.3	1.8	1.8	1.6	1.6	1.6	1.2
C_8-alcohols[(c)]	5.0	2.1	1.5	1.3	1.1	0.9	0.6	0.6

[(a)] *n*-butanol and *i*-butanol, [(b)] *n*-hexanol and *i*-hexanol, [(c)] *n*-octanol and *i*-octanol

The catalytic performances of catalyst were investigated under N_2 atmospheric pressure with a rate 160 mL/min at temperature 380 °C condition, which using contact time as 16.0 g.h/mol and run reaction for 8 h.

Table C6 Activity in Guerbet reaction over 7MgO/KNaX

Time on stream (min)	60	120	180	240	300	360	420	480
Conversion (%)	18.2	16.0	13.6	12.2	11.9	11.2	10.9	10.6
Yield of product (%)								
Ethylene	0.8	0.9	0.8	0.8	0.7	0.7	0.7	0.7
Acetaldehyde	1.5	1.8	1.9	2.1	2.2	2.2	2.2	2.2
Butadiene	2.7	2.3	1.9	1.9	1.7	1.6	1.5	1.4
C_4-aldehyde	1.5	1.3	1.0	0.9	0.9	0.8	0.7	0.7
C_4-alcohols[(a)]	5.9	5.6	4.8	4.0	4.2	3.8	3.8	3.8
C_6-alcohols[(b)]	3.0	2.5	1.8	1.5	1.5	1.2	1.1	1.1
C_8-alcohols[(c)]	2.7	1.6	1.3	0.9	0.8	0.7	0.6	0.6

[(a)] *n*-butanol and *i*-butanol, [(b)] *n*-hexanol and *i*-hexanol, [(c)] *n*-octanol and *i*-octanol

The catalytic performances of catalyst were investigated under N_2 atmospheric pressure with a rate 160 mL/min at temperature 380 °C condition, which using contact time as 16.0 g.h/mol and run reaction for 8 h.

Table C7 Activity in Guerbet reaction over 8MgO/KNaX

Time on stream (min)	60	120	180	240	300	360	420	480
Conversion (%)	9.0	7.1	6.5	5.6	5.9	5.6	5.6	5.5
Yield of product (%)								
Ethylene	1.0	0.9	0.9	0.9	1.0	0.9	1.0	1.0
Acetaldehyde	2.1	2.3	2.2	2.0	2.2	2.2	2.2	2.2
Butadiene	1.4	1.1	0.9	0.9	0.9	0.8	0.8	0.7
C_4-aldehyde	0.5	0.4	0.4	0.3	0.3	0.3	0.3	0.2
C_4-alcohols[(a)]	2.4	2.0	1.8	1.5	1.6	1.3	1.4	1.3
C_6-alcohols[(b)]	0.6	0.1	0.1	0.0	0.0	0.0	0.0	0.0
C_8-alcohols[(c)]	0.7	0.3	0.2	0.0	0.0	0.0	0.0	0.0

[(a)] *n*-butanol and *i*-butanol, [(b)] *n*-hexanol and *i*-hexanol, [(c)] *n*-octanol and *i*-octanol

The catalytic performances of catalyst were investigated under N_2 atmospheric pressure with a rate 160 mL/min at temperature 380 °C condition, which using contact time as 16.0 g.h/mol and run reaction for 8 h.

Table C8 Activity in Guerbet reaction over MgKNaX

Time on stream (min)	30	60	90	120	150	180	210	240
Conversion (%)	35.3	0.0	32.3	29.2	27.4	28.4	0.0	26.8
Yield of product (%)								
Ethylene	31.3	0.0	28.7	25.2	23.0	24.2	0.0	22.4
Acetaldehyde	1.0	0.0	0.9	0.9	0.9	0.8	0.0	0.8
Diethyl ether	3.0	0.0	2.8	3.1	3.5	3.4	0.0	3.6

[a] *n*-butanol and *i*-butanol, [b] *n*-hexanol and *i*-hexanol, [c] *n*-octanol and *i*-octanol

The catalytic performances of catalyst were investigated under N_2 atmospheric pressure with a rate 160 mL/min at temperature 380 ˚C condition, which using contact time as 16.0 g.h/mol and run reaction for 8 h.

Table C9 Activity in Guerbet reaction over 6MgO/KNaX(Imp)

Time on stream (min)	60	120	180	240	300	360	420	480
Conversion (%)	14.0	12.4	10.1	9.8	9.6	8.8	9.0	9.2
Yield of product (%)								
Ethylene	0.6	0.6	0.6	0.6	0.6	0.6	0.6	0.6
Acetaldehyde	2.8	2.9	2.7	2.8	2.9	2.7	2.8	3.0
Butadiene	1.5	1.2	1.1	1.0	0.9	0.8	0.9	0.9
C_4-aldehyde	0.9	0.7	0.6	0.5	0.5	0.5	0.4	0.4
C_4-alcohols[(a)]	5.2	4.7	3.7	3.6	3.5	3.1	3.3	3.3
C_6-alcohols[(b)]	2.1	1.6	1.1	1.1	1.0	0.8	0.9	0.9
C_8-alcohols[(c)]	0.5	0.3	0.0	0.0	0.0	0.0	0.0	0.0

[(a)] *n*-butanol and *i*-butanol, [(b)] *n*-hexanol and *i*-hexanol, [(c)] *n*-octanol and *i*-octanol

The catalytic performances of catalyst were investigated under N_2 atmospheric pressure with a rate 160 mL/min at temperature 380 °C condition, which using contact time as 16.0 g.h/mol and run reaction for 8 h.

Table C10 Activity in Guerbet reaction over 5MgO/KNaX(PB)

Time on stream (min)	60	120	180	240	300	360	420	480
Conversion (%)	3.5	2.5	2.7	2.6	2.7	2.7	2.7	2.8
Yield of product (%)								
Ethylene	1.0	0.9	0.9	0.9	0.8	0.8	0.8	0.8
Acetaldehyde	1.1	1.1	1.3	1.2	1.3	1.2	1.2	1.3
Butadiene	0.1	0.1	0.1	0.1	0.1	0.1	0.1	0.1
C_4-aldehyde								
C_4-alcohols[(a)]	0.4	0.4	0.4	0.5	0.5	0.6	0.5	0.6
C_6-alcohols[(b)]								
C_8-alcohols[(c)]								

[(a)] *n*-butanol and *i*-butanol, [(b)] *n*-hexanol and *i*-hexanol, [(c)] *n*-octanol and *i*-octanol

The catalytic performances of catalyst were investigated under N_2 atmospheric pressure with a rate 160 mL/min at temperature 380 °C condition, which using contact time as 16.0 g.h/mol and run reaction for 8 h.

Table C11 Activity in Guerbet reaction over 5MgO/KNaX(St)

Time on stream (min)	60	120	180	240	300	360	420	480
Conversion (%)		12.8	11.8	11.5	10.5	10.2	10.4	10.0
Yield of product (%)								
Ethylene		1.0	1.0	1.0	1.0	1.0	1.0	1.0
Acetaldehyde		1.8	1.8	2.0	1.9	2.0	2.1	2.0
Butadiene		1.6	1.6	1.5	1.3	1.3	1.3	1.4
C_4-aldehyde		0.9	0.8	0.9	0.7	0.6	0.7	0.6
C_4-alcohols[(a)]		4.6	4.2	3.9	3.7	3.5	3.8	3.6
C_6-alcohols[(b)]		2.1	1.8	1.7	1.5	1.3	1.4	1.3
C_8-alcohols[(c)]		0.8	0.5	0.5	0.4	0.3	0.2	0.2

[(a)] *n*-butanol and *i*-butanol, [(b)] *n*-hexanol and *i*-hexanol, [(c)] *n*-octanol and *i*-octanol

The catalytic performances of catalyst were investigated under N_2 atmospheric pressure with a rate 160 mL/min at temperature 380 °C condition, which using contact time as 16.0 g.h/mol and run reaction for 8 h.

Table C12 Activity in Guerbet reaction over 5MgO/KNaX-cycle 2

Time on stream (min)	540	600	660	720	780	840	900	960
Conversion (%)	15.7	12.8	11.2	11.0	10.5	10.2	10.3	10.0
Yield of product (%)								
Ethylene	0.8	0.8	0.7	0.7	0.7	0.7	0.6	0.7
Acetaldehyde	1.9	2.1	2.1	2.2	2.2	2.2	2.3	2.4
Butadiene	1.5	1.2	1.1	1.0	1.0	0.9	0.9	0.9
C_4-aldehyde	1.4	1.0	0.9	0.9	0.8	0.8	0.7	0.7
C_4-alcohols[(a)]	5.7	4.6	4.0	4.0	3.9	3.7	3.9	3.7
C_6-alcohols[(b)]	2.9	2.0	1.6	1.5	1.4	1.4	1.4	1.2
C_8-alcohols[(c)]	1.5	1.2	0.8	0.8	0.5	0.4	0.5	0.4

[(a)] *n*-butanol and *i*-butanol, [(b)] *n*-hexanol and *i*-hexanol, [(c)] *n*-octanol and *i*-octanol

The catalytic performances of catalyst were investigated under N_2 atmospheric pressure with a rate 160 mL/min at temperature 380 °C condition, which using contact time as 16.0 g.h/mol and run reaction for 8 h.

Table C13 Activity in Guerbet reaction over 5MgO/KNaX-cycle 3

Time on stream (min)	1020	1080	1140	1200	1260	1320	1380	1440
Conversion (%)	14.1	12.2	11.0	11.2	10.1	9.9	9.5	9.8
Yield of product (%)								
Ethylene	0.9	0.8	0.8	0.7	0.7	0.7	0.7	0.6
Acetaldehyde	2.0	2.2	2.2	1.9	2.3	2.3	2.3	2.3
Butadiene	1.6	1.3	1.1	1.0	1.0	1.0	0.9	0.9
C_4-aldehyde	1.9	1.0	0.9	0.9	0.8	0.7	0.7	0.7
C_4-alcohols[(a)]	4.9	4.1	3.8	4.1	3.5	3.6	3.4	3.7
C_6-alcohols[(b)]	2.3	1.9	1.5	1.7	1.3	1.2	1.2	1.2
C_8-alcohols[(c)]	0.7	0.9	0.7	0.8	0.5	0.5	0.3	0.4

[(a)] *n*-butanol and *i*-butanol, [(b)] *n*-hexanol and *i*-hexanol, [(c)] *n*-octanol and *i*-octanol

The catalytic performances of catalyst were investigated under N_2 atmospheric pressure with a rate 160 mL/min at temperature 380 °C condition, which using contact time as 16.0 g.h/mol and run reaction for 8 h.

Table C14 Activity in Guerbet reaction over 6MgO/KNaX

Time on stream (min)	60	120	180	240	300	360	420	480
Conversion (%)	38.8	31.9	29.2	26.2	24.1	0.0	0.0	0.0
Yield of product (%)								
Ethylene	1.0	1.0	1.0	0.9	0.9	0.0	0.0	0.0
Acetaldehyde	1.1	1.5	1.7	1.8	1.9	0.0	0.0	0.0
Butadiene	3.8	2.9	2.6	2.3	2.0	0.0	0.0	0.0
C_4-aldehyde	2.4	2.0	1.9	1.6	1.5	0.0	0.0	0.0
C_4-alcohols[(a)]	17.9	14.8	13.4	12.5	10.5	0.0	0.0	0.0
C_6-alcohols[(b)]	7.3	5.5	4.8	4.6	4.5	0.0	0.0	0.0
C_8-alcohols[(c)]	2.5	2.0	1.8	1.3	1.4	0.0	0.0	0.0
C_{10}-alcohols[(d)]	2.7	2.1	2.0	1.2	1.4	0.0	0.0	0.0

[(a)] *n*-butanol and *i*-butanol, [(b)] *n*-hexanol and *i*-hexanol, [(c)] *n*-octanol and *i*-octanol, [(d)] *n*-decanol

The catalytic performances of catalyst were investigated under N_2 atmospheric pressure with a rate 160 mL/min at temperature 380 °C condition, which using contact time as 48.0 g.h/mol and run reaction for 5 h.

APPENDIX D

CATALYTIC TIME ON STEAM PROFILES

The time on steam profiles of all catalysts was reported under N_2 atmospheric pressure with a rate 160 mL/min at temperature 380 ˚C condition, which using contact time as 16.0 g.h/mol. Except, Figure D14 was shown only profile of contact time as 48.0 g.h/mol, those data can be seen below respectively.

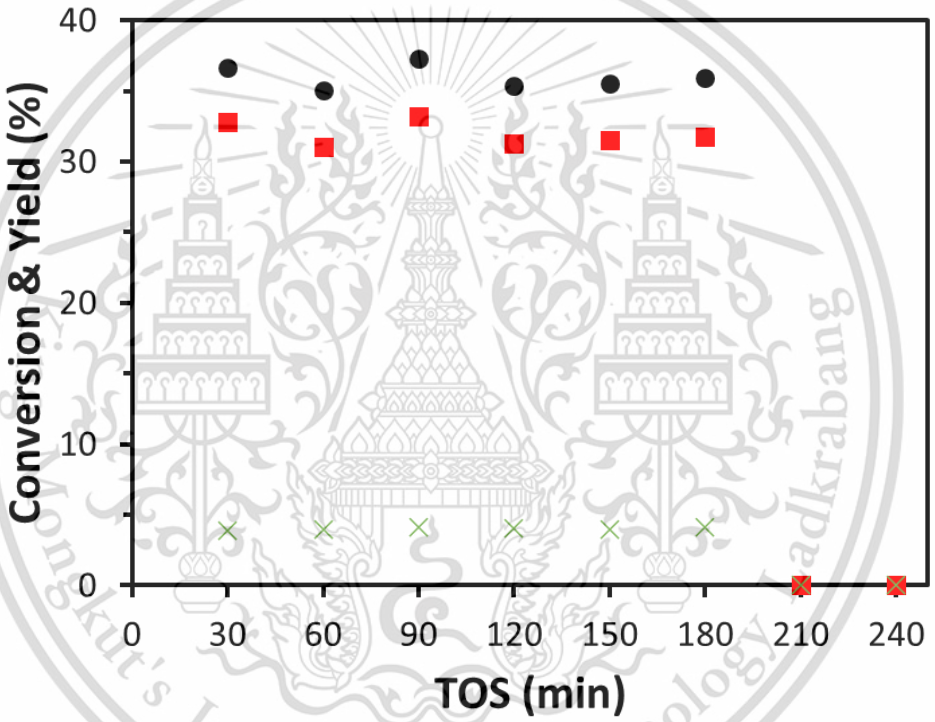

Figure D1 Time on steam profile over NaX

(●) Ethanol conversion, (■) Ethylene and (X) Diethyl ether

The catalytic performances of catalyst were investigated under N_2 atmospheric pressure with a rate 160 mL/min at temperature 380 ˚C condition, which using contact time as 16.0 g.h/mol and run reaction for 3 h.

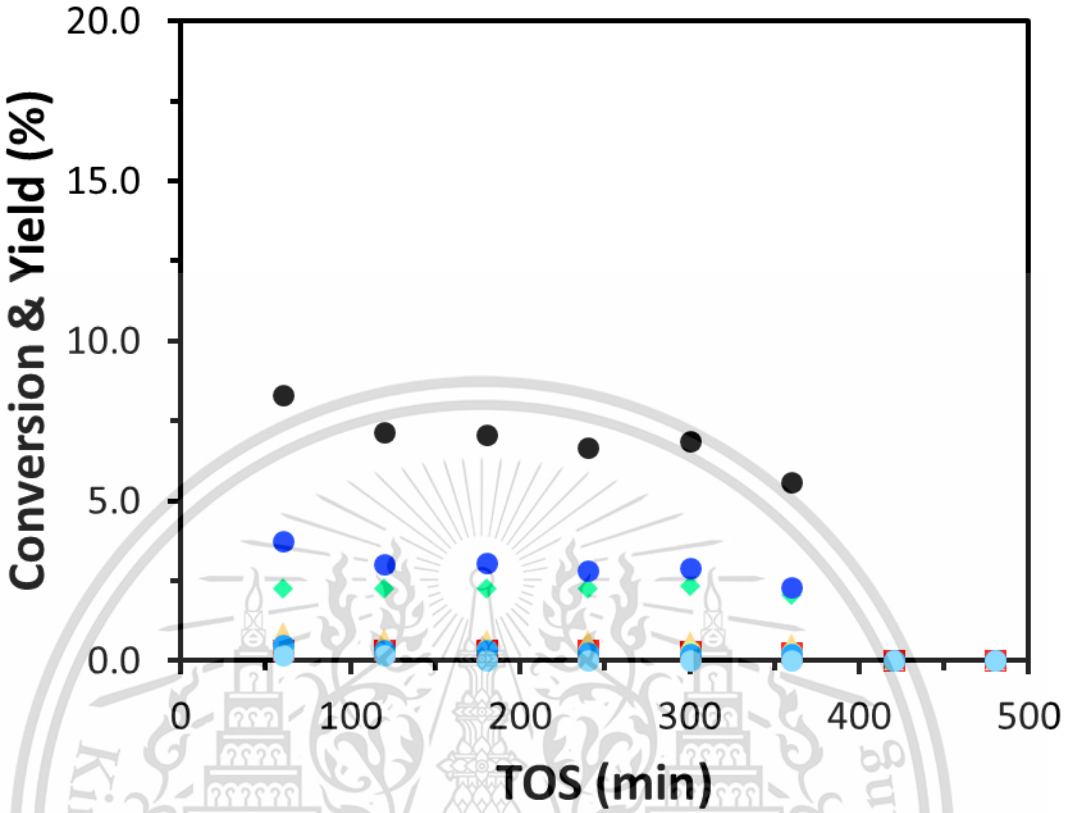

Figure D2 Time on steam profile over KNaX

(●) Ethanol conversion, (■) Ethylene, (◆) Acetaldehyde, (▲) butadiene, (●) C4-aldehyde, (●) C4-alcohol, (●) C6-alcohol, and (●) C8-alcohol

The catalytic performances of catalyst were investigated under N_2 atmospheric pressure with a rate 160 mL/min at temperature 380 °C condition, which using contact time as 16.0 g.h/mol and run reaction for 8 h.

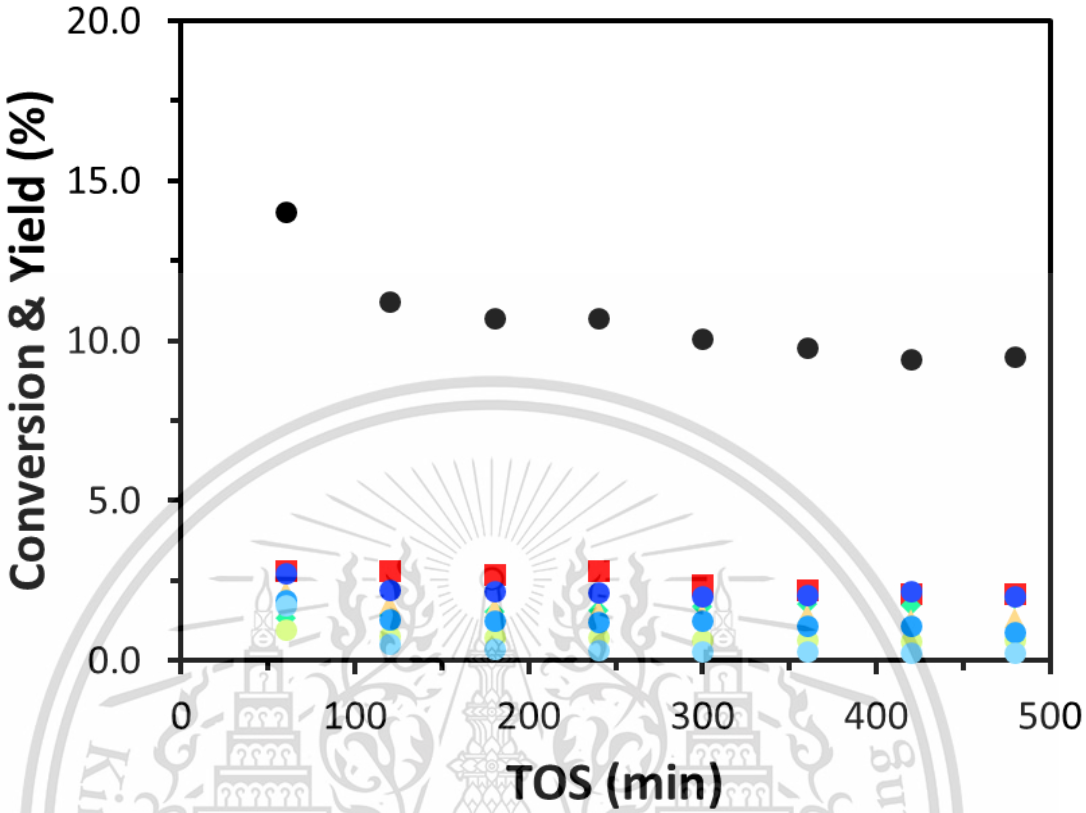

Figure D3 Time on steam profile over 4MgO/KNaX

(●) Ethanol conversion, (■) Ethylene, (◆) Acetaldehyde, (▲) butadiene, (●) C4-aldehyde, (●) C4-alcohol, (●) C6-alcohol, and (●) C8-alcohol

The catalytic performances of catalyst were investigated under N_2 atmospheric pressure with a rate 160 mL/min at temperature 380 °C condition, which using contact time as 16.0 g.h/mol and run reaction for 8 h.

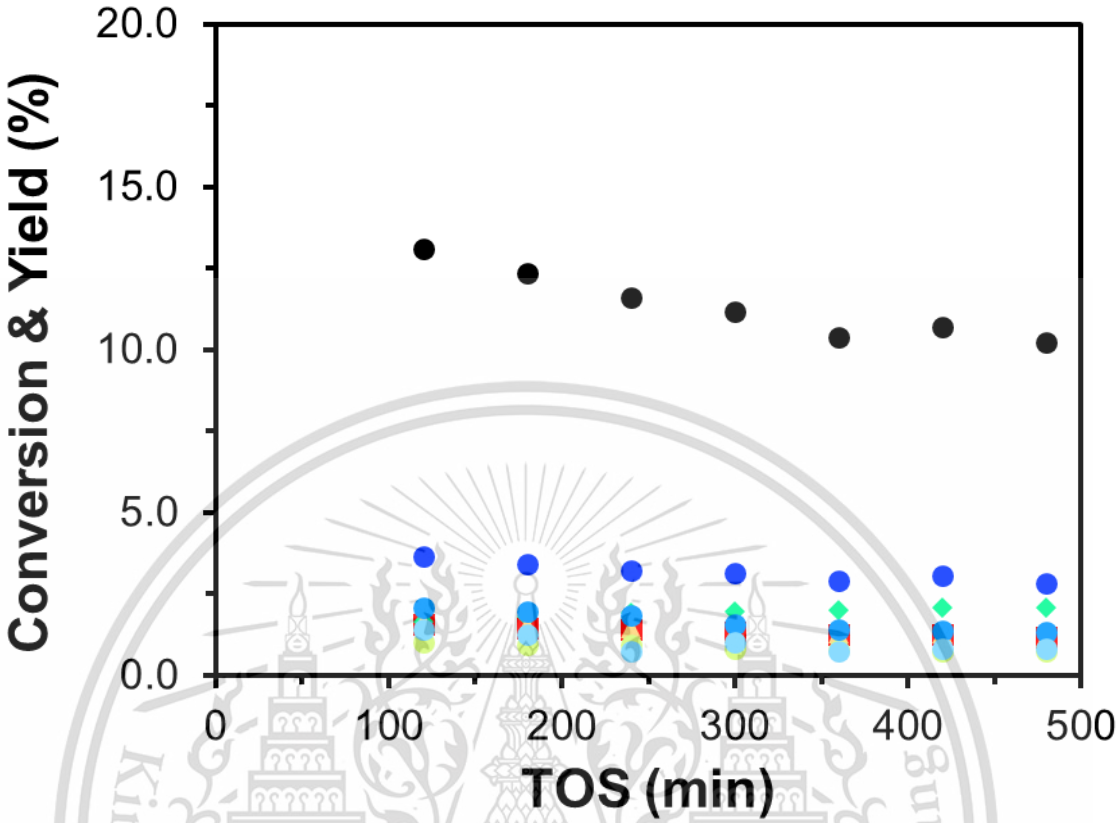

Figure D4 Time on steam profile over 5MgO/KNaX (●) Ethanol conversion, (■) Ethylene, (◆) Acetaldehyde, (▲) butadiene, (●) C4-aldehyde, (●) C4-alcohol, (●) C6-alcohol, and (●) C8-alcohol

The catalytic performances of catalyst were investigated under N_2 atmospheric pressure with a rate 160 mL/min at temperature 380 ˚C condition, which using contact time as 16.0 g.h/mol and run reaction for 8 h.

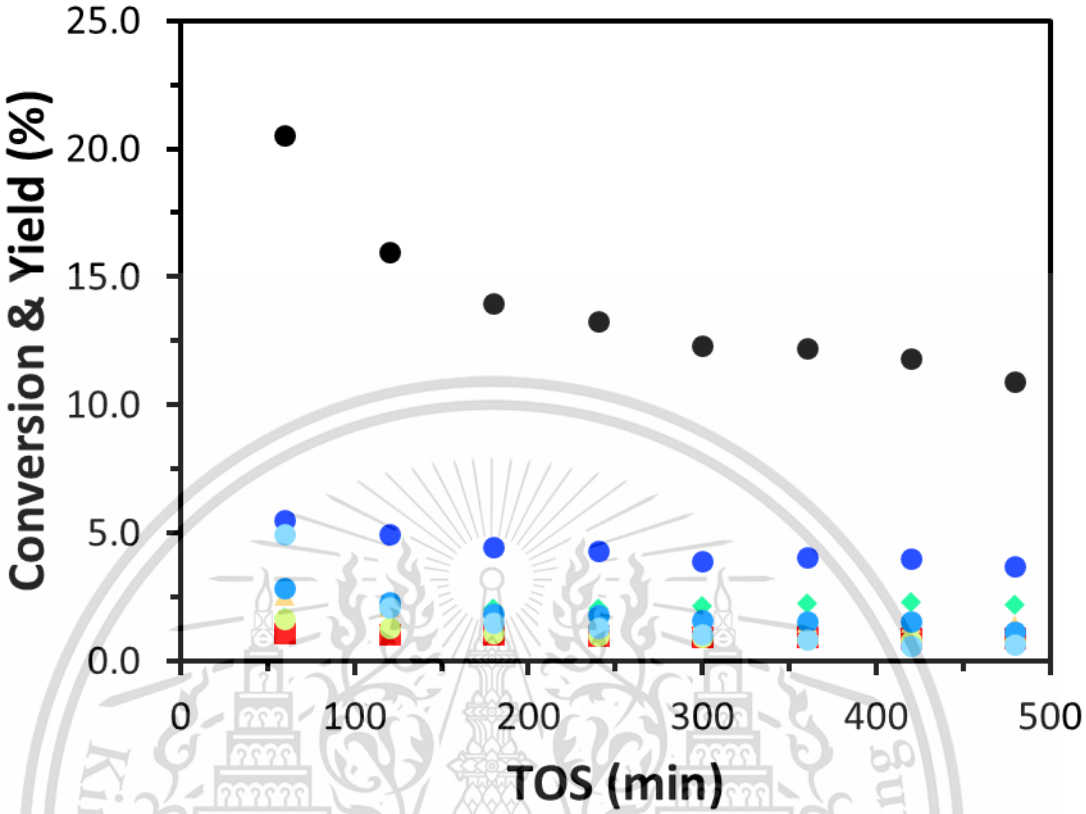

Figure D5 Time on steam profile over 6MgO/KNaX

(●) Ethanol conversion, (■) Ethylene, (◆) Acetaldehyde, (▲) butadiene, (●) C4-aldehyde, (●) C4-alcohol, (●) C6-alcohol, and (●) C8-alcohol

The catalytic performances of catalyst were investigated under N_2 atmospheric pressure with a rate 160 mL/min at temperature 380 °C condition, which using contact time as 16.0 g.h/mol and run reaction for 8 h.

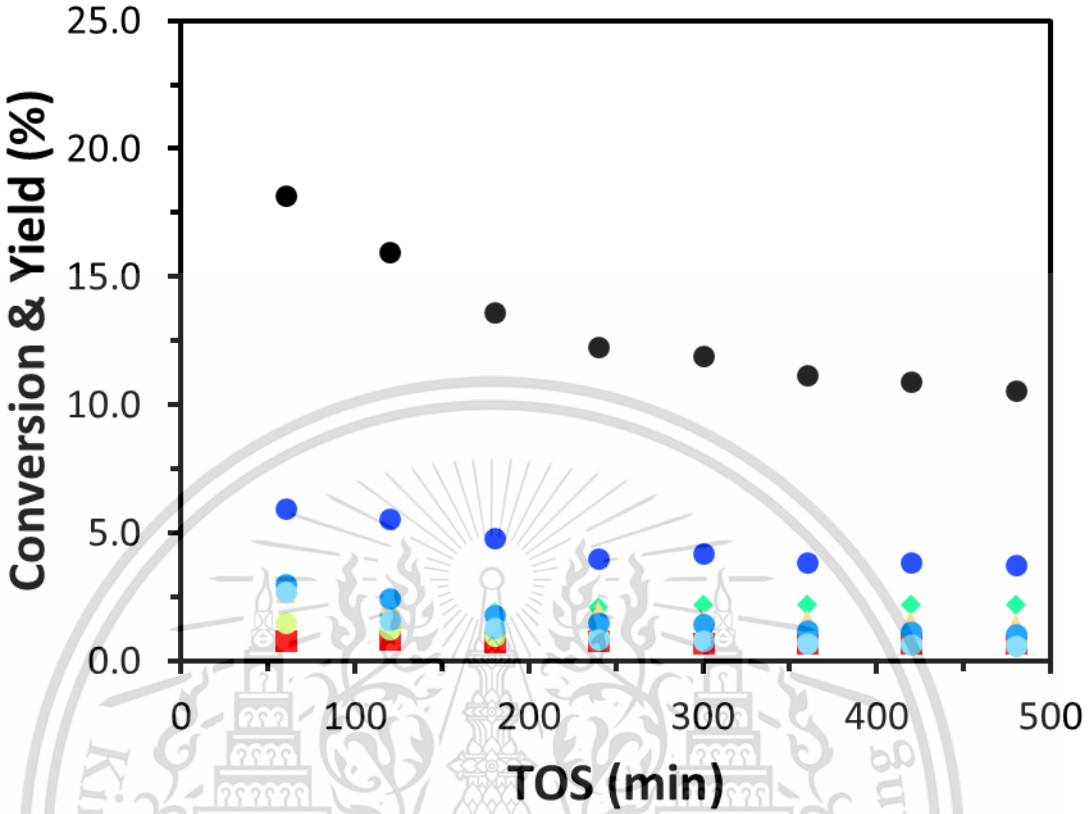

Figure D6 Time on steam profile over 7MgO/KNaX

(●) Ethanol conversion, (■) Ethylene, (◆) Acetaldehyde, (▲) butadiene, (●) C4-aldehyde, (●) C4-alcohol, (●) C6-alcohol, and (●) C8-alcohol

The catalytic performances of catalyst were investigated under N_2 atmospheric pressure with a rate 160 mL/min at temperature 380 °C condition, which using contact time as 16.0 g.h/mol and run reaction for 8 h.

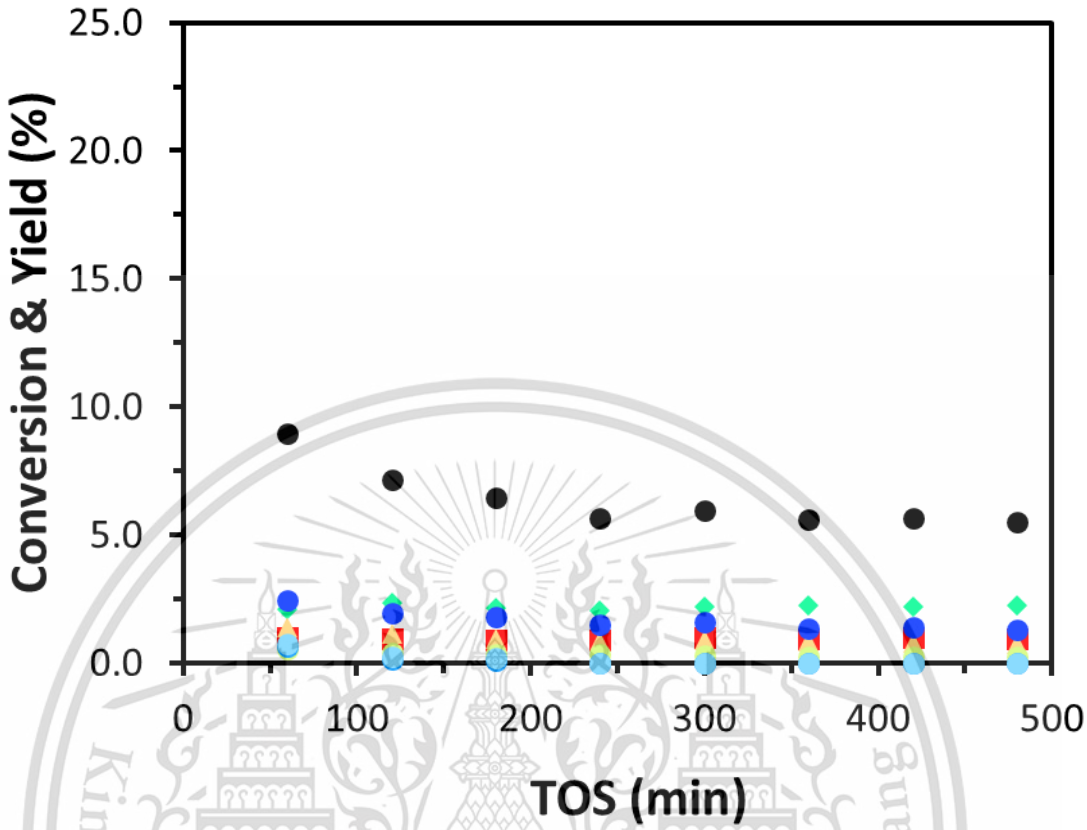

Figure D7 Time on steam profile over 8MgO/KNaX

(●) Ethanol conversion, (■) Ethylene, (◆) Acetaldehyde, (▲) butadiene, (●) C4-aldehyde, (●) C4-alcohol, (●) C6-alcohol, and (●) C8-alcohol

The catalytic performances of catalyst were investigated under N_2 atmospheric pressure with a rate 160 mL/min at temperature 380 °C condition, which using contact time as 16.0 g.h/mol and run reaction for 8 h.

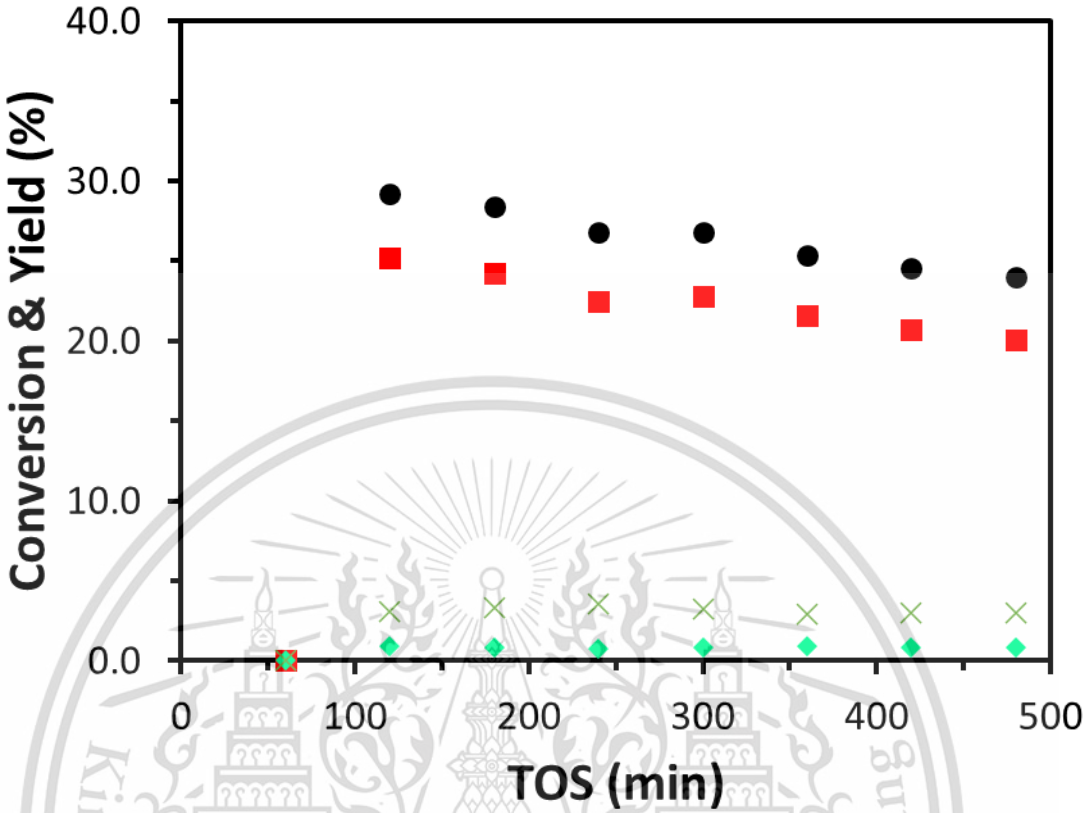

Figure D8 Time on steam profile over MgKNaX

(●) Ethanol conversion, (■) Ethylene, (◆) Acetaldehyde, (▲) butadiene, (●) C4-aldehyde, (●) C4-alcohol, (●) C6-alcohol, and (●) C8-alcohol

The catalytic performances of catalyst were investigated under N_2 atmospheric pressure with a rate 160 mL/min at temperature 380 °C condition, which using contact time as 16.0 g.h/mol and run reaction for 8 h.

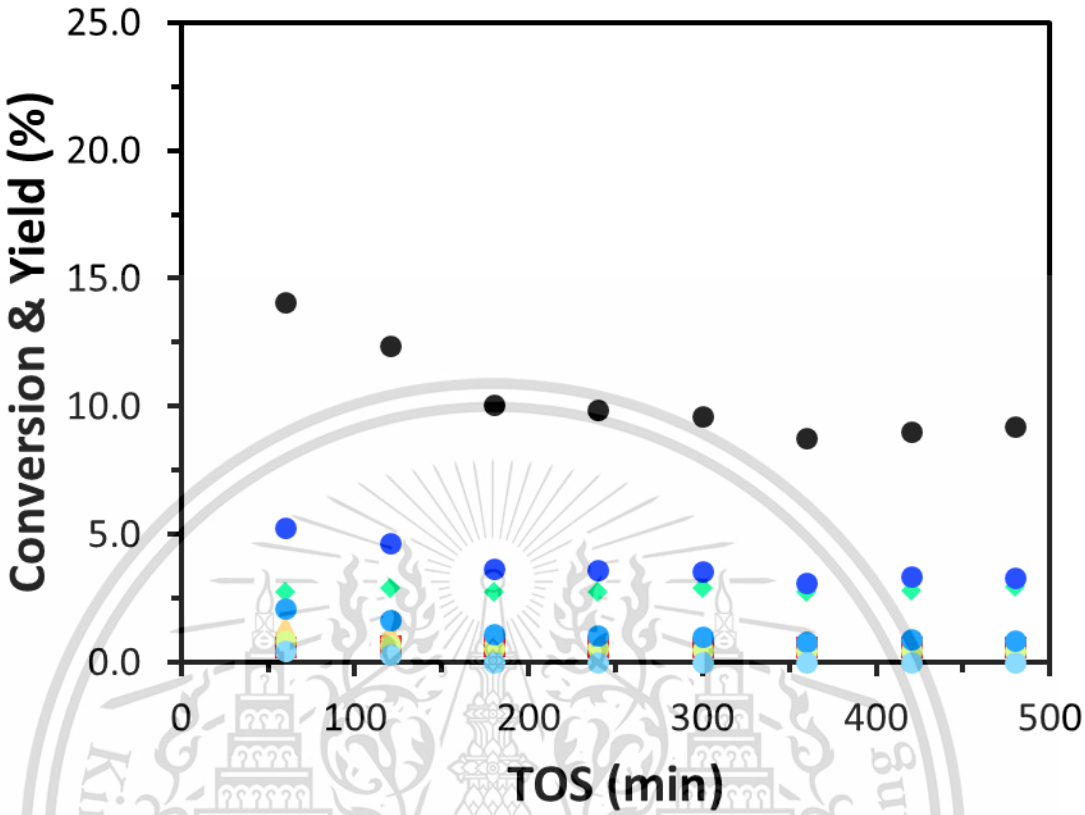

Figure D9 Time on steam profile over 6MgO/KNaX(Imp).

(●) Ethanol conversion, (■) Ethylene, (◆) Acetaldehyde, (▲) butadiene, (●) C4-aldehyde, (●) C4-alcohol, (●) C6-alcohol, and (●) C8-alcohol

The catalytic performances of catalyst were investigated under N_2 atmospheric pressure with a rate 160 mL/min at temperature 380 °C condition, which using contact time as 16.0 g.h/mol and run reaction for 8 h.

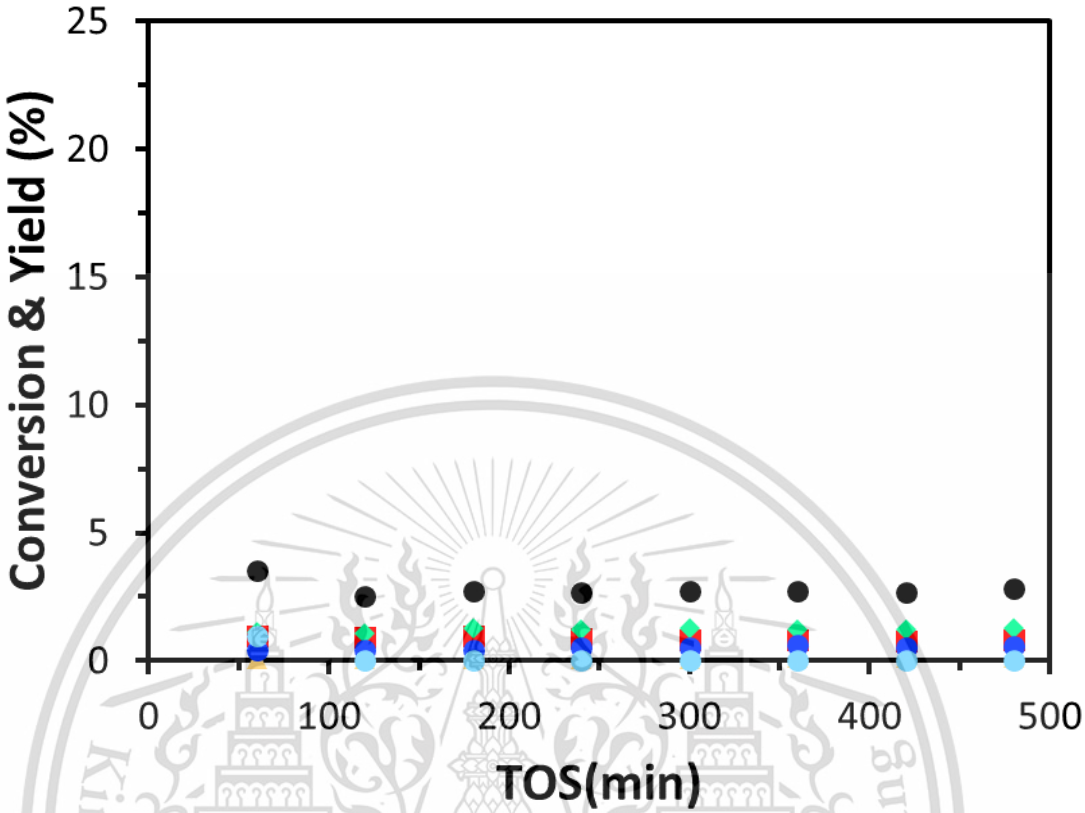

Figure D10 Time on steam profile over 5MgO/KNaX(PB).

(●) Ethanol conversion, (■) Ethylene, (◆) Acetaldehyde, (▲) butadiene, (●) C4-aldehyde, (●) C4-alcohol, (●) C6-alcohol, and (●) C8-alcohol

The catalytic performances of catalyst were investigated under N_2 atmospheric pressure with a rate 160 mL/min at temperature 380 °C condition, which using contact time as 16.0 g.h/mol and run reaction for 8 h.

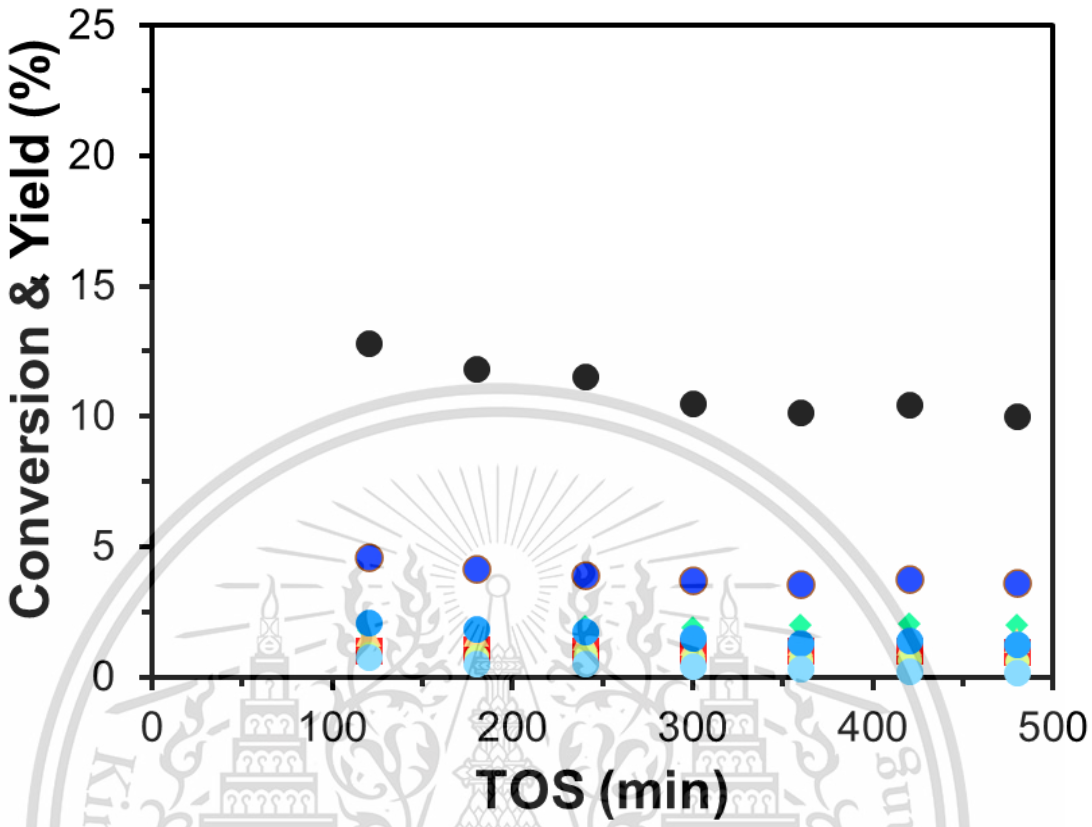

Figure D11 Time on steam profile over 5MgO/KNaX(St).

(●) Ethanol conversion, (■) Ethylene, (◆) Acetaldehyde, (▲) butadiene, (●) C4-aldehyde, (●) C4-alcohol, (●) C6-alcohol, and (●) C8-alcohol

The catalytic performances of catalyst were investigated under N_2 atmospheric pressure with a rate 160 mL/min at temperature 380 °C condition, which using contact time as 16.0 g.h/mol and run reaction for 8 h.

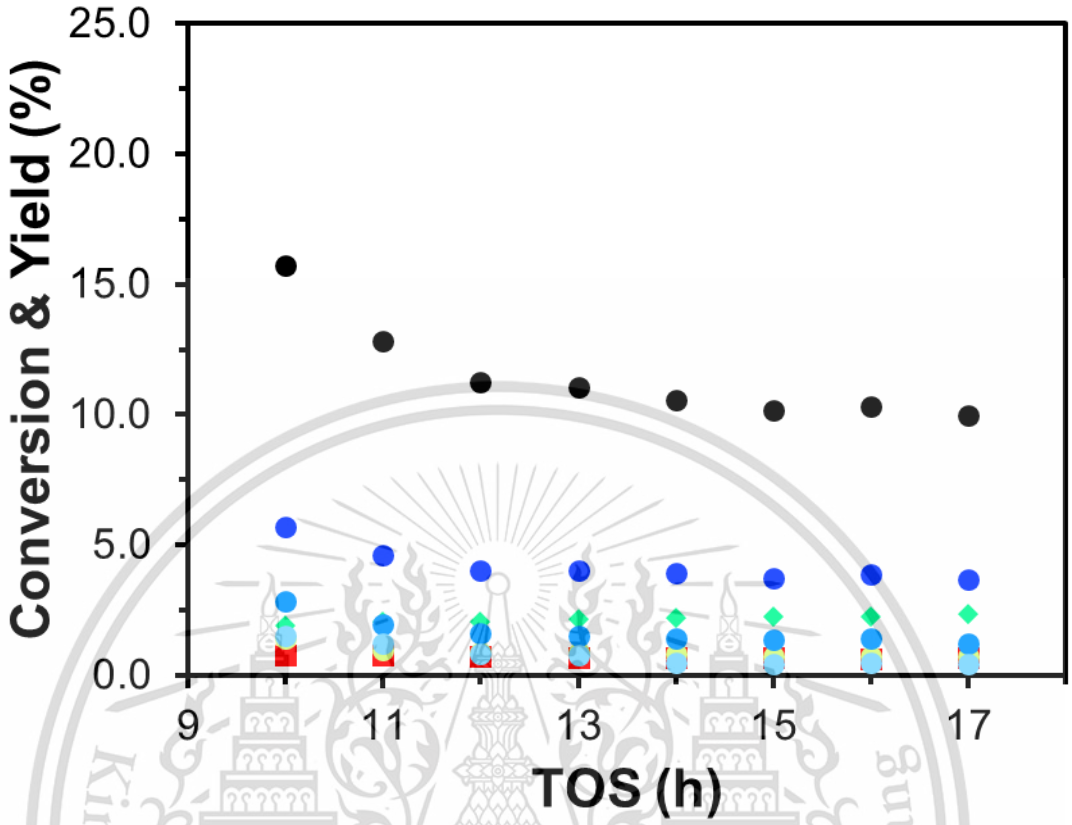

Figure D12 Time on steam profile over 6MgO/KNaX cycle2.

(●) Ethanol conversion, (■) Ethylene, (◆) Acetaldehyde, (▲) butadiene, (●) C4-aldehyde, (●) C4-alcohol, (●) C6-alcohol, and (●) C8-alcohol

The catalytic performances of catalyst were investigated under N_2 atmospheric pressure with a rate 160 mL/min at temperature 380 °C condition, which using contact time as 16.0 g.h/mol and run reaction for 8 h.

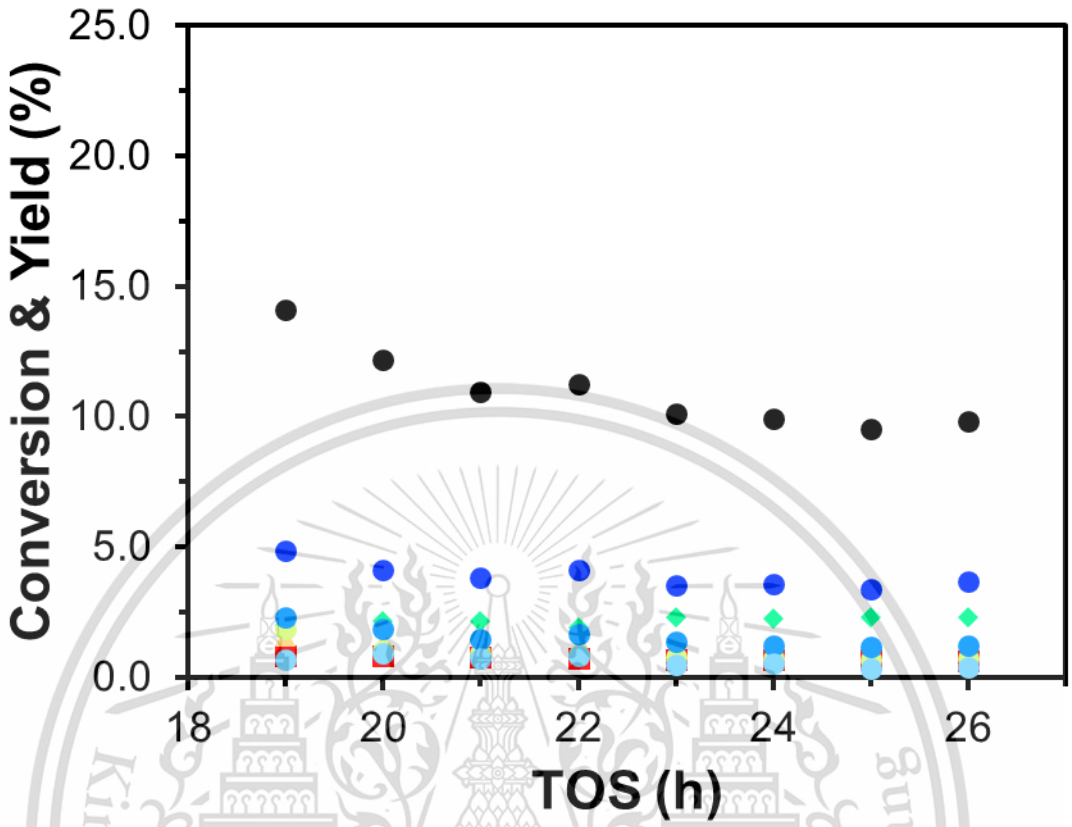

Figure D13 Time on steam profile over 6MgO/KNaX cycle3.

(●) Ethanol conversion, (■) Ethylene, (◆) Acetaldehyde, (▲) butadiene, (●) C4-aldehyde, (●) C4-alcohol, (●) C6-alcohol, and (●) C8-alcohol

The catalytic performances of catalyst were investigated under N_2 atmospheric pressure with a rate 160 mL/min at temperature 380 °C condition, which using contact time as 16.0 g.h/mol and run reaction for 8 h.

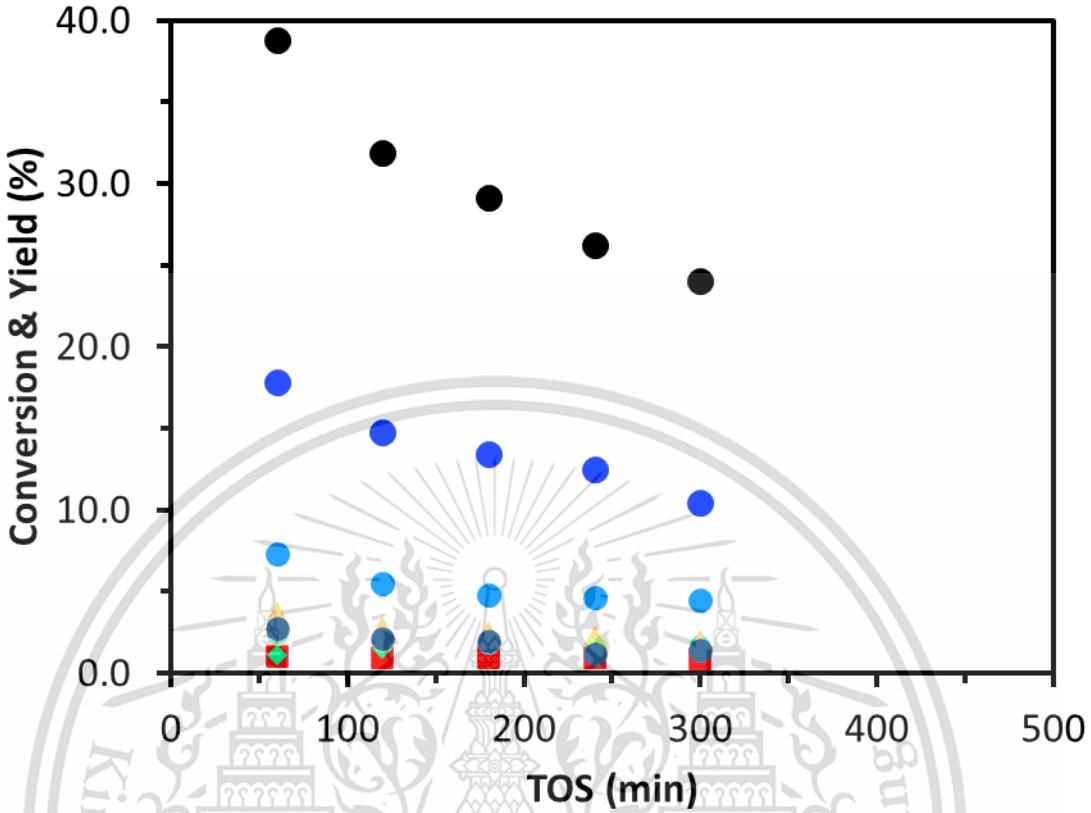

Figure D14 Time on steam profile over 6MgO/KNaX

(●) Ethanol conversion, (■) Ethylene, (◆) Acetaldehyde, (▲) butadiene, (●) C4-aldehyde, (●) C4-alcohol, (●) C6-alcohol, (●) C8-alcohol and (●) C10-alcohol

The catalytic performances of catalyst were investigated under N_2 atmospheric pressure with a rate 160 mL/min at temperature 380 ˚C condition, which using contact time as 48.0 g.h/mol and run reaction for 5 h.

APPENDIX E

Temperature profile of NH_3- and CO_2-TPD

More detail, after the sample was activated with air zero (30 ml/min) for an hour. Then, waiting the reactor was cooled to 30 ˚C, then adsorption with NH_3 or CO_2 gas at least 1 h, for emphasize that the sample was adsorption to maximum point. Continuously, this sample was thoroughly flushed with reference gas until the baseline is stable (approximate 1 h in this work). Afterward, the sample was heated using rate 10 ˚C/min up to 900 ˚C and hold for an hour, which recorded the signal at 50-900 ˚C. Finally, this sample was pulsed with standard gas during hold time at 900 ˚C, as follow the time profile below.

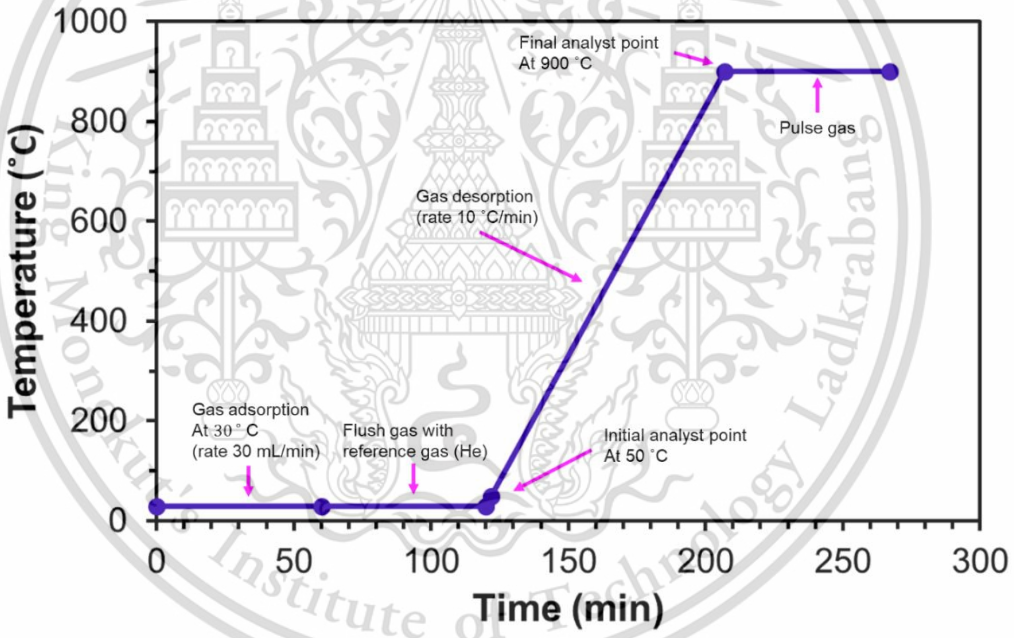

Figure E1 Analysis temperature profile of NH_3- and CO_2-TPD.

APPENDIX F

N_2 physisorption isotherm of all catalysts.

More detail, the samples were necessary calcined before analysis process. Surface area of the catalysts was measured via a gas absorption analyzer (Quantachrome Autosorb-1). Nitrogen (N_2) was used as probe molecules. The sample weight approximate 0.03-0.05 g was putted in sample cell, then attached to the outgassing station equipped and activated this sample to cleaning by vacuum at 300 ˚C. Until the sample was completely outgases process. The cell was filled by nitrogen then moved to analysis station rapidly. Adsorption isotherm was measured in a pressure range of 10-6 to 1.0 P/P_0 at -203 ˚C cooling by liquid nitrogen. After the analysis, the cell was uninstalled and closed immediately. The cell with catalyst was weighted and compared to the blank cell for certain amount of catalyst without humidity. The surface area of the catalysts was calculated by using Brunauer, Emmett, and Teller equation (BET). The N_2 physisorption isotherm of all catalysts was presence below.

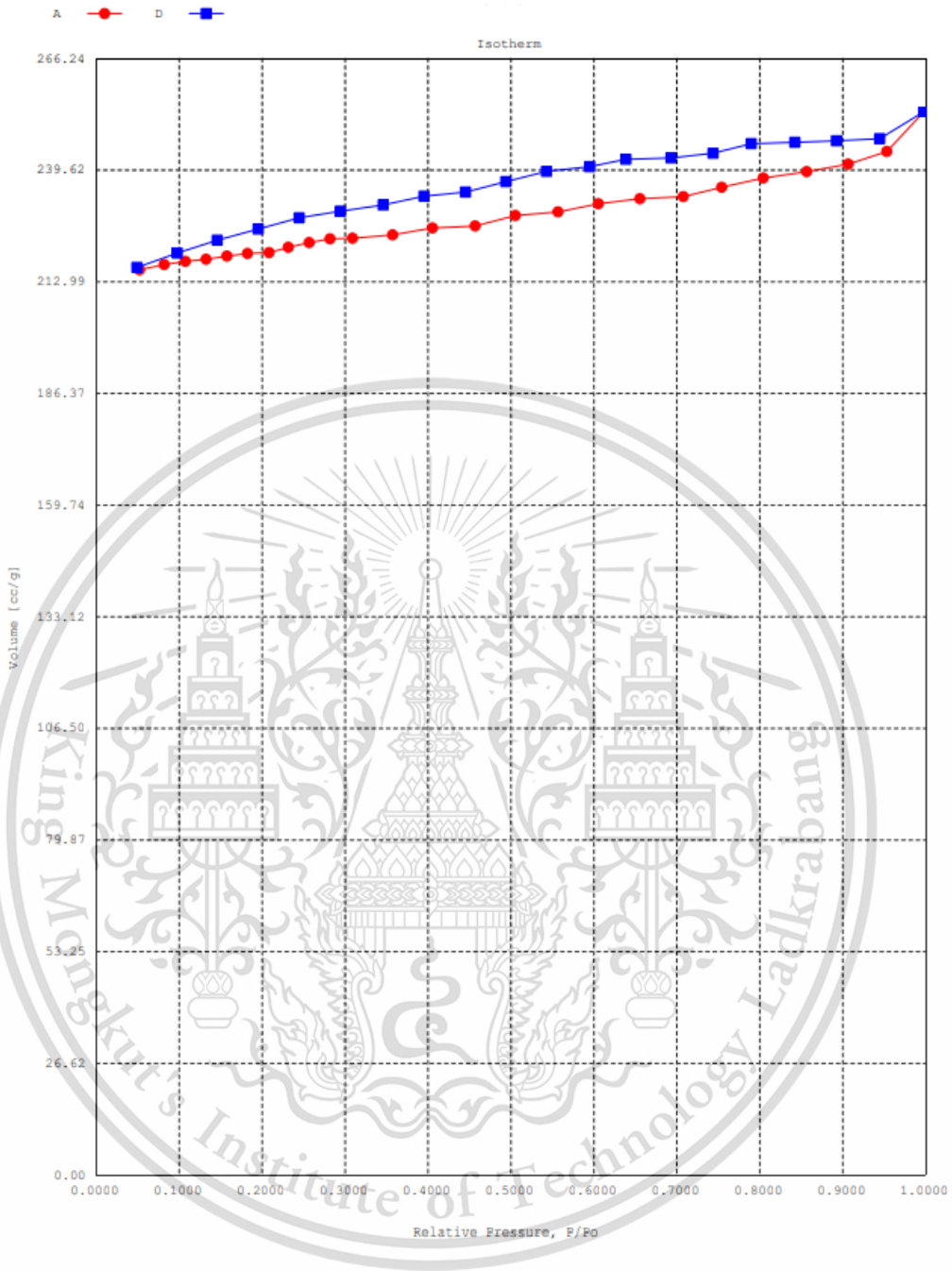

Figure F1 N_2 adsorption-desorption isotherm of NaX

Sample weight after out gases: 0.038 g and analysis time: 380.1 min.

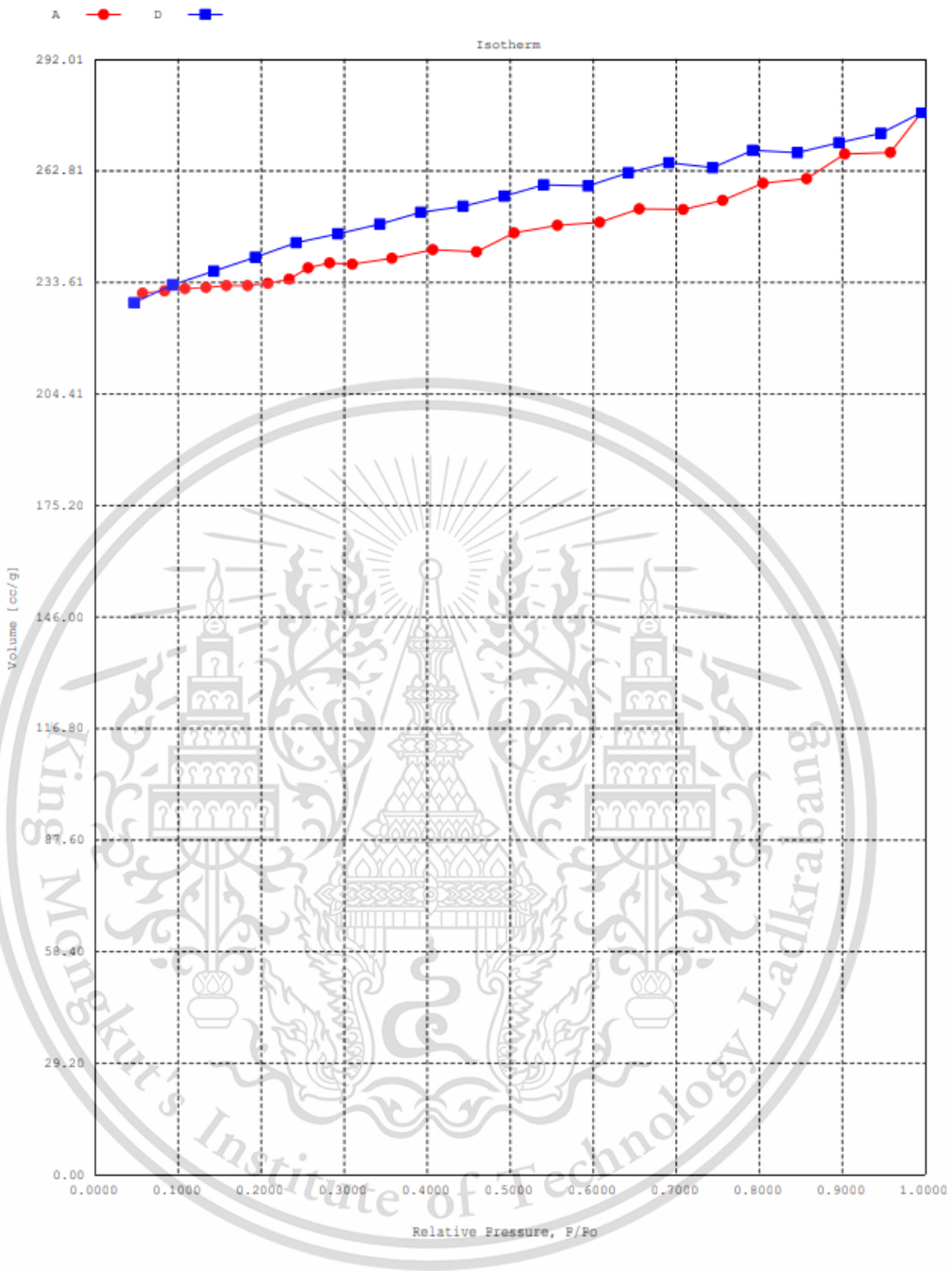

Figure F2 N_2 adsorption-desorption isotherm of KNaX

Sample weight after out gases: 0.018 g and analysis time: 367.9 min.

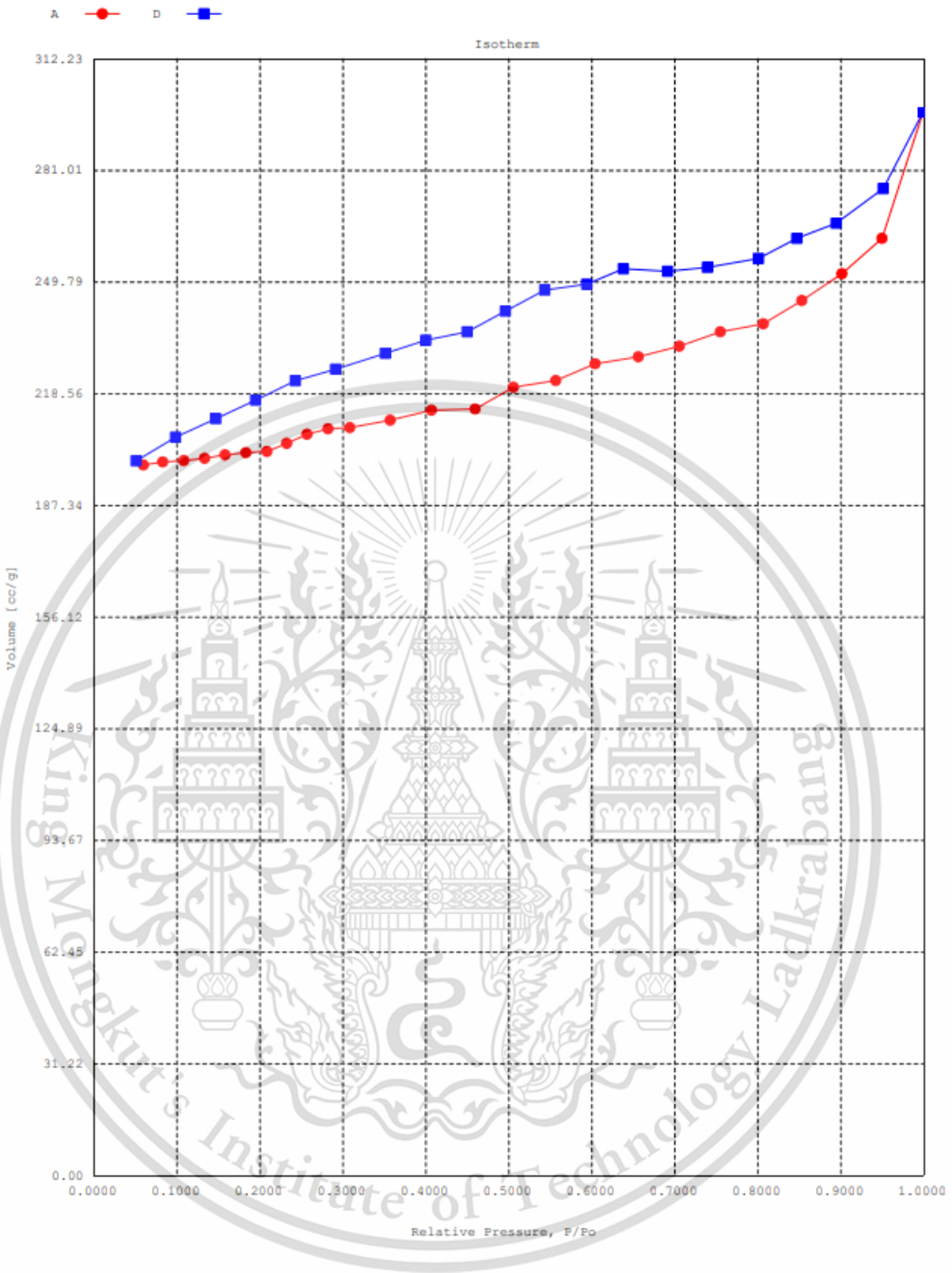

Figure F3 N_2 adsorption-desorption isotherm of 4MgO/KNaX

Sample weight after out gases: 0.0197 g and analysis time: 387.0 min.

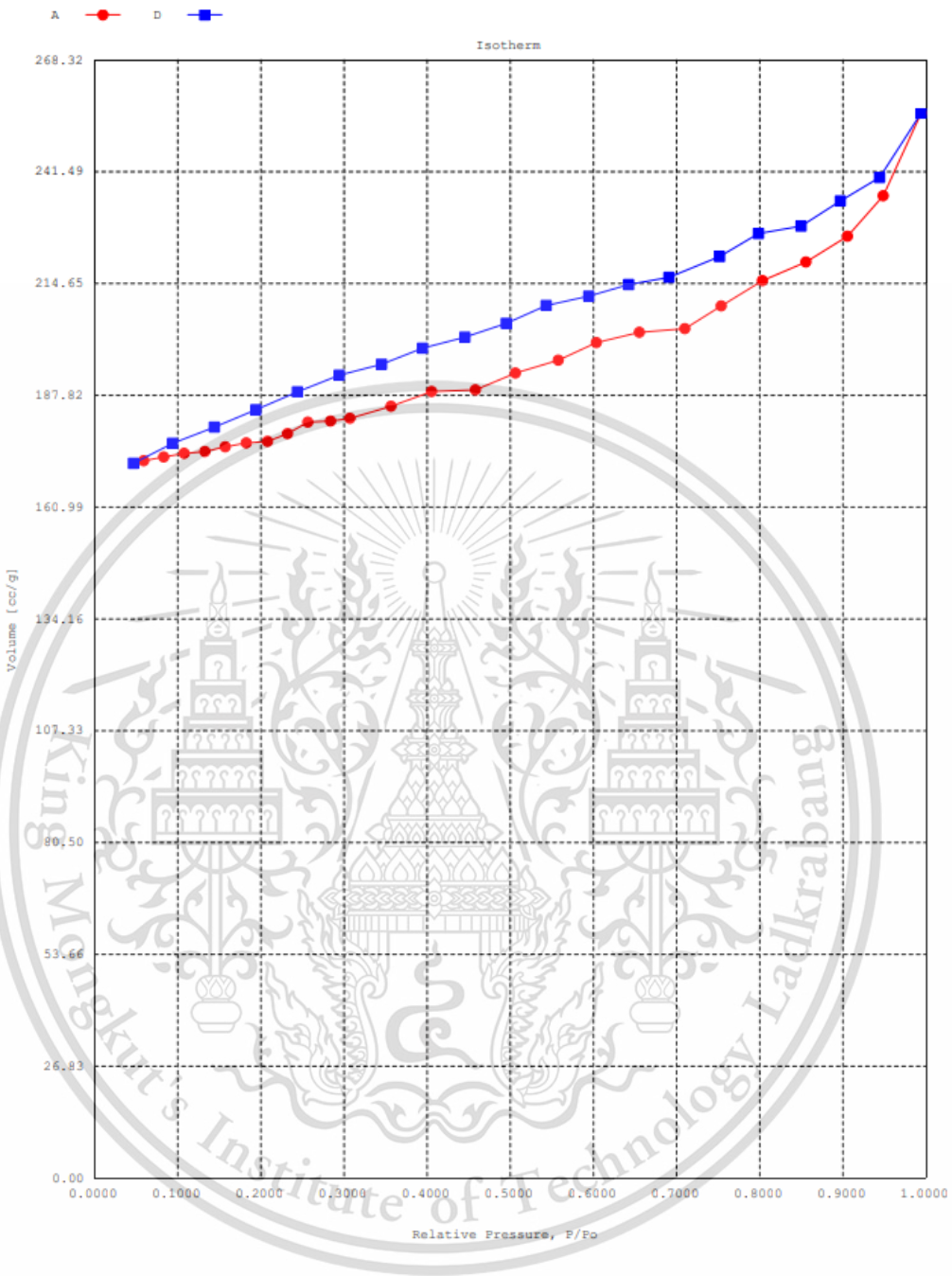

Figure F4 N_2 adsorption-desorption isotherm of 5MgO/KNaX

Sample weight after out gases: 0.0214 g and analysis time: 377.1 min.

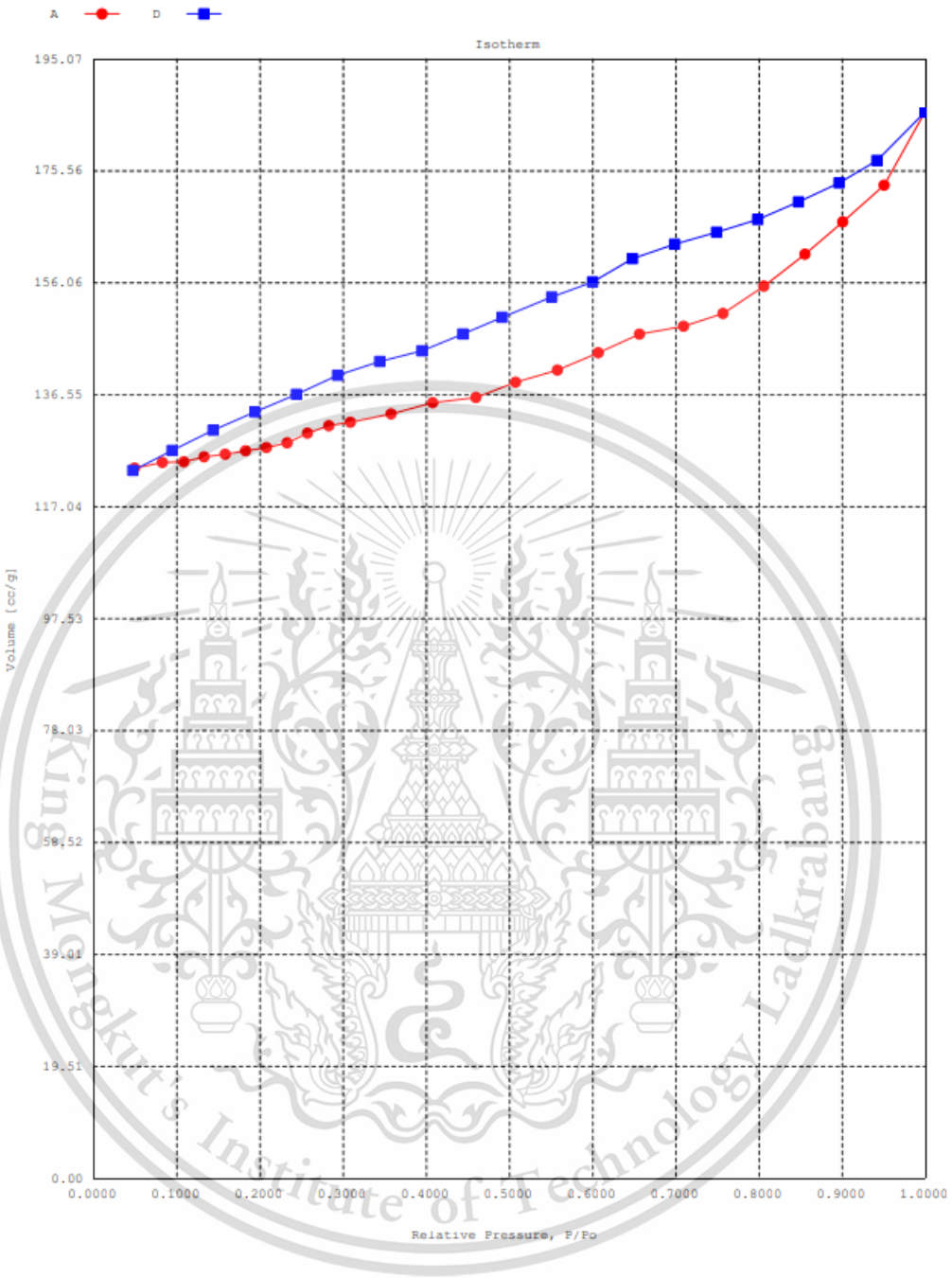

Figure F5 N_2 adsorption-desorption isotherm of 6MgO/KNaX

Sample weight after out gases: 0.0273 g and analysis time: 376.7 min.

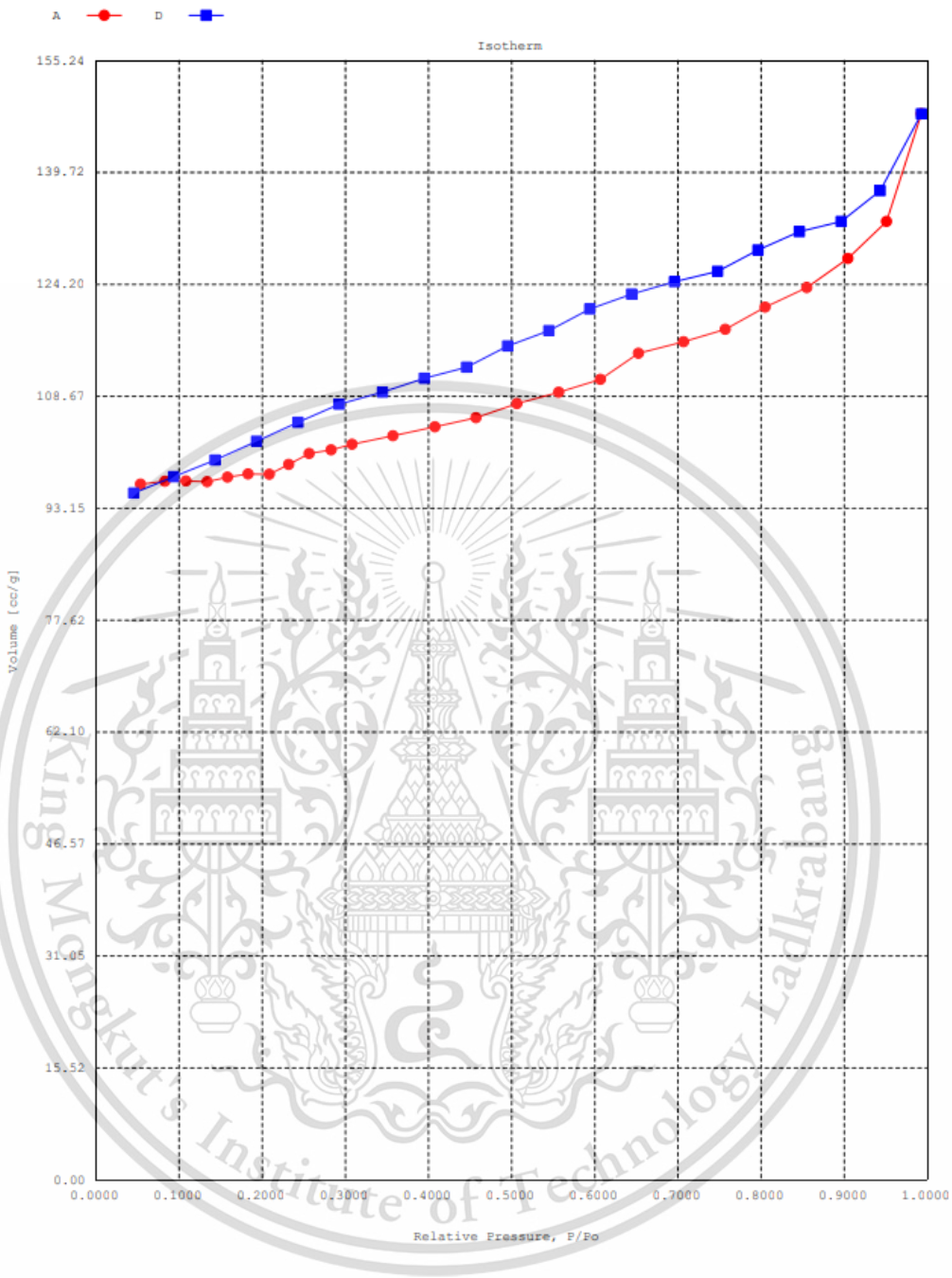

Figure F6 N_2 adsorption-desorption isotherm of 7MgO/KNaX

Sample weight after out gases: 0.0319 g and analysis time: 370.2 min.

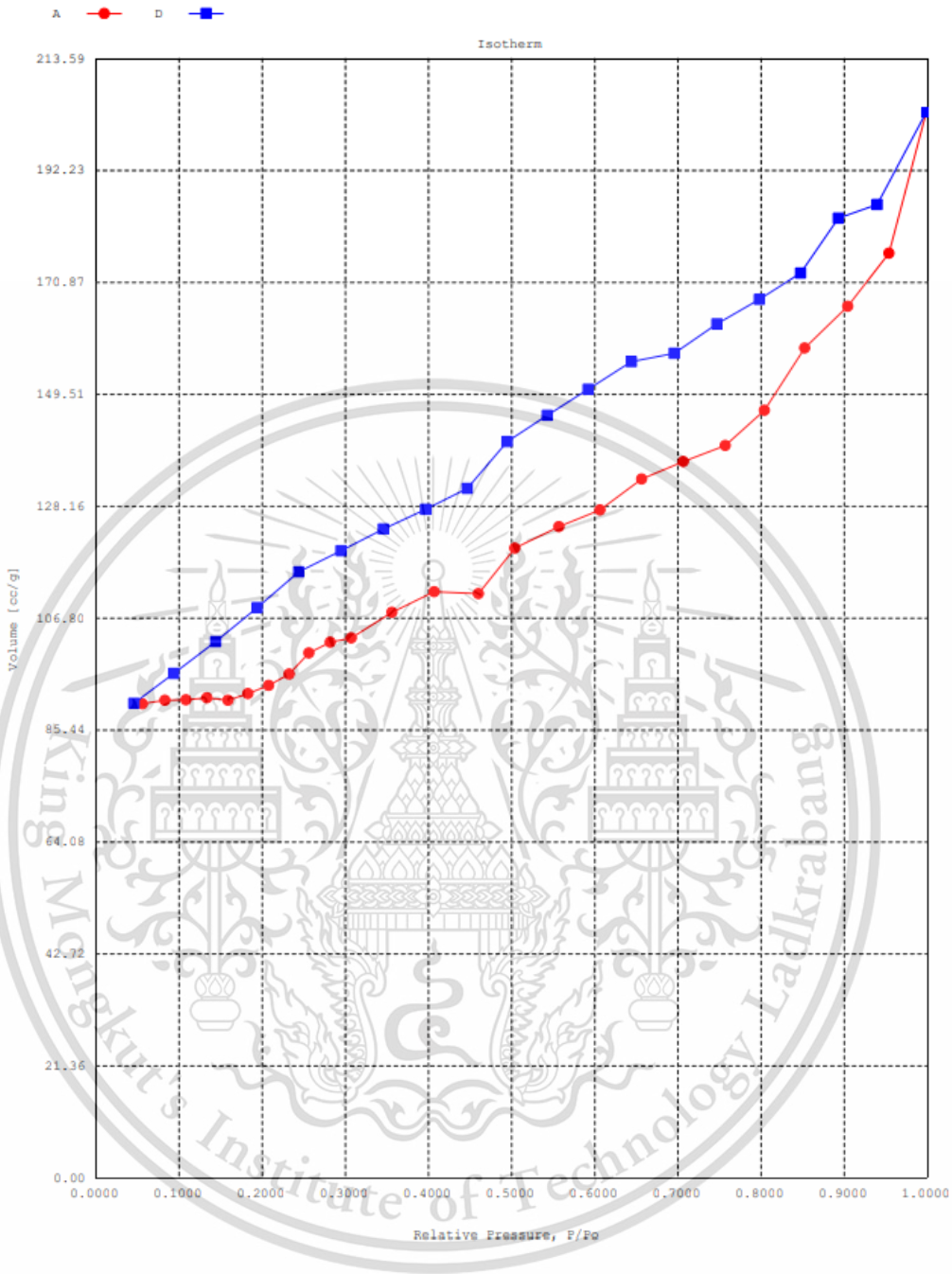

Figure F7 N_2 adsorption-desorption isotherm of 8MgO/KNaX

Sample weight after out gases: 0.0125 g and analysis time: 364.2 min.

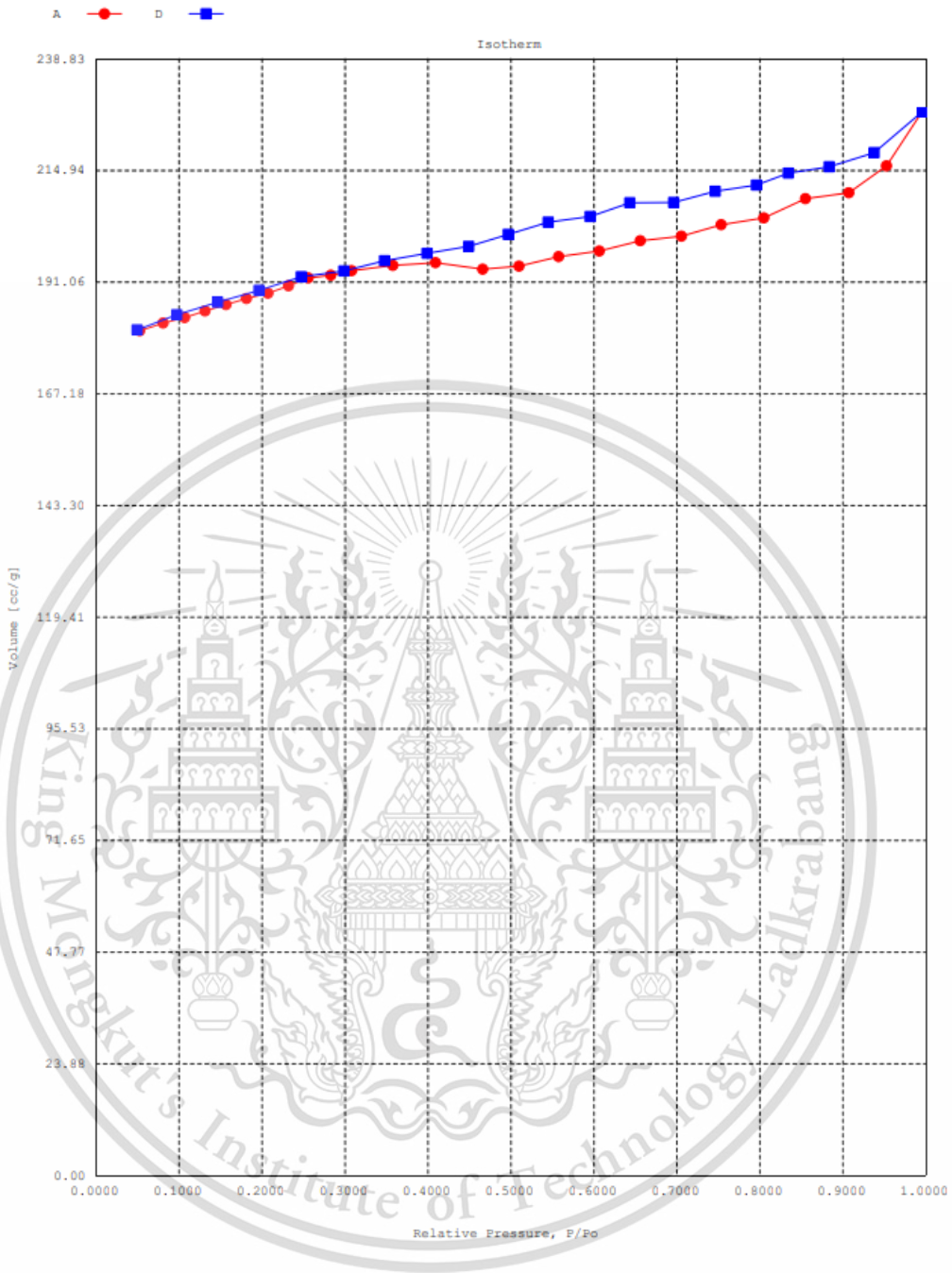

Figure F8 N_2 adsorption-desorption isotherm of MgKNaX

Sample weight after out gases: 0.0441 g and analysis time: 409.0 min.

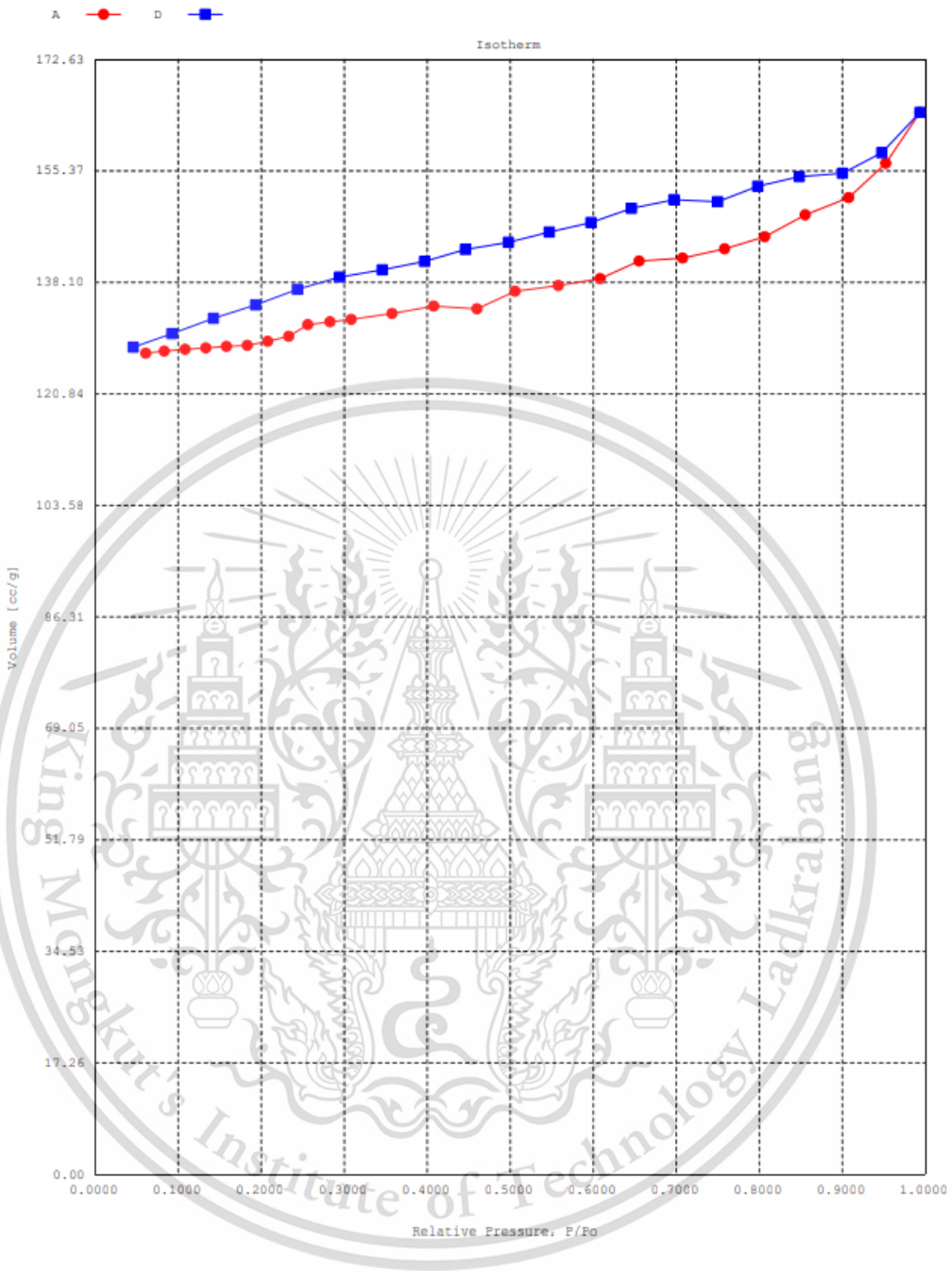

Figure F9 N_2 adsorption-desorption isotherm of 6MgO/KNaX(Imp)

Sample weight after out gases: 0.0261 g and analysis time: 401.6 min.

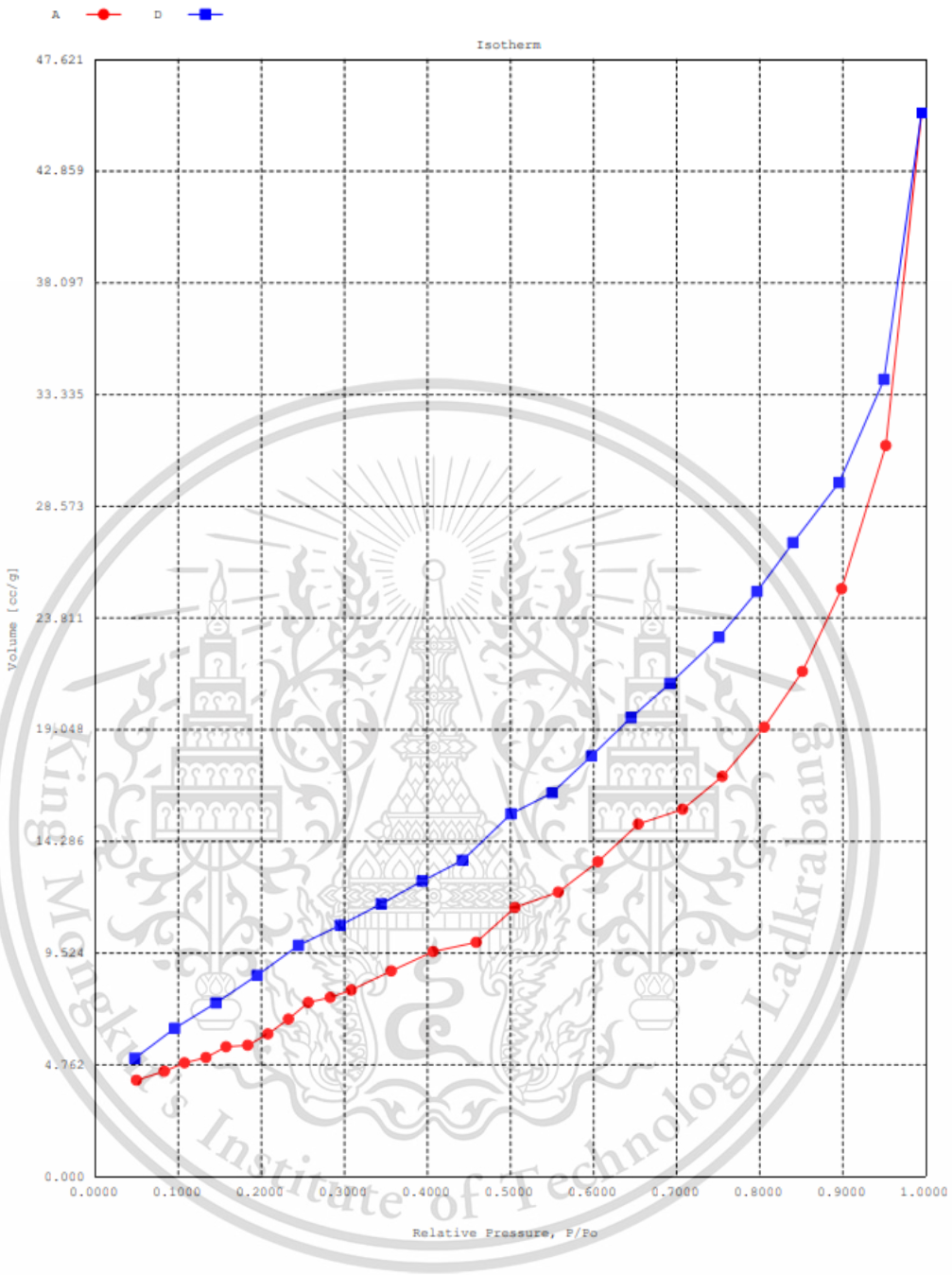

Figure F10 N_2 adsorption-desorption isotherm of 5MgO/KNaX(PB)

Sample weight after out gases: 0.0676 g and analysis time: 394.7 min.

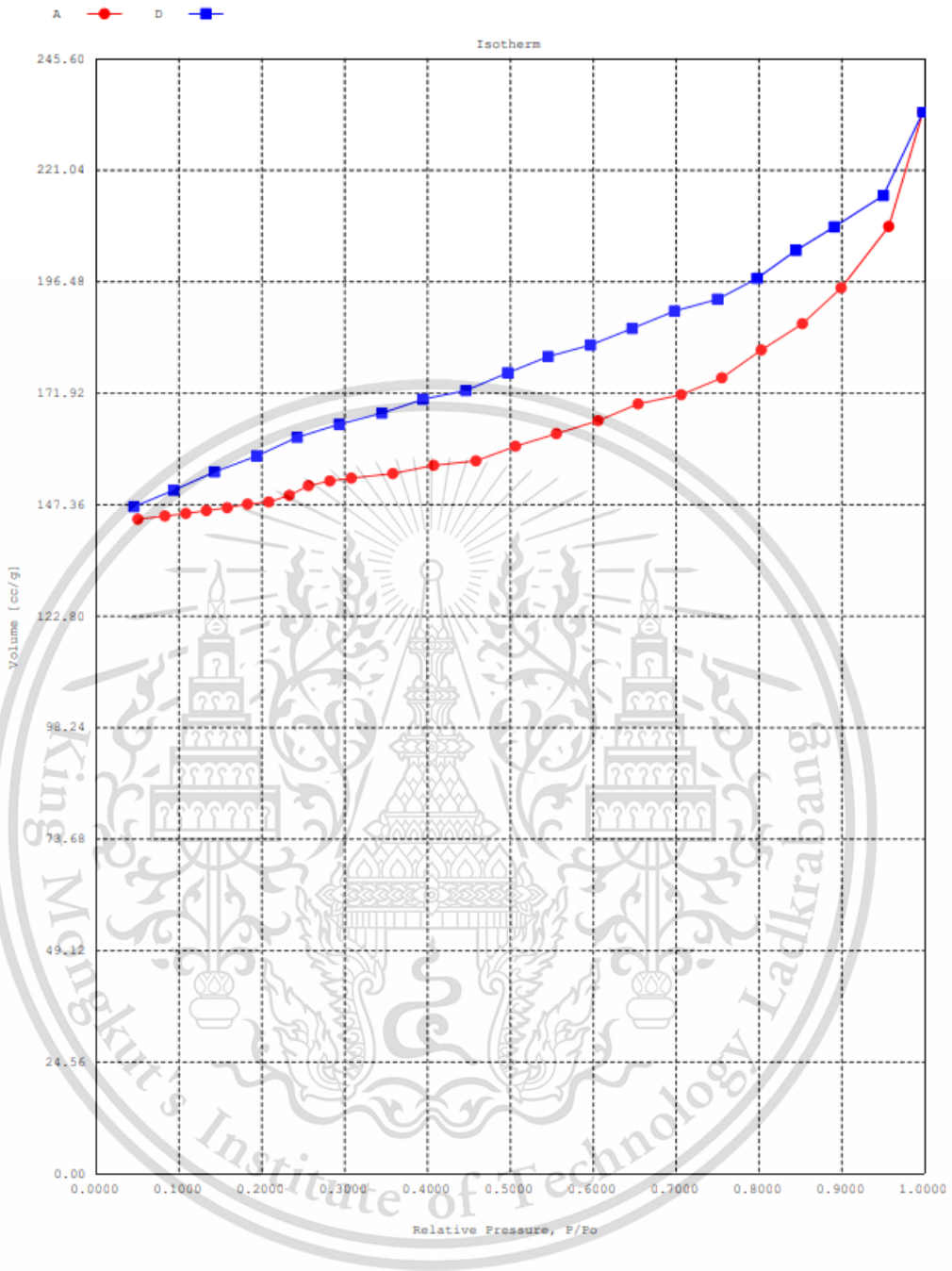

Figure F11 N_2 adsorption-desorption isotherm of 5MgO/KNaX(St)

Sample weight after out gases: 0.0227 g and analysis time: 413.3 min.

Author Biography

Name Mr. Nattapol Yotkkham

Date of Birth Day Month Year 10-03-1997

Address

Education (2018) Bachelor of Science in Industrial chemistry GPA 2.99
King Mongkut's Institute of Technology Ladkrabang

(2021) Master of Science in Applied chemistry GPA 4.00
King Mongkut's Institute of Technology Ladkrabang

Scholarship The authors are grateful for financial support from the School of Science, KMITL (Grant No. RA/TA-2562-M-030 and 2565-02-05-022) and National Research Council of Thailand.

Academic publication

[1] N. Yotkkham, K. Choojun, P. Promchana, X. Fan, and T. Sooknoi, **"Higher alcohol production from ethanol over occluded $[Mg_4(OH)_4]^{4+}$ clusters in MgO/KNaX,"** *Appl. Catal. Gen.*, vol. 632, p. 118502, Feb. 2022, doi: 10.1016/j.apcata.2022.118502.